2012

Mathematical Modeling and Simulation of a One-Dimensional Transient Entrained-flow GEE/Texaco Coal Gasifier

Job S. Kasule
West Virginia University

Mathematical Modeling and Simulation of a One-Dimensional Transient Entrained-flow GEE/Texaco Coal Gasifier

Job S. Kasule

A Dissertation Submitted to the
Benjamin M. Statler College of Engineering and Mineral Resources
at West Virginia University
in partial fulfillment of the requirements
for the Degree of

Doctor of Philosophy
in
Chemical Engineering

Richard Turton, Ph.D., Chair
Charter Stinespring, Ph.D
Stephen E. Zitney, Ph.D
John Zondlo, Ph.D
David Klinke, Ph.D

Department of Chemical Engineering

Morgantown, West Virginia

2012.

Keywords: Mathematical Modeling; Entrained-flow; Gasifier; Coal gasification; Aspen Custom Modeler; IGCC

ABSTRACT

Mathematical Modeling and Simulation of a One-Dimensional Transient Entrained-flow GEE/Texaco Coal Gasifier

Job S. Kasule

Numerous gasifier models of varying complexity have been developed to study the various aspects of gasifier performance. These range from simple one-dimensional (1D) models to rigorous higher order 3D models based on computational fluid dynamics (CFD). Even though high-fidelity CFD models can accurately predict many key aspects of gasifier performance, they are computationally expensive and typically take hours to days to execute even on high-performance computers. Therefore, faster 1D partial differential equation (PDE)-based models are required for use in dynamic simulation studies, control system analysis, and training applications.

In the current study, a 1D transient model of a single-stage downward-firing entrained flow General Electric Energy (GEE)/Texaco-type gasifier has been developed. The model comprises mass, momentum and energy balances for the gas and solid phases. A detailed energy balance across the wall of the gasifier has been incorporated in the model to calculate the wall temperature profile along the gasifier length. This balance considers a detailed radiative transfer model with variable view factors between the various surfaces of the gasifier and with the solid particles. The model considers the initial gasification processes of water evaporation and coal devolatilization. In addition, the key heterogeneous and homogeneous chemical reactions have been modeled. The resulting time-dependent PDE model is solved using the method of lines in Aspen Custom Modeler®, whereby the PDEs are discretized in the spatial domain and the resulting differential algebraic equations (DAEs) are then integrated over time using a variable step integrator.

Results from the steady-state model and parametric studies have been presented. These results include the gas, solid, and wall temperature profiles, concentrations profiles of the solid and gas species, effects of the oxygen-to-coal ratio and water-to-coal ratio on temperature, conversion, cold gas efficiency, and species compositions. In addition, the dynamic response of the gasifier to the disturbances commonly encountered in real-life is presented. These disturbances include ramp and step changes in input variables such as coal flow rate, oxygen-to-coal ratio, and water-to-coal ratio among others. The results from the steady-state and dynamic models compare very well with the data from pilot plants, operating plants, and previous studies.

Dedication

This work is dedicated to my beloved mother Rosette Nansubuga, my late father Kizza Godfrey, my late uncle Micheal Ssebunya and the rest of my family.

Acknowledgements

I am highly indebted to my Advisor, Prof. Richard Turton for his guidance, patience, support, and unwavering belief in me during this research experience. Special thanks to Dr. Debangsu Bhattacharyya for his selfless help and insightful suggestions throughout this work. Many thanks to Dr. Stephen Zitney for his help with Aspen Custom Modeler® as well his useful suggestions during the course of this research. I cannot fail to recognize my PhD committee members for their suggestions and corrections, which ensured that this manuscript met the acceptable standards. I would like to thank; the Faculty of the Chemical Engineering Department for the invaluable knowledge impacted to me through their excellent teaching skills; the staff especially Linda Rogers, Bonnie and Jim Hall for their cordial reception and various forms of support during my study.

Furthermore, I would like to extend my heartfelt gratitude towards the National Energy Technology Laboratory (NETL) of the United States Department of Energy (DOE), Morgantown WV for financing this research. Thanks to my fellow students (Kiran Chaudhari, Justin Jones, Prokash Paul, Pratik Pednekar, and Qiang Zhang) for their help and good company.

Last but not least, special thanks go to my wife, the one and only one Mary Immaculate B. Kasule for her selfless sacrifice, care, emotional support, and patience throughout this thrill of a journey, thank you dear!

Table of Contents

List of Figures

List of Tables

Nomenclature

A_t	Cross sectional area of reactor (cm^2)
ρ_s	Density of solid phase (g/cm^3)
ρ_g	Density of gas phase (g/cm^3)
ρ_w	Density of the gasifier wall
ε	Gas volume fraction
σ	Stefan-Boltzmann constant ($cal/cm^2.s.K^4$)
x_{sj}	Mass fraction of the jth solid specie
y_{gi}	Mass fraction of the ith gas specie
Γ_{s-g}	Net rate of consumption of the solid phase (coal) by the heterogeneous reactions ($g/cm^3.s$)
U_s	Solid phase velocity (cm/s)
U_g	Gas phase velocity (cm/s)
P_t	Total pressure in the gasifier (atm)
ΔH	Enthalpy of reaction (cal/g)
ΔH_k	Enthalpy of kth reaction (cal/g)
ΔH_j	Enthalpy of jth reaction (cal/g)
h_{eff}	Effective heat transfer coefficient ($cal/cm^2.s.K$).
$C_{p,g}$	Specific heat capacity of the gas phase (cal/g/K)
$C_{p,s}$	Specific heat capacity of the solid phase (cal/g/K)
$C_{p,w}$	Specific heat capacity of the gasifier wall (cal/g/K)
D_i	Inner gasifier diameter (cm)
D_o	Outer gasifier diameter (cm)
Δx	Discretization length step
d_p	Coal particle diameter (cm)

e_g	Emissivity of gas phase
e_w	Emissivity of wall
η_{cg}	Cold gas efficiency (%)
g	Acceleration due to gravity (cm/s^2)
$h_{\text{g-s}}$	Convective heat transfer coefficient between gas and solid (cal/cm^2.K.s)
$h_{\text{w-g}}$	Convective heat transfer coefficient between wall and gas (cal/cm^2.K.s)
Mw_i	Molar weight of specie *i* (g/mol)
C_D	Drag force correlation
Re	Reynolds number
R	Universal gas constant (cal/gmol.K)
μ_g	Gas viscosity (g/cm.s)
Nu	Nusselt number
k	Reaction rate constant
k_0	Arrhenius constant
VM	Volatile matter
V	Volatile content at time t
V^*	Effective volatile content of the coal
k_{diff}	Gas film diffusion coefficient (*g/cm^2 atm s*)
k_{ash}	Ash layer diffusion coefficient (*g/cm^2 atm s*)
k_s	Surface reaction constant (*g/cm^2 atm s*)
Y	Ratio of the radius of the unreacted core to the original particle radius
R_{gi}	Net rate of generation or consumption of gas species *i* (g/cm^3.s)
R_{Sj}	Net rate of generation or consumption of solid species *j* (g/cm^3.s)
P_i	Partial pressure of the gaseous species (atm)
f_s	Drag force per unit volume of particles (N/cm^3)
q_{loss}	Heat loss from the gasifier wall to the surrounding (cal/cm/s)
$q_{rad,w-s}$	Radiative heat flux transfer between wall and solid particles (cal/cm^2.s)

$q_{rad,w-g}$ Radiative heat flux transfer between wall and gas molecules (cal/cm^2.s)

$q_{rad,g-s}$ Radiative heat flux transfer between gas molecules and solid particles (cal/cm^2.s)

T_w, T_s, T_g are the wall, solid and gas temperatures (K).

$F_{w-s}, F_{w-g}, F_{g-s}$ are the wall-solid, wall-gas and gas-solid view factors respectively where for example F_{w-s} represents the fraction of radiation emitted by the wall that is received by the solid.

Greek letters

ε	void fraction
σ	Stefan-Boltzmann constant
ρ	density
α	recirculation ratio
$\Gamma_{g\text{-}s}$	rate of char consumption

Subscripts

w, g, s	wall, gas and solid respectively
rg	recirculated gas flow out of recirculation gas
mg	recirculated gas flow in mixing zone
cg	cold gas

Superscripts

*	Equilibrium values

Chapter 1

1.0 Introduction

Coal accounts for 65% of the world's fossil fuel reserves (World Coal Institute). A number of valuable products can be obtained from coal through the process of coal gasification. In this process, solid coal is thermally converted into its constituent gaseous components which include synthesis gas (H_2 and CO), CO_2, H_2S, and CH_4 among others. These gaseous species can then be used as feedstocks for chemical manufacturing plants, liquid fuels production, and electricity generating plants among others.

With the continued depletion of crude oil and natural gas resources from traditional oil producing countries, energy costs have increased rendering coal a more important role as an energy source for meeting the future energy requirements in both developed and developing countries. For example, in the United States, more than 50% of the electric energy is generated from coal combustion. However, coal is also one of the main sources of major environmental pollutants such as CO_2, mercury, and sulfur-based compounds. There is evidence to suggest that greenhouse gases, such as CO_2, cause global warming. Thus, an efficient and environmentally sustainable utilization of the vast coal resources to meet the increasing energy requirements remains a formidable challenge.

For decades, conventional coal-fired power plants have been at the forefront of generating electricity in the United States. However, they are less efficient and environmentally unattractive. As a result, a more efficient and environmentally competitive technology is necessary to avert the shortcomings of the direct coal-fired power plants.

The Integrated Gasification Combined Cycle (IGCC) plant technology, developed in the early 1980's has emerged as a suitable and efficient replacement for conventional power plants. These plants are known to be more efficient and cleaner (Holt and Alpert, (2004), Maurstad (2005), Minchener, J. A. (2005), Bhattacharyya et al. (2010)) than alternative coal-fired power plants, particularly when CO_2 is captured. A simplified schematic of the IGCC is shown in Figure 1.1

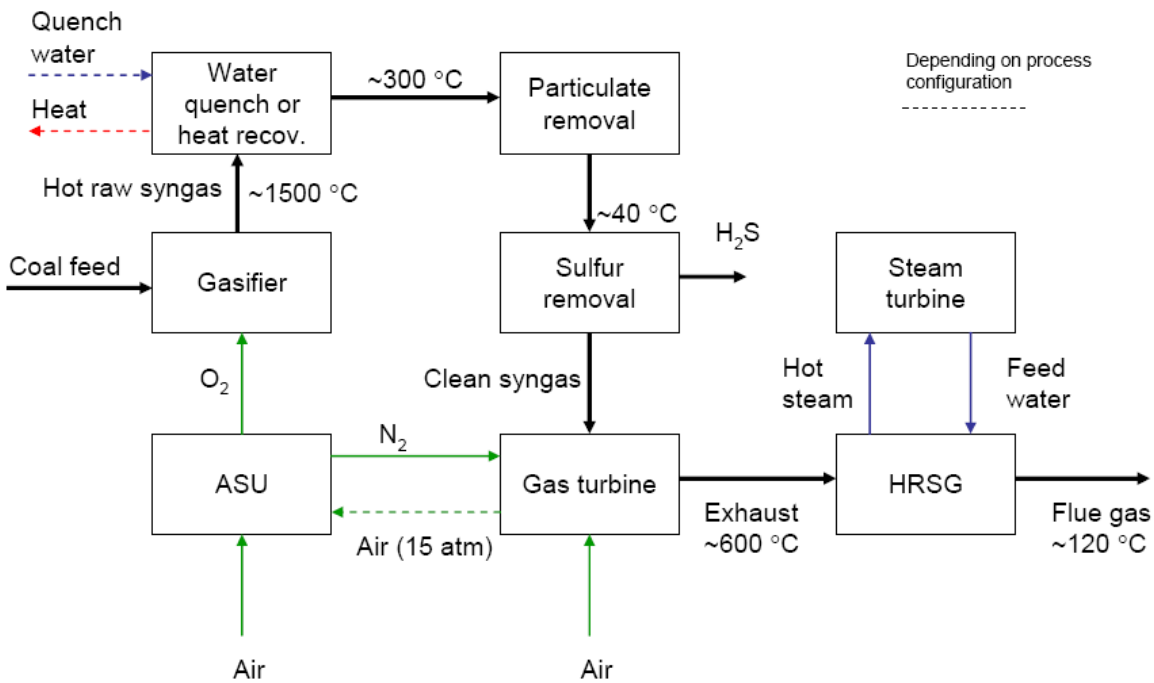

Figure 1.1: A Simplified Schematic of the IGCC Process [Ola Maurstad, "An Overview of Coal based Integrated Gasification Combined Cycle (IGCC) Technology", September 2005, MIT LFEE 2005-002 WP]

1.1 Brief Description of IGCC Power Plant

The solid (coal) or liquid fuel is fed to the gasifier where it is partially oxidized under pressure (30-80bar) using either oxygen or air as oxidant to form a synthetic gas stream (syngas),

which is a mixture of mainly carbon monoxide (CO) and hydrogen (H_2). In most IGCC plants that use oxygen, an air separation unit (ASU) is installed as part of the plant to provide this oxygen requirement. The syngas is then subjected to a series of purification processes in which the particulate matter (fly ash), CO_2, H_2S and mercury are removed prior to being fed to a combustion turbine where it is combusted to release energy that is converted to electricity by a generator. The high temperature waste streams are then fed to a heat recovery steam generator (HRSG) where high, intermediate, and low pressure steam is generated and fed to a steam turbine to generate more electricity, hence the name combined cycle. A more detailed description of the IGCC plant can be found in the literature, for example in (Holt and Alpert, (2004), Maurstad (2005)).The composition of the syngas is dependent on the type of gasifier, operating conditions inside the gasifier, and coal type. A number of gasification technologies are currently in use. The most common ones, illustrated in Figure 1.2 and whose main characteristics given in Table 1, are:

- Moving- (fixed-) bed gasifier
- Fluidized bed and gasifier
- Entrained bed gasifier.

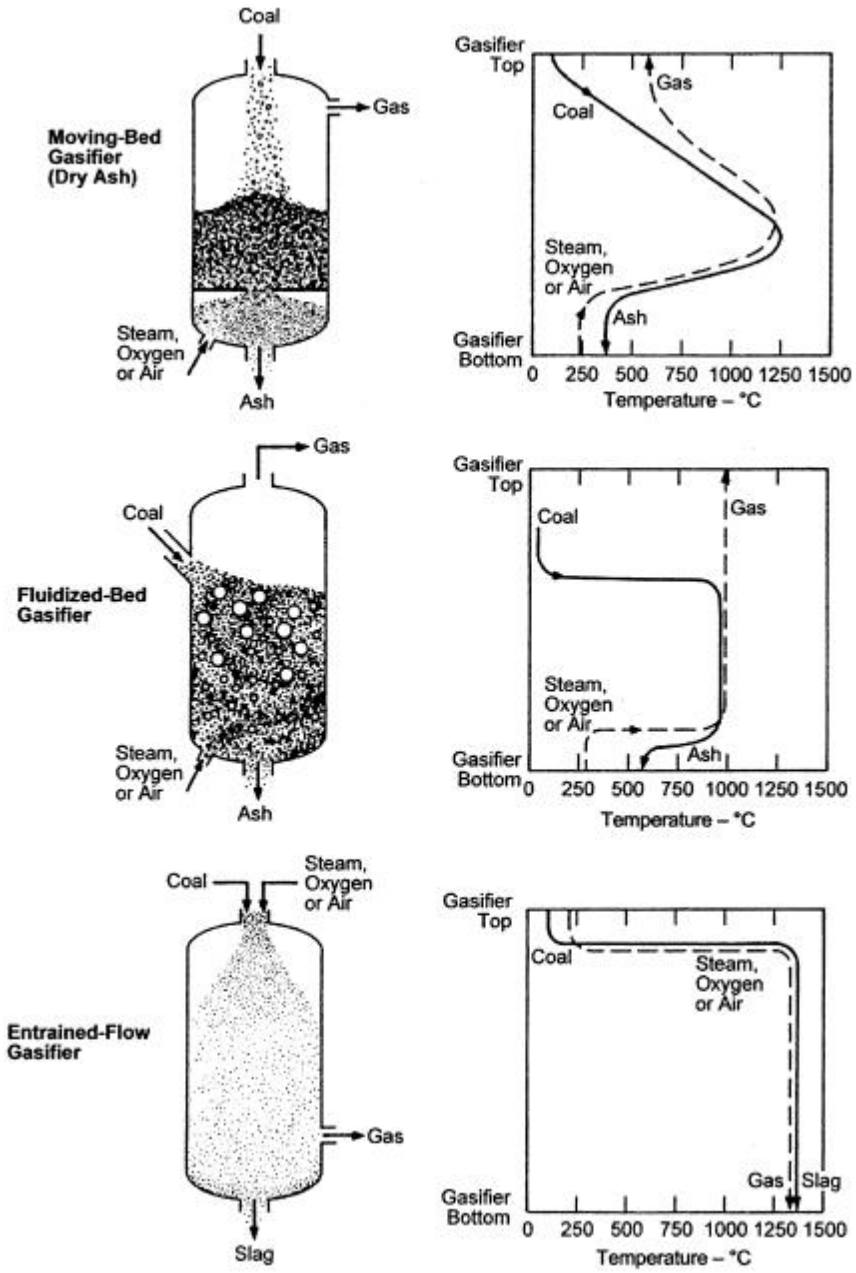

Figure 1.2: The three major types of gasification processes [Holt and Alpert, "Integrated Gasification Combined-Cycle Power Plants", *Encyclopedia of Physical Science and Technology*, **2004,** *18*, 897-924.]

Table1: Characteristics of different gasifier types [Maurstad (2005)**]**

Gasifier type	Fixed/Moving bed	Fluidized bed	Entrained-Flow
Outlet temperature	Low (425-600 ^{o}C)	Moderate (900-1050 ^{o}C)	High (1250 -1600 ^{o}C)
Oxidant demand	Low	Moderate	High
Ash conditions	Dry ash or slagging	Dry ash or agglomerating	Slagging
Size of coal feed	6-50 mm	6-10mm	<100µm
Acceptability of fines	Limited	Good	Unlimited
Other characteristics	Methane, tars & oils present in syngas	Low carbon conversion	Pure syngas, high carbon conversion

In the moving-bed/fixed-bed gasifiers, the gases flow relatively slowly upward through the bed of coal feed. They are only suitable for solid fuels and can process coals with biomass and/or wastes. Both concurrent and counter-current technologies are available but the former is more common.

In fluidized-bed gasification, the coal particles are suspended in an upward gas (either air or oxygen/steam) flow with feed particles continuously mixed with the particles undergoing gasification. They can only operate with solid crushed fuels (0.5-5mm), with the exception of the transport reactor which is midway between a fluidized-bed and an entrained-flow gasifier and as such operates with pulverized coals.

Lastly, in the entrained-flow gasifier, coal and/or other solid particles cocurrently flow and react with steam and oxygen or air in a suspension flow mode. They are the most widely used type for coal gasification; they are very versatile as they can accept both solid and liquid fuels, and they have higher gasification rates and are easier to operate. The high operating

temperatures in the entrained-gasifier lead to a product gas that is relatively free of higher hydrocarbons particularly any tarry material (Govind and Shah (1984)).

The major entrained-flow gasifier technologies/vendors are General Electric Energy (GEE, formerly Texaco), Shell and ConocoPhillips's E-gas gasification technologies. These technologies differ in many ways but share certain general production characteristics. Their typical gasification feedstocks include coal, petroleum based materials (crude oil, high sulfur fuel oil, petroleum coke and other refinery residues), gases or low value waste streams.

The Shell gasification technology is a single-stage, dry-feed process while the GEE/Texaco and ConocoPhillips gasifying processes use a wet(slurry) feed and a single-stage and two-stage feed systems, respectively. The GEE and ConocoPhillips gasifiers use a refractory–lined gasification chamber that, in general, increases the operation and maintenance costs as compared to the Shell process, which uses a membrane gasifier wall. Both the Shell and ConocoPhillips gasifiers are upflow systems, while the GEE/Texaco gasifier is a downflow system (Zheng and Furinsky, 2005).

Other distinguishing features of these technologies lie in the type of quenching/ heat recovery systems and operating pressure ranges. The GEE/Texaco gasifier is offered with a quench or with heat recovery and has the widest operation pressure range (500-1000 psig) as compared to the Shell (up to 600 psig) and the ConocoPhillips (up to 500 psig) both of which are only offered with heat recovery systems. These technologies have been widely utilized in many industrial electrical generating and chemical gasification plants as given in Minchener (2005).

1.2 Importance of the Study

The heart of any IGCC power plant is the gasifier. The downstream processes and efficiency of the IGCC is dependent on the performance of the gasifier. Thus, a good understanding of gasifier operation is crucial to the design and optimization of IGCC plants. Coal is a multi-component fuel that can undergo many highly complex reactions with widely varying residence/reaction times. Additionally, the extremely high operating temperatures and pressures typical in entrained-flow gasifiers make it hard for laboratory experiments to be conducted at these process conditions.

As a result, mathematical modeling and numerical simulations of gasification processes became a natural choice for studying the gasification processes. Their use is cheaper, more efficient, and allows the extreme process conditions to be studied easily.

With mathematical models, the main processes taking place within the gasifier such as mass, momentum and heat transfer processes, and chemical reactions can be simulated to obtain concentration, temperature and velocity profiles of the reacting gas and solids in the gasifier. Additional sensitivity studies can be conducted easily in order to understand the effects of changes in feed and operating conditions on the conversion of solid fuel and gas composition at the gasifier outlet.

A number of mathematical models have been developed (Ubhayakar et al., 1977, Wen and Chaung, 1979; Govind and Shah, 1984; Brown et al., 1988; Ni et al., 1995; Vamvuka, 1995a,b; Bearth, 1996; Wanatabe and Otaka, 2006; Chen et al., 2000a,b; Liu et al., 2000; Shi et al., 2006; Choi et al., 2001; Monaghan et al., 2010; Yang et al., 2011; etc.) to study different aspects of the gasification process. Due to the very complex nature of the processes taking place in the gasifier, most of these models are simplified 1-D models that have included at least two of

the transport phenomena processes above under steady-state conditions. However, actual gasifier operation is transient and the processes involved take place in more than one-dimensional space. Thus, dynamic models are needed to further understand the operation of gasifiers. Whereas multidimensional dynamic models have been recently developed, they are computationally expensive and may not find direct design applicability. Therefore, one-dimensional dynamic models are still needed to further elucidate the complex processes within the gasifier and to aid efficient design and optimization of gasifier operation.

In the current study, therefore, a 1-D transient entrained-flow gasifier model will be developed and simulated using Aspen Custom Modeler® (ACM), a product of Aspen Technology Inc. a leading developer of industrial process simulators. Unlike in most commercial process simulators, and other AspenTech simulation products in which built-in process models/routines are used, in ACM, the user can custom build a variety of models to simulate processes of relative complexity. Thus, a working 1-D ACM-based gasifier model will be an important building step for future design of more complex gasifier models that may be incorporated easily in plant-wide IGCC studies.

1.3 Objectives of the study

The general objective of the current study is to model and simulate the performance of a single-stage, downward-firing, GEE/Texaco-type, entrained-flow gasifier in a one-dimensional domain using Aspen Custom Modeler®. This will then be incorporated in the general plant-wide IGCC dynamic simulator model that West Virginia University is developing in collaboration with researchers at the National Energy Technology Laboratory's (NETL) Advanced Virtual Energy Simulation Training And Research (AVESTAR) Center. .

1.3.1 Specific Objectives

1. Develop a steady-state entrained-flow gasifier model that will incorporate:
    - Mass, momentum and heat transfer between the gaseous and solid fuel phases.
    - Conduction, convection and radiation as heat transfer mechanisms between coal particles and gaseous phases.
    - Pyrolysis, devolatilization, gasification and combustion reactions.
2. Extend the steady-state model above to a transient model incorporating the above phenomena.
3. Validate the results of the steady-state model with other models of similar gasifiers in the literature and/or industrial data.
4. Perform sensitivity studies of the gasifier model to investigate the effect of process parameters such as coal quality, feed conditions and operating conditions both in steady-state and dynamic modes.
5. Validate the dynamic model with any available experimental /plant data

Chapter 2

Literature Review

2.1 Introduction

Coal is a very complex mixture of mineral matter whose exact composition has not been fully established and varies widely with coal type. The proximate and ultimate analyses are the standard ways of determining coal composition. In the former, the composition of coal is given in terms of the percentage moisture, volatile matter (VM), fixed carbon (FC) and ash content while in the later, the elemental composition of coal is determined and given as percentage carbon (C), nitrogen (N), oxygen (O), hydrogen (H) and sulfur (S) content. In its raw solid form, coal may be pulverized and combusted to produce electricity via conventional steam turbines. However, through the process of gasification described in the previous chapter, coal can also be converted to a number of useful gaseous products that have a wide range of industrial applications as well as being used for power generation.

Coal gasification has been widely studied for a long time but due to the complex nature of the process, it is not surprising that much research is still directed towards this field. A number of experimental and numerical simulation studies of coal gasification are available in the literature and outline in this section, a literature review of the studies related to the current study is presented. An overview of the entrained gasifier is also presented in which the main chemical reactions taking place in the gasifier and the main components of the numerical model are briefly discussed.

2.2 Entrained-Flow Coal Gasifier

The entrained-flow coal gasifier is the most widely used gasification technology. In this type of gasifier, a pulverized coal feed (dry or in slurry form depending on gasifying technology) and a hot gas stream of steam and oxygen, at adjusted predetermined ratios are mixed at the gasifier entrance and travel concurrently throughout the gasifier. The gasifiers are operated at high temperatures and pressures and thus high carbon conversions can be achieved with the gasification products relatively free of higher hydrocarbons.

However, they also have disadvantages that can be attributed to the high operating temperatures. These include: difficulty in the selection of refractory and construction material in the combustion zone of the gasifier; difficulty in the recovery of sensible heat in order to obtain efficient utilization of the high-temperature gas product; and the large amounts of oxygen needed to maintain the high-temperature operating conditions.

2.3 General Model Description

In order to model the entrained-flow gasification process, there are several key processes that must be considered. These are mainly the chemical reactions taking place in the gasifier and other physical processes such as momentum and heat transfer. A brief description of the chemical reactions taking place in a gasifier is given below. The heat transfer model components are covered later in Chapter 3, which describes the model development for the current study.

2.4 Reactions in an Entrained-Flow Gasifier

In the gasifier, coal can undergo many different reactions due to its complex nature. However, it is common practice that only the main reactions are considered in order to ensure tractability of the models. These are divided into the following categories: thermal decomposition reactions, commonly known as pyrolysis or devolatilization; heterogeneous gas-solid reactions; and the homogeneous gas-phase reactions.

2.4.1 Pyrolysis/Devolatilization

Pyrolysis or devolatilization is one of the early stage processes that is undergone by coal when coal is heated. The coal decomposes to release volatiles, which consist of a mixture of combustible gases (CO, H_2, and CH_4), carbon dioxide (CO_2), hydrogen sulfide (H_2S), nitrogen, water vapor and tar. This is a very complex reaction but can be represented by reaction (2.1) below:

$$\underset{(Raw\ coal)}{C_{\alpha i}H_{\beta i}O_{\gamma i}N_{\delta i}S_{\varepsilon i}Ash} \xrightarrow{\Delta} \underset{(Char)}{C_{\alpha}H_{\beta}O_{\gamma}N_{\delta}S_{\varepsilon}Ash} + \underset{(CO+H_2+CH_4+H_2S+N_2+tar)}{Volatiles} \tag{2.1}$$

Char, tar, and gas are the major products of the pyrolysis reaction and according to Wen and Onozaki (1982), the char is defined as the undistillable material which remains in solid form. The volatiles are comprised of two fractions; gas that is comprised of small molecules, and distillable liquid that is comprised of material with a molecular weight larger than C_6 (referred to as tar) and components lighter than C_6.

Over the years, a substantial amount of experimental research has been directed towards studying the pyrolysis reaction (Howard and Essenhigh, 1967; Badzioch and Hawksley, 1970;

Loison and Chauvin, 1964; Badzioch, 1961), Antony and Howard, 1976, Anthony et al., 1976) with the aim of understanding the mechanisms for volatile release, kinetics and the factors affecting volatile yield. The pyrolysis reaction is extremely complex and the mechanisms and the influence of the many experimental variables are still not well understood. However, there is strong evidence that the devolatilization reaction is a chemical decomposition reaction (Antony and Howard, 1976). It is known that the devolatilization does not start until the temperature reaches between 350°-400°C after which its extent becomes a strong function of temperature and heating rate. The heat causes the complex coal structure to decompose, the weaker bonds rupturing at lower temperatures and the stronger ones at higher temperatures. At the same time, fragments that are volatile attempt to escape from the particles, some of which are highly reactive free radicals subject to a variety of secondary reactions such as cracking and repolymerization.

These secondary reactions are usually undesirable as they tend to deposit part of the volatile matter as a solid (char) and reduce the gas and liquid yields. Their extent can, however, be reduced by enhancing the transport of volatiles away from the reactive environment, such as by operating at reduced pressures with smaller and more widely dispersed particles. Besides this carbon enrichment, the release of volatiles has a profound effect on the physical structure of the coal, with the enlargement and increase in the number of pores and changes in the shape of the particles, as some of the volatiles are trapped and act as solvents liquefying or softening the coal (Bearth, 1996).

It is not easy to study devolatilization experimentally as the process is extremely rapid at the temperatures conditions used for combustion and particularly in a reactive environment, the changes in the coal due to devolatilization are difficult to distinguish from those due to

heterogeneous reactions. Therefore, many researchers have preferred to study pyrolysis of coal under inert or reducing atmospheric conditions implicitly assuming that the behavior of coal in devolatilization under combustion or gasification conditions is similar to that measured experimentally with a less reactive environment. To some extent, this assumption is not valid as it is almost impossible to replicate the heating conditions of an igniting particle, possibly with heterogeneous ignition if oxygen concentration is high, in an inert atmosphere (Bearth, 1996).

From a modeling point of view, the factors that should be considered are the rate, the yield of volatiles, their composition, and the resultant structural changes of the char particles that are known to play a significant role in the subsequent heterogeneous reactions. The temperatures in the gasifier during gasification are usually high and as a result lead to rapid rates of devolatilization. However, the actual devolatilization rate is expected to have only a minor effect on the overall gasification process as the devolatilization time is negligible compared to the overall gasification time. On the other hand, it is the volatile yield that is important as it determines the residual amount of char that is yet to be gasified. The composition of volatiles is also expected to have a minor impact because the gaseous species usually change very rapidly due to the combustion and gasification reactions.

The process of devolatilization has been studied extensively and the literature is rich in related work (Anthony et al., 1976; Badzioch and Hawskey, 1970; Anthony and Howard, 1976; Suuberg, 1977) and confirmed through later studies such as Niksa (1988), Niksa (1991), and Lee (1991) that established the main factors that affect the rate and amount of volatiles released during the process.

It has been established that the total amount of volatiles released during devolatilization is strongly dependent on the type (rank) of coal with low-rank coals generally giving off more

volatiles than high ranking coals. Another factor known to affect the amount of volatiles released is the maximum temperature achieved during devolatilization and the duration of time the devolatilizing particles spend at this temperature. At high heating rates, the total volatile yields have been shown to exceed the volatile matter established through the ASTM proximate analysis.

Pressure is another factor that strongly affects the yield of volatiles during devolatilization. It has been reported by a number of investigators (Anthony, 1976; Suuberg, 1977; Bautista, 1986; Niksa, 1991; Lee, 1991) that increases in pressure resulted in substantial decreases in the amounts of volatile yields. Although the exact reasons for this is still uncertain, it is generally believed that high pressures lead to increases in secondary char-forming reactions of volatiles (Anthony, 1976; Lee, 1991); an increase in pressure increases the resistance of volatiles to escape from the coal melt and subsequently enhancing secondary reactions of volatiles trapped inside the coal melt. In addition, it is believed that the increase in boiling point of liquid hydrocarbons at high pressures leads to reduced vapor pressures of the volatiles (Niksa, 1991).

Particle size is another factor that can have an appreciable effect on the yield of volatiles from a devolatilization reaction. However, for particles smaller than about 1mm (typical of those in entrained-flow gasifier feed), yields and product distributions are independent of particle size (Wagner, 1985; Niksa, 1988). In larger particles, such factors as diffusion and pore structural changes may also affect the volatiles yield.

2.4.1.1 Devolatilization Kinetics

Because devolatilization or pyrolysis is more than just a chemical process but rather a complex series of processes and reactions consisting of phase changes, mass and heat transfer, the use of the term kinetics to describe the rate of pyrolysis may not be appropriate from a rigorous point of view (de Souza-Santos, 2004). Any kinetic model for pyrolysis is just a crude approximation to reality and it is, therefore, not surprising that a number of dissimilar devolatilization models have been developed with widely varying ranges of precision.

A number of experimental studies have been carried out over time and a number of devolatilization kinetic models have been developed but it is the most widely used models that are described briefly below. These models fall into the following categories:

- Single First-Order Reaction Model
- Distributed Activation Energy (DAE) Model and
- Two-Step Reaction Model

The first category of models (Badzioch and Hawksley, 1970; Anthony and Howard, 1976; Anthony, 1976) is the simplest and is based on the concept that the rate of pyrolysis is proportional to the amount of volatile content remaining in the coal. Thus the rate of devolatilization is represented as

$$\frac{dV}{dt} = k(V^* - V) \tag{2.2}$$

where $k = k_0 \exp(-E/RT)$ and $V \to V^*$ as $t \to \infty$ with the unknown parameters k and V^* being determined from the kinetic studies data. V^* is the effective volatile content of the coal, which is, in general different from the VM determined by proximate analysis.

However, the simple first-order model above has its limitations. The rate parameters are fit from data taken at a particular devolatilization history and thus may not describe devolatilization over a broad range of heating rates. Besides, the volatile yields from the first order rate expression (2.2) are reported to be higher than the volatile matter ascertained by proximate yields, with some results reported (Anthony and Howard, 1976) with discrepancies in yields as high as 80%. Although, variations to equation (2.2), including n^{th} order rate kinetics have been developed in order to improve its utility, they have a serious shortcoming in that the apparent asymptotic yield (V^*) appears to be a function of the final temperature, which is neither mechanistically consistent with nor mathematically amenable to the equations.

The second type of model is more complicated and assumes that devolatilization occurs through several parallel simultaneous first-order reactions. First proposed by Pitt (1962), who had unreasonably assumed isothermal conditions from the start to the end of the pyrolysis process, the method was later generalized by Anthony et al. (1976) for non-isothermal conditions for which the amount of volatiles from the start to a time t could be obtained. The model also assumes that the number of reactions is large enough to permit the activation energy to be represented as a continuous function, $f(E)$ unlike in the previous model in which the activation energy is assumed to be a constant. Thus the DAE model (Anthony, 1976) assumes that the activation energy follows a Gaussian distribution with mean E_0 and standard deviation of σ and according to this model, the rate of devolatilization is given by

$$\frac{dV}{dt} = V^* \int_0^\infty A\exp(-\frac{E}{RT})\exp\left[-\int_0^t A\exp(-\frac{E}{RT})dt'\right] f(E)dE \tag{2.3}$$

where E is a particular activation energy in a continuous distribution function, $f(E)$, which is given by the following normal distribution function:

$$f(E) = \frac{1}{\sqrt{2\pi}\sigma} \exp(-\frac{(E-E_0)^2}{2\sigma^2}) \tag{2.4}$$

and σ is the standard deviation about the mean energy E_0.

The above model was able to represent the impact of temperature and heating rate variations on devolatilization rates and it achieved considerable improvements in the predictions of total volatile release rates over a wide range of temperatures compared to the simple first-order reaction model. However, just like in the previous model, it still has a hypothetical ultimate yield parameter and thus cannot predict the impact of heating rate on devolatilization yields.

In the third type of approach (Kobayashi et al., 1976; Ubhayakar et al., 1977; Brown et al., 1988; Choi et al., 2001), the pyrolysis process is represented by a competing two-step reaction model based on two competitive reaction channels that simultaneously convert the coal reactant into both volatiles and char.

$$\begin{aligned} m_c &\xrightarrow{k_1} y_1 V_1 + (1-y_1) C_1 \\ m_c &\xrightarrow{k_2} y_2 V_2 + (1-y_2) C_2 \end{aligned} \tag{2.5}$$

where m_c is the devolatilizing coal mass, V_1 and V_2 are the instantaneous volatile yields generated through routes 1 and 2 respectively while C_1 and C_2 are the corresponding instantaneous char yields, respectively, while y_1 and y_2 are the stoichiometric coefficients and k_1, k_2 are the two Arrhenius rate constants for the above reactions. It is normally interpreted that one of the channels occurs at low temperature and the other at high temperature; although, it is more preferred to interpret route 1 as the tar production route and 2 as the gas formation route as explained in the PC Coal Lab V4.0, User's Guide and Manual, (2004). This means that channels 1 and 2 are low and high activation reactions respectively. The rate law corresponding to this model is given as

$$\frac{dV(t)}{dt} = \int_0^t y_1 k_1(t') + y_2 k_2(t') S(t') dt', \tag{2.6}$$

where,

$$S = S_0 \exp(-\int_0^t (k_1 + k_2) dt') \tag{2.7}$$

This type of model is capable of describing the effect of temperature on volatile yields as well as predicting the devolatilization rates at higher temperatures. It also has an added advantage that the apparent ultimate yield parameter, V^*, which has been at the focus of kinetic studies, does not appear in the formulation.

Anthony et al. (1976), in an experimental study of coal pyrolysis and hydrogasification, showed that the volatile yield increases significantly with decreasing pressure, increasing hydrogen partial pressure, and increasing final temperature attained but only slightly with increasing rate of heating. The effect of pressure on volatile yield was explained by a mathematical model that considered the competition between diffusional escape and secondary reaction of reactive volatile species during a pyrolysis process as

$$V^* = V_{nr*} + V_{r**} / (1 + 0.56 P_t) \tag{2.8}$$

Where V_{nr*} is the ultimate volatiles yield at very high pressure (greater than 100 atm), and V_{r**} is the portion of volatile yield in excess of V_{nr*} at very low pressure (less than 0.001 atm). But, the values of these parameters vary from coal to coal and since not enough experimental data are available, expression. (2.8) cannot be used directly in a general gasification model. With most experimental data on volatile yield taken at 1atm, a more usable form that accounts for the pressure effects is obtained by linear interpolation of the data and this is given as

$$V^* = V^*_{(at\ 1\ atm)} (1 - a \ln P_t) \tag{2.9}$$

where a is approximately 0.066 for bituminous coal.

The above expression can be used to estimate the total yield of volatiles if the total pressure in the gasifier is between 0.1 and 50 atm.

Lee (1991) studied the effect of pressure on devolatilization and swelling behavior of a softening coal during rapid heating. He observed that increasing the applied pyrolysis pressure slowed the rates of volatiles release, lowered the asymptotic volatiles yields, enhanced secondary reactions of the volatiles, reduced the tar yield and changed the gas yields in a complex manner.

Bearth (1996) correlated the results obtained by Lee (1991) to predict the effect of pressure on volatile yield and obtained the expression given in Equation (2.10) below

$$V_p^* = V_{1atm}^* / P^{0.13} \tag{2.10}$$

Where the atmospheric volatile yield, V_{1atm}^* in the above was calculated using the simple expression given by Neoh and Gannon (1984), and P is the pressure in atm.

2.4.1.2 Composition of Volatile Products

Although the models above achieved reasonably accurate predictions of the amounts of tar, gases, and char released during pyrolysis, they could not predict the composition or stoichiometry of the product mixture and there is not much work in the literature regarding this point. This is not a trivial task as it depends significantly on fuel properties and operating conditions in addition to solid residence time. It needs special correlations to determine the stoichiometry or ratios of individual gases released in the process.

The work of Loison and Chauvin (1964) is the first noticeable effort in trying to establish the stoichiometry of the volatile products. They studied the rapid devolatilization of several coals

and determined the mass fractions of the component gas species in the product mixture. The correlations for these mass fractions are shown in de Souza-Santos (1989).

Their data were helpful in later studies such as Wen and Chaung (1979) and Govind and Shah (1984) who graphically summarized their data as shown in Figure 2.1 and used the ratios of CO/CO_2 and H_2O/CO_2 in addition to the elemental balances to determine the product distribution.

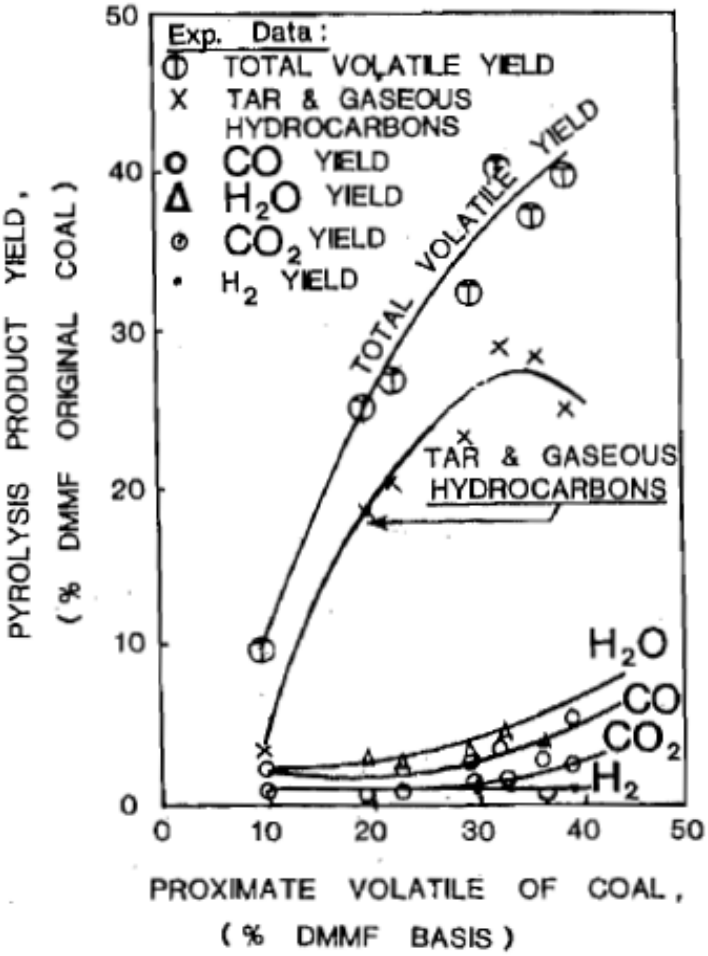

Figure 2.1: Product yield of coal pyrolysis (Loison and Chauvin, 1964): at 103 ^{o}C/s to 1,050 ^{o}C (obtained from Govind and Shah, 1984)

In other efforts, an average overall composition of the devolatilization products was given (Fuller, 1982) but such values, just like the correlations of Loison and Chauvin (1964),

were obtained at a particular set of conditions and may not reflect the effect of other factors such as temperature, heating rate, and pressure and thus may be limited in application to other conditions.

However, with advances in analytical techniques, particularly the pressurized drop tube furnace (PDTF) or thermo-gravimetric analyzer (TGA), more knowledge regarding the internal and chemical constitution of solid fuels in general has been obtained and this has led to an increasingly sophisticated representation of models for the devolatilization process (Gavalas et al., 1981; Niksa and Kerstein, 1986; Niksa, 1986; Niksa and Keistein, 1987; Solomon, 1988; Niksa, 1988; Niksa, 1991). These models fall in a particular category of devolatilization reactions called structural models that in general try to account for the coal structural changes and internal bond and chemical composition.

Perhaps the most detailed of these is the FLASHCHAIN model described in Niksa (1988) and then in more detail in Niksa (1991). This model is an improvement to the previous structural models above and it invoked a new model of coal constitution, chemical kinetics, chain statistics, and flash distillation to explain the devolatilization of various coals. These models can determine the rates of devolatilization of the individual gases from the breakdown of specific bond types. The difficulties of the previous simplified devolatilization models were eliminated by these structural models, as the composition of product gas and tar are readily obtained.

Based on this model, Niksa Energy Associates LLC developed computational software called PC Coal Lab® that acts as a virtual laboratory for predicting the devolatilization behavior of any coal, biomass, and petroleum coke under any operating conditions, given only the coal's proximate and ultimate analyses and sets of well-defined operating conditions (see PC Coal Lab V4.0, User's Guide and Manual, (2004) for details). With this software, experimental data based

on the flashchain mechanisms can be generated and used to estimate, among other things, the parameters in the above devolatilization models (simple first order, distributed activation energy and two-step reaction models) needed for modeling purposes.

2.4.2 Heterogeneous Reactions

After devolatilization, the carbon-rich solid residue (char) is then gasified in the reactive gaseous environment. Many reactions are possible, but only the main heterogeneous reactions are usually considered in most of the gasification studies and these are: the char-combustion reaction; char-carbon dioxide gasification reaction; char-steam gasification and the char-hydrogen reaction. The heterogeneous reactions proceed when the flux of volatiles from the coal particles is sufficiently low to allow diffusion of reactant gases to the particles (Bearth, 1996). Owing to the rapid nature of the oxygen gasification reaction, as compared to other gasification reactions, it is expected to dominate in the presence of oxygen and will proceed until all the oxygen is consumed. Following the "combustion" zone, the carbon dioxide and steam gasification reactions dominate given their high concentrations as released from the combustion reaction. The hydrogen gasification reaction is slow and occurs when a substantial amount of hydrogen is present, for example, in large, high pressure gasifiers with relatively high carbon conversion. A detailed representation of the heterogeneous reactions adapted from Wen and Chaung (1979) is shown below:

Char-Oxygen Reaction

$$C_\alpha H_\beta O_\gamma N_\delta S_\varepsilon A + \left(\frac{\alpha}{\phi} - \frac{\gamma}{2} + \frac{\beta}{4} - \frac{\varepsilon}{2}\right) O_2 \rightarrow 2\left(1 - \frac{1}{\phi}\right)\alpha CO + \left(\frac{2}{\phi} - 1\right)\alpha CO_2 + \left(\frac{\beta}{2} - \varepsilon\right) H_2O + \varepsilon H_2S + \frac{\delta}{2} N_2 + ash \quad (2.11)$$

Char-Carbon dioxide Reaction

$$C_\alpha H_\beta O_\gamma N_\delta S_\varepsilon A + \alpha CO_2 \rightarrow 2\alpha CO + \gamma H_2O + \left(\frac{\beta}{2} - \varepsilon - \gamma\right) H_2 + \varepsilon H_2S + \frac{\delta}{2} N_2 + ash \tag{2.12}$$

Char-Steam Reaction

$$C_\alpha H_\beta O_\gamma N_\delta S_\varepsilon A + (\alpha - \gamma) H_2O \rightarrow \alpha CO + \left(\alpha - \gamma + \frac{\beta}{2} - \varepsilon\right) H_2 + \varepsilon H_2S + \frac{\delta}{2} N_2 + ash \tag{2.13}$$

Char-Hydrogen Reaction

$$C_\alpha H_\beta O_\gamma N_\delta S_\varepsilon A + 2\left(\alpha + \gamma + \varepsilon - \frac{\beta}{2}\right) H_2 \rightarrow \alpha CH_4 + \gamma H_2O + \varepsilon H_2S + \frac{\delta}{2} N_2 + ash \tag{2.14}$$

It should be noted that the stoichiometric coefficients presented in the char-oxygen (2.11) and char-carbon dioxide (2.12) reaction equations above are slightly different from the original versions given in (Wen and Chaung, 1979). The stoichiometric coefficients in the original equations, fails to conserve the oxygen and hydrogen elemental balances as pointed out by Spenik (NETL, Morgantown, WV) whose corrected versions are shown above.

However, most studies have used simplified versions of the above equations in which coal is usually represented as pure carbon, even though the effects of structural changes may be important in modeling the gasification kinetics. It is known that during devolatilization, a range of changes in the structure of the particles may occur, for example, large pores may form as the gases escape from the particles and in high temperature devolatilization, increasing amounts of material separating from the char matrix increases the formation of gases in the particle that would in turn cause swelling.

The reaction kinetics of the gasification reactions have been studied and will be discussed in chapter three.

2.4.3 Homogeneous Reactions

The gaseous products from the devolatilization and gasification reactions discussed above participate in a number of homogeneous reactions within the gasifier. The main reactions commonly considered in most gasifier models, along with the standard heats of reaction are given below:

$$CH_4 + 1/2\,O_2 \xrightarrow{k_1} CO + 2H_2 \qquad \Delta H = -35.7\ MJ/kmol \tag{2.15}$$

$$H_2 + 1/2\,O_2 \xrightarrow{k_2} H_2O \qquad \Delta H = -242\ MJ/kmol \tag{2.16}$$

$$CO + 1/2\,O_2 \xrightarrow{k_3} CO_2 \qquad \Delta H = -283 MJ/kmol \tag{2.17}$$

$$CO + H_2O \underset{k_5}{\overset{k_4}{\leftrightarrow}} CO_2 + H_2 \qquad \Delta H = -41.1 MJ/kmol \tag{2.18}$$

$$CH_4 + H_2O \xrightarrow{k_6} CO + 3H_2 \qquad \Delta H = +206 MJ/kmol \tag{2.19}$$

$$CO + 3H_2 \xrightarrow{k_7} CH_4 + H_2O \qquad \Delta H = -206 MJ/kmol \tag{2.20}$$

$$\tfrac{1}{2} N_2 + \tfrac{3}{2} H_2 \xrightarrow{k_8} NH_3 \qquad \Delta H = -46.1 MJ/kmol \tag{2.21}$$

$$NH_3 \xrightarrow{k_9} \tfrac{1}{2} H_2 + \tfrac{3}{2} H_2O \qquad \Delta H = +46.1 MJ/kmol \tag{2.22}$$

The homogeneous reactions above are a mixture of endothermic and exothermic reactions. The energy requirement for the endothermic reactions is obtained from the fuel combustion and other exothermic reactions which release high amounts of the energy. Some of this energy is also utilized in the endothermic gasification reactions. In the presence of oxygen, the combustion reactions are expected to dominate due to their rapid kinetics.

Other equilibrium reactions that can be significant in the gasifier but that are not included in the current study include:

$$SO_2 + 3H_2 \leftrightarrow 2H_2O + H_2S \tag{2.41}$$

$$COS + H_2O \leftrightarrow CO_2 + H_2S \tag{2.42}$$

The reactions based on nitrogen, its oxides and ammonia are also possible but have been usually neglected by most studies in the literature and are also neglected in the current model. The kinetics of the reactions considered in this study are discussed in the next chapter.

With a better understanding of the reaction kinetics scheme, many researchers have been able to develop mathematical models of varying complexity to study gasification processes in different reactor configurations at varying operating conditions that may not be possible to replicate under laboratory conditions, as well as for designing and scaling of industrial gasification facilities. Many such models developed for entrained gasifiers exist in the literature but only the main, relevant studies are given here.

In one of the earlier initiatives in modeling entrained gasification, Ubhayakar et al. (1976) developed an analytical model to describe the physical and chemical processes occurring in an entrained-bed coal gasifier. In their model, mixing (using empirical relationships) of the cold coal-carrier gas stream with the hot entraining gases, heat transfer to the coal particles, the devolatilization of the coal particles to char and volatiles, gas-phase reaction of these volatiles with the entraining gases and the thermal cracking of the volatiles in the gas phase were considered. Although their model solutions correlated well with data from an experimental coal gasifier, clearly, it was a very simplified model that neglected many aspects of the actual gasification processes, such as the heterogeneous reactions.

Wen and Chaung (1979) developed a 1-D model to simulate the Texaco downflow entrainment pilot plant gasifier using coal liquefaction residues and coal-water slurries as feedstocks. In the absence of experimental data to estimate the degree of mixing in the gasifier, the authors assumed that at the entrance of the gasifier, the gas phase is completely mixed and

that in the region that follows and throughout the entire reactor, plug flow of solid and gas phases was a reasonable approximation. They subsequently adopted a compartment-in-series approach to represent the gasifier hydrodynamics, an approach which employs a large first compartment and smaller sizes for each of the compartments that follow. The reaction schemes considered included the pyrolysis reaction; char-combustion; steam, CO_2 and H_2 gasification reactions in which the shrinking-core model was used to model the heterogeneous reactions; and gaseous combustion reactions as well as the methanation and water-shift gas reaction. Based on the reactions taking place, they divided the gasifier into three zones: the pyrolysis and volatile combustion zone; the combustion and gasification zone and the gasification zone. The mass and heat balances were then solved to obtain temperature and concentration profiles for both the solid and gas phases along the reactor while the solid particles velocity was obtained using a Stokes law approximation.

Govind and Shah (1984), following a similar approach, refined the model of Wen and Chaung (1979) by including momentum balances and solving for both the solid and gas phase velocities in addition to the mass and energy balances. Both models were steady-state and parametric studies were carried out to provide a better understanding of the reactor performance for various feed conditions and the results were compared to the Texaco-pilot plant experimental data. The gas composition exiting the gasifier was found to depend on three major parameters; the fuel feed rate; the oxygen-to-fuel ratio, and the steam-to-fuel ratio. It was found that the oxygen-to-fuel ratio affected the carbon conversion more than the steam-to-fuel ratio, while the steam-to-fuel ratio significantly affected the gas composition.

Vamvuka et al. (1995) developed a one-dimensional, steady-state, entrained-flow, gasifier state model that incorporated gravimetric analysis data for a bituminous coal type. They

based their model on mass and energy balances, heterogeneous reaction rates and homogeneous gas-phase equilibria, and solved the resulting system of non-linear mixed ordinary differential-implicit algebraic equations using the modified Euler method in combination with a non-linear algebraic equation solver. Temperature, reaction rates, and composition profiles in the gasifier at operating pressures of 0.1 and 2 Mpa were then predicted at constant feed rates. They concluded that realistic conversions of carbon could not be predicted if the devolatilization reaction and the heterogeneous surface reactions between the coal and oxygen and steam were assumed to occur sequentially and showed that combustion was much faster than gasification and that a temperature maxima for both solid particles and gas occurs at the point of final consumption of oxygen while gasification proceeded only in the absence of oxygen. However, some anomalies are observed with the model; although equilibrium was assumed for the homogeneous combustion reactions, negligible oxygen is left behind at the end of the reactions. Also, it was observed that carbon monoxide; hydrogen and methane do not co-exist with oxygen and because the methanation reaction was not considered in the model, predictions of high methane composition would arise as there is no other mechanism by which methane is consumed.

In a subsequent paper, Vamvuka *et al*. (1992) carried out parametric studies to provide a better understanding of the reactor performance in terms of coal conversion, product gas composition, calorific value and temperature profiles along the reactor under various operating conditions such as feed flow rate, particle size and system pressure. In agreement with earlier studies, their results suggest that the critical parameters in gasification are the steam-to-coal and oxygen-to-coal feed ratios and the gasifier pressure. They observed that the maximum reactor temperature could be controlled by the steam-to-coal ratio but its location strongly depended on pressure. Regarding the throughput and calorific value of product gas, the authors found that the

performance of the reactor would be improved with lower steam and oxygen feed rates and higher system pressure, with higher conversion observed at higher system pressures.

Ni and Williams (1994) devised a multivariate model to study the performance of an entrained-flow gasifier. They set up their model based on equilibrium mass and energy balances and simulated a Shell type gasifier using dry pulverized coal as feed. They optimized the performance of the gasifier model using non-linear programming, obtained the equilibrium compositions, and showed the region in which the results were applicable for a given set of feedstocks. They studied the effects of coal-to-oxygen (RCO) and coal-to-steam (RCS) ratios, the temperature, and the pressure of the gasified products and steam production. Their results showed that the oxygen-to-coal ratio is the most important control variable for the gasifier operation in all cases considered in their study. They deduced that high cold gas efficiency (CGE), the efficiency of the gas when it is combusted after being cooled, could be obtained at low oxygen feed rates while keeping a stable carbon conversion. The CGE also increased with increasing temperature for any feed flow but its optimal value may not take place at the maximum temperature in the feasible region. The steam-to-coal ratio influenced gaseous product compositions but its impact on CGE and steam efficiency (SE) depended on the RCO. At high RCO values, RCS almost makes no change to CGE and SE while at very low RCO values, increasing RCS will cause CGE to rise with its maximum occurring at the boundary of the feasible region. This indicated that there was a critical RCO for control of CGE for which the RCS was sensitive. Pressure was shown to have almost no effect on the gasifier performance in the region studied.

Bearth (1996) developed a mathematical model for entrained flow coal gasification with the aim of predicting the influence of coal properties and gasification conditions on the

performance of entrained flow gasifiers operating at pressures up to 21 atm. Using correlations from a comprehensive review of literature and experimental data, he was able to predict the coal properties. He predicted coal properties through use of correlations from extensive literature sources and others developed from experimental data in the literature. He modeled the gasifier as a plug flow reactor thus neglecting any mixing or turbulence and based his model on mass and energy balances neglecting any aspect of fluid dynamics. His model sensitivity analysis indicated that errors in the calculated values of the volatile yield, carbon dioxide gasification reactivity and steam gasification may significantly affect the model predictions. In the same way, errors in the input values for gasifier wall temperatures and gasifier diameter, when affected by slagging, could also cause errors in the model predictions. However, the model predictions were comparable with the experimental gasification results for a range of atmospheric and high-pressure gasifiers. Most of the atmospheric pressure results used in their comparisons were obtained by the Commonwealth Scientific and Industrial Research Organization (CSIRO) for a range of coals and the predictions for the majority of the results were accurate over a wide range of gas feed rates. However, uncertainties existed for high pressure gasifiers due to the limited range of experimental data; although, accurate predictions were provided for the majority of available results. The model was also used to determine reaction mechanisms and optimum gasifier feed mixtures. The predictions suggested that the reactions at the particle surface occurred in a sequence; commencing with devolatilization then oxygen gasification followed by carbon dioxide and steam gasification, with some overlap between the reactions. The optimum feed conditions and maximum gasifier performance varied with changing gasifier pressure, gasifier diameter and feed coal.

Similar in some ways to previous one-dimensional gasifier model studies, a new approach to modeling the entrained gasifier is the use of the reactor network model as employed by Monaghan et al. (2010) and later adopted by Yang et al. (2011). In this approach, the gasifier is divided into different areas based on the flow characteristics in the reactor. Each area was represented by either zero-dimensional well-stirred reactors (WSRs) or one-dimensional plug flow reactors (PFRs). Monaghan et al. developed a dynamic one-dimensional reduced order model for the entrained flow gasifier that incorporated a slagging model for the slag behavior inside the gasifier.

Based on Monaghan et al. (2010)'s space division concept, Yang et al.(2011) developed a dynamic model to simulate a new type of oxygen-staged gasifier that has been recently developed in China. They simulated two types of oxygen-staged gasifiers: the refractory wall and the membrane wall gasifiers. In their study, they included a widely accepted slag layer model to simulate the time-variation slag accumulation and flow on the wall and the heat transfer process through the wall.

Recently, CFD-based models (Chen et al., 2000; Chen et al., 2001; Watanabe and Otaka, 2006) have been developed to simulate entrained flow coal gasification.

In the first part of the study by Chen et al. (2000), a comprehensive three-dimensional model of an entrained flow gasifier was developed and a series of numerical simulations were performed for a 200t/d two-stage air-blown, up-flow, entrained gasifier consisting of lower combustor and an upper reductor sections separated by a throat. They used an extended coal gas mixture fraction model with Multi-Solids Progress Variables (MSPV) to simulate the gasification reactions and mixing process. The variable off-gas from coal devolatilization, char-O_2, char-CO_2, and Char-H_2 reactions were separately tracked by using four conserved mixture

fractions. The authors used the Random Pore Model to model the heterogeneous reaction kinetics and included the influence of turbulence on the gas properties. The gas temperature generally decreased along the reactor height and was related to the gas composition such that the high CO_2 and H_2O concentrations in the combustor were responsible for the high combustor temperatures while the high CO and H_2 production in the reductor was responsible for the low reductor temperatures. The turbulent fluctuations in the volatiles and the char-oxygen reactions were shown to affect temperature and gas compositions significantly and should not be neglected in model development.

Most recently, Watanabe and Otaka (2006) developed a three-dimensional model that was aimed at evaluating and optimizing the performance of an air-blown, two-stage, entrained-flow, coal-fed gasifier. The two stages in the gasifier were the combustor and reductor stages and the simulation was performed on the CRIEPI 2 tons/day (T/D) research scale coal gasifier (Japan). Their gasification model consisted of a pyrolysis model consisting of a Heaviside type function, the char gasification model for which the Random Pore Model was used to model the reaction kinetics and a gas-phase reaction model. An initial particle size distribution of the Rossin-Rammler type was also included in the model. They studied the influence of the air ratio on gasification performance, such as the per-pass carbon conversion efficiency, amount of product char, heating value of product gas, and cold gas efficiency.

The results of the model show that the gas temperature in the combustor is much higher than that in the reductor as the air ratio in the combustor is higher than that in the reductor. A rapid decrease in temperature observed at the bottom part of the reductor was attributed to the endothermic nature of the dominant char gasification reactions. H_2 and CO concentrations

increased with increasing air ratios but with an overestimation of steam at the expense of hydrogen. In general, their results agreed well with the experimental results.

2.4.4 Conclusion of Literature Review

The studies discussed here have used a number of model formulations, varying in complexity from one-dimensional to three-dimensional, to study the gasification process. The main differences in most of them are reflected in the details of dimensions, reaction models and whether or not fluid dynamics are incorporated in the model. The CFD-based models considered the fluid dynamics with turbulence in addition to reaction model schemes but the large number of parameters does not make such models easily applicable for design related purposes and thus lower dimensional models are still useful in this regard.

However, most of the one-dimensional models discussed are steady-state in nature. In practice, the gasifier operation is dynamic in nature and thus dynamic models are required to further our understanding of the gasification process and for the dynamic response and control of such equipment.

It is therefore the objective of the current study to develop a one-dimensional transient model of the entrained GEE/Texaco type coal gasifier that solves mass momentum and energy balances. The model is similar in some ways to that of Govind and Shah (1984) in which the steady-state mass, momentum and heat balance equations are also solved. However, the model incorporates a detailed radiative energy balance model with variable view factors and no a priori wall temperature profile is assumed as in many of the models above.

The model is solved in Aspen Custom Modeler® (ACM), a simulation environment in which custom models can be built with varying levels of complexity, and is used to implement

the model. The main advantage of using ACM is the accessibility of physical properties from the Aspen database for most of the components involved during the gasification process. This makes it easier to calculate relevant component properties, using the in-built routines.

Chapter 3

Mathematical Description of the Model

3.1 Introduction

In order to develop a working mathematical model for the entrained coal gasifier, a thorough understanding of the processes, chemical kinetics, and hydrodynamics taking place is required. The process of modeling then involves the use of mathematical expressions/equations to represent these processes. These processes, which are both physical and chemical, include the exchange of mass, momentum, and energy between the gas and solid species as they flow along the gasifier. However, they are not only highly nonlinear but they also occur at very different rates and thus development of a mathematical model that can track all the time scales of the processes is very difficult. This is made more difficult by the complex nature of coal whose chemical properties are still a subject of contention. In order to obtain a tractable problem, a number of simplifying assumptions have been made in order to develop a model that is mathematically and computationally well-behaved and yet at the same time retains the major characteristics of the process.

3.2 Model Description

In the current study, a one-dimensional dynamic model is developed to simulate the GEE/Texaco down-flow type gasifier, which is operated at high temperature and pressure. A schematic of this gasifier type is shown in Figure 3.1 for which coal slurry and oxygen streams are fed with the exit syngas stream and any remaining char and slag fed to the radiant syngas cooler (RSC). The RSC cooler was modeled separately as reported in Section 4.2.1.

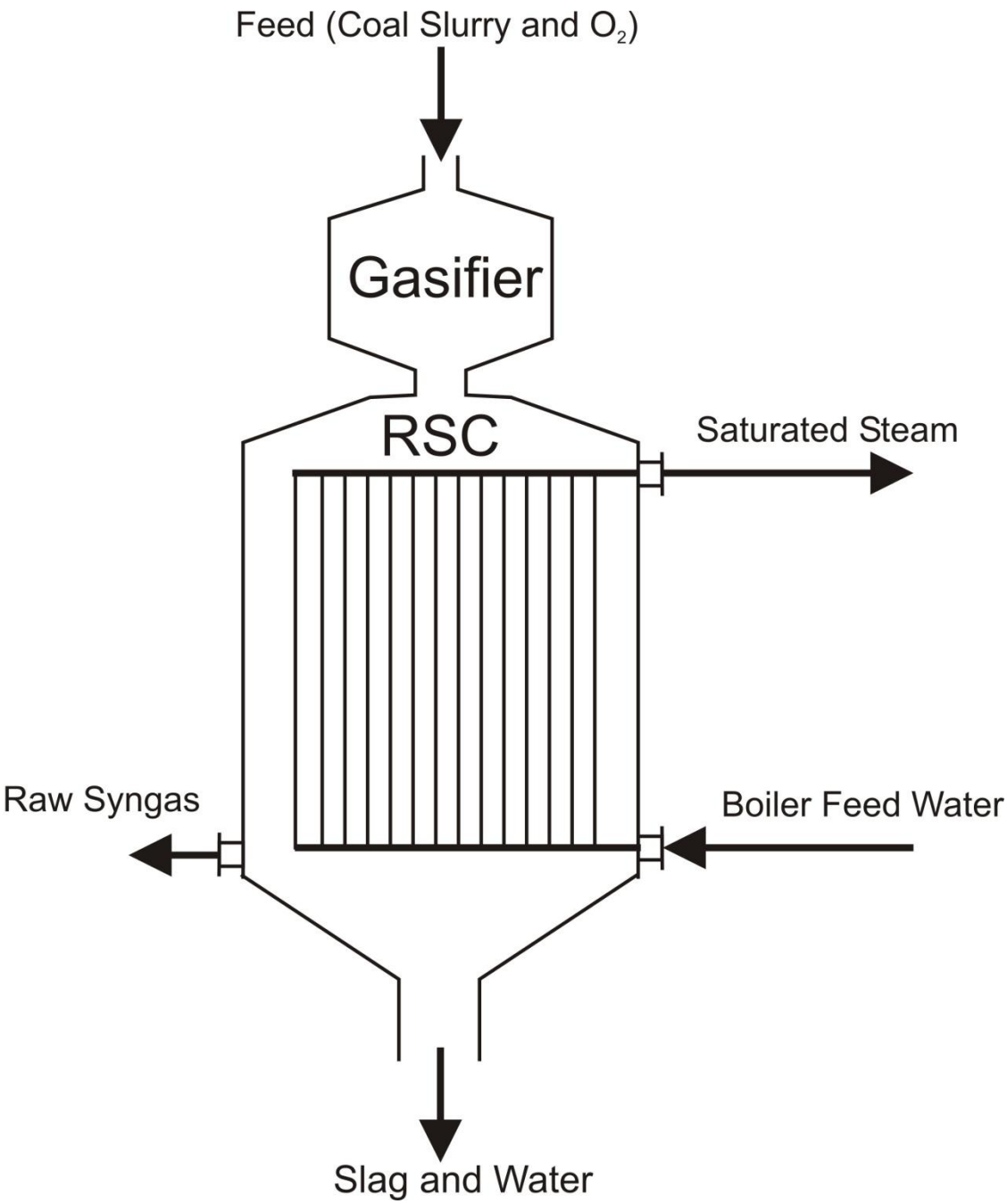

Figure 3.1: The schematic of the GEE/Texaco gasifier with RSC considered in the study.

In modeling the gasification processes inside the gasifier, unsteady-state mass, momentum and energy balance equations are written and solved based on a number of simplifying assumptions, **which** are given below.

3.2.1 Simplifying Assumptions

The basic assumptions made during the development of the current model include the following:

- The radial dispersion of mass, momentum, and energy are neglected.
- The system is assumed to be very dilute in the solid phase such that the inter-particle interactions are neglected. The ash layer formed as the coal particle reacts is assumed to remain on the particle surface and consequently the shrinking core model is assumed.
- The ideal gas equation of state is assumed to hold for the gaseous phase.
- The temperature inside the solid particle is assumed to be uniform i.e. there are no temperature gradients within the particle.
- The ash is assumed to be inert and thus its effect as a catalyst is indirectly neglected, although; this may have been implicitly accounted for when the kinetic equations were developed.
- In considering the energy balance, potential and kinetic energies of the system are considered to be negligible as compared to the thermal energy due to the very high temperatures in the gasifier.
- Furthermore, no particle attrition is considered in the model.

Any additional assumptions that were made in the model development are explicitly stated in the respective sections.

In addition, a heuristic recirculation model similar to that of Smoot and Smith,(1988) and simpler than that in Monaghan et al., (2009) is incorporated in the model to capture the mixing and recirculation phenomena that exist at the entrance region in the actual gasifier operation due to the turbulence caused by the inlet burner. Within these mixing and recirculation zones, there

is an improved energy transfer that helps in promoting the initial gasification processes of slurry-water evaporation and coal devolatilization that are modeled in the current study. Details of such burner designs may not be fully incorporated in a 1D model, and a heuristic approach, details of which appear in the appendix, was used to achieve a similar purpose.

In what follows, the governing equations for the model are introduced and briefly described.

3.2.2 Continuity and Momentum Equations:

The two-phase system in the gasifier is modeled by a two-fluid Eulerian based model. This is a continuous method in which both phases are modeled as an interpenetrating continuum. This method has been extensively used by the CFD community (MFIX, CFX, FLUENT, etc) because of its generally low computational demand. In the two-phase model, conservation equations for mass, momentum, and energy for each phase are developed and solved in conjunction with some closure constitutive equations that will be presented later. The theory and derivation of these governing equations for gas-solid systems and general transport mechanism appear in many standardized textbooks which include Bird et al., (2002), Fan and Zhu (1998), Gidaspow (1994) among others, and as a result only a brief description and derivation of the these equations is presented. The reader interested in a more comprehensive description of these equations should consult the respective texts.

A schematic of a slice of the reactor is shown in Figure 3.1 below on which the balance equations for mass, momentum and energy is carried out to obtain the governing equations.

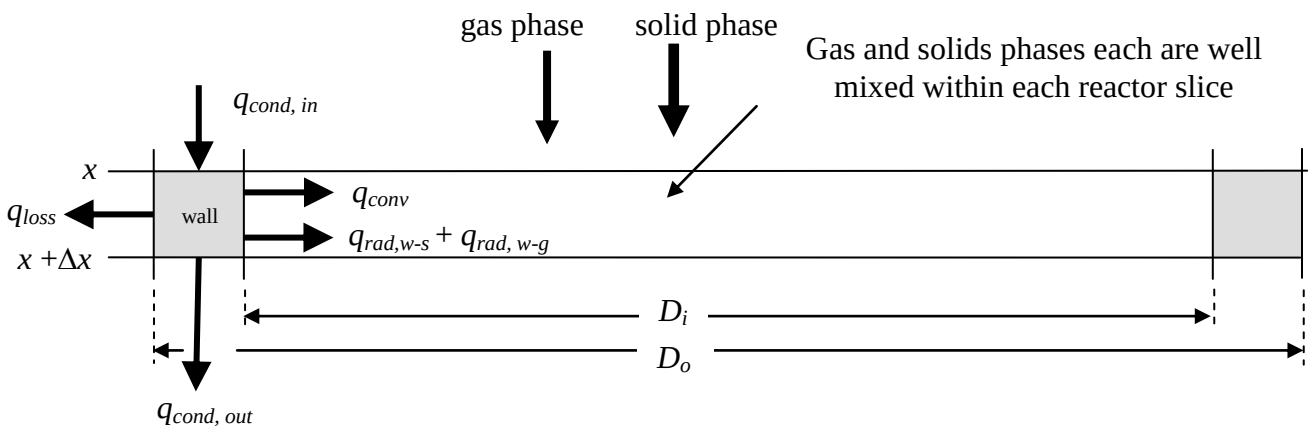

Figure 3.2 A schematic of a slice across the gasifier

3.2.2.1 Continuity Equations

The continuity equations for the solid and gas phases are obtained by carrying out a mass balance across a slice of the reactor shown in Figure 3.1 above and as a means of illustration, a balance is carried out for the solid phase as shown below:

In (flow) = Out (Flow) + Consumption (reaction) + Accumulation (3.1)

$$A_R \rho_s (1-\varepsilon) U_s \big|_x = A_R \rho_s (1-\varepsilon) U_s \big|_{x+\Delta x} + A_R \Delta x (1-\varepsilon) \Gamma_{s-g} + A_R \Delta x \frac{\partial(\rho_s (1-\varepsilon))}{\partial t} \tag{3.2}$$

such that in the limit that as $\Delta x \to 0$, we obtain

$$\frac{\partial(\rho_s (1-\varepsilon))}{\partial t} + \frac{\partial(\rho_s (1-\varepsilon) U_s)}{\partial x} = -(1-\varepsilon)\Gamma_{s-g} \tag{3.3}$$

The gas continuity equation is similarly obtained as

$$\frac{\partial(\varepsilon \rho_g)}{\partial t} + \frac{\partial(\rho_g \varepsilon U_g)}{\partial x} = (1-\varepsilon)\Gamma_{s-g} - m_{rg} + m_{mg} \tag{3.4}$$

where

$A_R = \frac{\pi}{4} D_i^2$, is the internal cross sectional area of the gasifier,

ρ_s and ρ_g are the densities of the solid and gas phases respectively,

ε, is the void fraction in the gasifier and

Γ_{s-g}, is the net rate of consumption of the solid phase (coal) by the heterogeneous reactions (g/cm^3.s), which must be specified per unit of reactor volume and is a positive quantity. The last two terms on the right hand side of Eqn. (2) account for the mass recirculated from the hotter combustion region to the colder inlet region as illustrated in the Appendix. The term, m_{rg}, represents the mass that enters a control volume (CV) while the term, m_{mg}, represents the mass that leaves a CV.

In addition to the overall mass balances for the solid and gas phases, the species involved in the reactions must be conserved and thus species balance equations are written and solved.

3.2.2.2 Species balance equations

The species balance equations are given by:

$$\frac{\partial}{\partial t}(\varepsilon\rho_g y_{gi}) + \frac{\partial}{\partial x}(\varepsilon\rho_g U_g y_{gi}) = R_{gi} - m_{rg} y_{gi} + m_{mg}\omega_{gi} \tag{3.6}$$

$$\frac{\partial}{\partial t}((1-\varepsilon)\rho_s x_{sj}) + \frac{\partial}{\partial x}(\varepsilon\rho_s U_s x_{sj}) = R_{sj} \tag{3.7}$$

where y_{gi} and x_{sj} are the mass fractions of the ith gas and j^{th} solid species participating in the homogeneous and heterogeneous chemical reactions in the reactor; R_{gi}, R_{sj} are the net rates of generation or disappearance of the given species depending on whether the species are reactants or products. As before the last two terms in Equation (3.6) relate to the mass of gas added or removed from a control volume due to the recirculation as explained in the Appendix **.

3.2.2.3 Momentum Balance Equations

The momentum balance equations for each of the phases are similarly obtained by carrying out a force balance across the slice of the reactor shown above. Although, many forces are theoretically known to be in play in such systems (Syamlal et al., 1982; Fan and Zhu, 1998), the forces considered here are: the gravitational force, the normal surface force (pressure), and the momentum transfer force between the gas and solid phases. The shear forces are neglected as well as the particle-particle forces. The equations are accordingly obtained as

$$\frac{\partial(\rho_g \varepsilon U_g)}{\partial t} + \frac{\partial\left\lfloor \varepsilon \rho_g U_g^2 \right\rfloor}{\partial x} = -\varepsilon \frac{\partial P_t}{\partial x} + \varepsilon \rho_g g - (1-\varepsilon) f_s \tag{3.8}$$

$$\frac{\partial(\rho_s (1-\varepsilon) U_s)}{\partial t} + \frac{\partial\left\lfloor (1-\varepsilon) \rho_s U_s^2 \right\rfloor}{\partial x} = -(1-\varepsilon) \frac{\partial P_t}{\partial x} + (1-\varepsilon) \rho_s g + (1-\varepsilon) f_s \tag{3.9}$$

where, the first term on the left represents the net rate of momentum increase while the second term represents the net rate of momentum transfer by convection. The first and the second term on the right hand side are related to the buoyancy and the gravitational forces respectively. The third term is the interaction force representing the momentum transfer between the fluid and solid phases, i.e. f_s is the drag force per unit volume of particles. It should be said that in another formulation, the pressure gradient term is modeled differently from the current model in such a way that the voidage term is inside the pressure gradient, i.e., a pressure gradient is included in each phase. U_s and U_g are the solid and gas phase velocities and P_t is the total pressure in the system, taken to be the same as the gas phase temperature.

3.2.3 Energy Balance Equations

In the gasifier, the temperatures of the solid particles, gas, and the gasifier wall are different. This is due to the difference in the distribution of thermal energy between the solid particles, gas, and the reactor wall, which in turn depends on the heat transfer processes that vary along the reactor. These heat transfer processes are important to the progress of the gasification process, for example, the heating of gas and solid on entering the hot gasifier and the loss of heat from the gas and solids to the wall as they move along the gasifier.

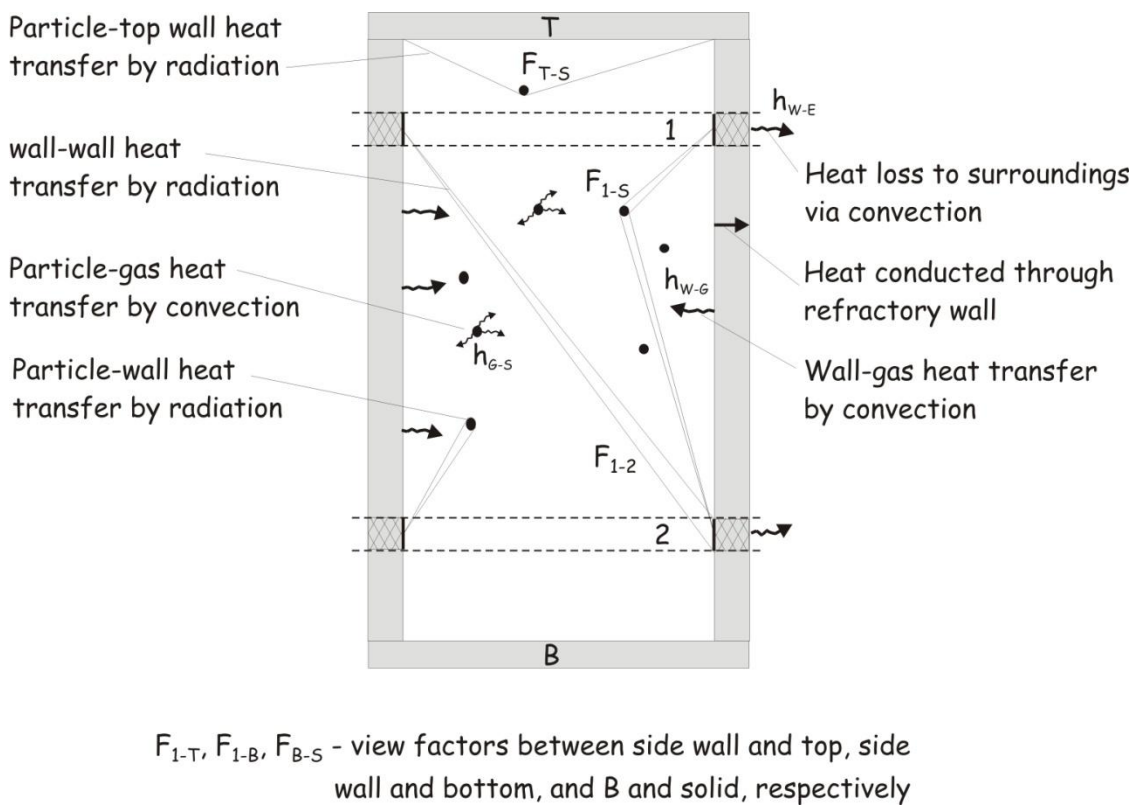

Figure 3.3: An idealized gasifier model showing heat transfer interactions considered in the current energy balance model.

These energy/heat interactions occur by the standard heat transfer processes namely; conduction (thermal diffusion), convection, and radiation as illustrated in Figure 3.3. It is

common to assume that these processes are fully independent with no cross-influences (Bearth, 1996); although, in reality, some inter-relations can exist. Because the temperatures are usually high during gasification, the heat transfer by conduction can be neglected while that due to convection tends to be significant in cooler parts of the gasifier. As a result, many studies have considered radiation and convection as the major heat transfer processes.

The energy balance equations for the system are obtained by carrying out an energy balance on the reactor wall and across the slice of the gasifier for the gas and solid phases as shown in Figure 3.1.

3.2.3.1 Overall Energy Balance on Reactor Wall

In order to model the transient behavior of the reactor, it is necessary to complete an energy balance that incorporates the wall of the reactor. Various heat transfer mechanisms take place inside the gasifier and some of the major heat transfer mechanisms between the various surfaces of the gasifier and the gas and solid phases are shown in an idealized representation of Figure 3.3. For this 1-D unsteady-state model, it is assumed that heat loss from the reactor wall can be modeled using an effective heat transfer coefficient, h_{eff}. The energy balance across the wall can be written as:

In (conduction) = Out (conduction, convection, radiation + losses) + Accumulation

$$A_W q_{cond}\big|_x = A_W q_{cond}\big|_{x+\Delta x} + \pi D_i \Delta x\left[q_{conv} + q_{rad,w-s} + q_{rad,w-g}\right] + \pi D_o \Delta x q_{loss} + A_w \Delta x \rho_w c_{p,w}\frac{\partial T_w}{\partial t}$$

By rearrangement we get

$$\frac{\partial q_{cond}}{\partial x} = -\frac{4D_i}{D_o^2 - D_i^2}\left[q_{conv} + q_{rad,w-s} + q_{rad,w-g}\right] - \frac{4D_o}{D_o^2 - D_i^2} q_{loss} - \rho_w c_{p,w}\frac{\partial T_w}{\partial t} \qquad (3.10)$$

where

$$q_{cond} = -k\frac{\partial T_w}{\partial x},\ q_{conv} = h_{w-g}(T_w - T_g),\ q_{loss} = h_{eff}(T_w - T_{surr}),\ q_{rad,w-s} = F_{w-s}\sigma(T_w^4 - T_s^4)$$
$$q_{rad,w-g} = e_g F_{w-g}\sigma(T_w^4 - T_g^4) \tag{3.11}$$

T_w, T_s, T_g, and T_{surr}, are the wall, solid, gas, and surrounding temperatures, respectively. F_{w-g}, and F_{w-s} are the view factors (shape factors) representing the fraction of radiation emitted by the wall that is directly intercepted by the gas solid respectively and h_{w-g} is the convective heat transfer coefficient between gas and wall. Finally, e_g is the emissivity of the gas phase.

3.2.3.2 Gas and Solid Phase Energy Balance

In a similar manner, the solid and gas phase energy balance equations were obtained from:

In (flow) + In (radiation from wall) + In (convection from wall) = Out (flow) + Out (radiation to solids) + Out (convection to solids) + Consumption (heat consumed in gas-phase reactions) + Accumulation

Giving the equations as:

$$\frac{\partial\left\lfloor \varepsilon\rho_g C_{p,g} T_g \right\rfloor}{\partial t} + \frac{\partial(U_g \varepsilon\rho_g C_{p,g} T_g)}{\partial x} = \frac{\pi D_i}{A_R}\left\{e_g F_{w-g}\sigma\left[T_w^4 - T_g^4\right] + h_{w-g}\left[T_w - T_g\right]\right\}$$
$$-(1-\varepsilon)\frac{6}{d_p}\left\{e_g F_{g-s}\sigma(T_g^4 - T_s^4) + h_{g-s}(T_g - T_s)\right\} + \sum_{j}^{\text{gas-phase reactions}} \varepsilon\left(-\Delta H_j\right) r_j \tag{3.12}$$

$$\frac{\partial\lfloor(1-\varepsilon)\rho_s C_{p,s}T_s\rfloor}{\partial t}+\frac{\partial\lfloor U_s(1-\varepsilon)\rho_s C_{p,s}T_s\rfloor}{\partial x}=\frac{\pi D_i}{A_R}F_{w-s}\sigma\left[T_w^4-T_s^4\right]$$
$$+(1-\varepsilon)\frac{6}{d_p}\left\{e_g F_{g-s}\sigma\left[T_g^4-T_s^4\right]+h_{g-s}\left[T_g-T_s\right]\right\}+\sum_{k}^{\text{solid-phase reactions}}(1-\varepsilon)\left(-\Delta H_k\right)r_k \tag{3.13}$$

where, the $6/d_p$ term is the ratio of the surface area of a particle to its volume. It is further assumed that all reaction rates, r_k are specified per unit volume of the reactor and hence the fraction of gas, ε, in the reactor is used as a multiplier for this term. Note that the view factors, $F_{g\text{-}s}$ and $F_{w\text{-}g}$ used in the radiation terms must correctly account for the change in area between the emitting and receiving body.

In order to successfully apply the above balance equations to the solution of physical processes, several closure relations including the reaction kinetics must to be determined.

3.2.4 Closure Laws

A number of constitutive relations that are either fundamentally represented or empirically established are needed to describe certain variables that appear in the above conservation equations and are briefly described below.

3.2.4.1 Fluid Phase Density

The gas phase can be modeled as a compressible gas obeying an ideal gas equation of state (EOS):

$$P_g=\frac{RT_g}{V_g} \tag{3.14}$$

Thus, the gas phase density is calculated from the following equation:

$$\frac{1}{\rho_g} = \frac{RT_g}{P_g} \sum_{i=1}^{N} (x_i / MW_i) \tag{3.15}$$

where, x_i and MW_i are the mass fraction and molar weight of the ith gaseous species, respectively and N is the total number of gaseous species. P_g, the gas phase pressure can be assumed to be equal to the total pressure P_t since the gasifier is dilute in solid particles.

3.2.4.2 Drag Coefficient

The momentum transfer between the gas and solid phase represented by the drag force per unit volume, f_s in the momentum balance equations can be obtained experimentally from pressure drop measurements and a number of correlations have been developed for the drag coefficient. Some of these correlations were summarized by Benyahia et al. (2005). The correlation used in the current study is given by Arastroopour and Gidaspow (1979) as:

$$f_s = \frac{3C_D \rho_g \varepsilon^{-2.65} \left[U_g - U_s \right]^2}{4d_p} \tag{3.16}$$

where the drag coefficient, C_D, is given by Rowe and Henwood (1961) as:

$$C_D = \begin{cases} \frac{24}{Re}\left[1 + 0.15 Re^{0.687}\right], & Re < 1{,}000 \\ 0.44 & Re \geq 1{,}000 \end{cases} \tag{3.17}$$

The particle Reynolds number, Re is given by

$$\mathrm{Re} = \varepsilon \rho_g d_p \frac{|U_g - U_s|}{\mu_g} \tag{3.18}$$

where d_p and μ_g are the particle diameter and dynamic viscosity of the gas phase respectively.

3.2.4.3 Interphase Heat Transfer

The energy balances above considered conductive, convective, and radiative heat transfer mechanisms between the solid, gas and the inner gasifier walls as well as the convective heat loss from the outside gasifier wall to the surroundings.

Heat transfer by conduction is a fairly well known and easier process to model. It is the molecular transfer of energy between two surfaces in contact. The set of information needed to model this process, as defined in the above equations, is the thermal conductivity of the solid particles and the gasifier wall refractories.

The heat transfer by convection is rather a difficult process to model analytically due to the complex flow patterns. However, empirical correlations have been found that approximate the process of heat transfer between the gas and both the gasifier wall and the solid particles, which are assumed to be spherical in shape. These correlations appear in the form of the convective heat transfer coefficients. The Ranz-Marshall correlation given by eqn. 3.19 is used to model the convective heat transfer:

$$Nu = 2.0 + 0.6\,\mathrm{Re}^{1/2}\,\mathrm{Pr}^{1/3}, \tag{3.19}$$

where, *Nu*, *Re*, *Pr* are the dimensionless Nusselt number, particle Reynolds number, and Prandtl number, respectively. Because the coal particles are usually very small, the Reynolds number, Re, can be neglected and as a consequence, the Nusselt number is assumed to be 2.

On the other hand, heat transfer by radiation in the gasifier is very complicated and more challenging to model compared to the previous two mechanisms. The presence of emissive gases in the gasifier namely CO_2 and H_2O complicates the process as they interfere with radiation

transfer between the wall and solid particles. These gases can absorb, emit or transmit radiation and in addition, their emissivity depends on the temperature, pressure and the gas composition of the system as well as the width or other characteristic length, L of the enclosure (Themelis, 1995). For solid particles and the wall, the emissive properties are independent of temperature and not significantly affected by pressure (Liu et al. 2000). In addition, view factors are required to compute the radiative heat flux from and to each of the surfaces involved.

3.2.4.4 Radiation view factors

The various view factors that appear in the energy balance equations described above are calculated using formulae shown in Table 3.1, which were adapted from Siegel and Howell, (1981).

Table 3.1: The view factors with their corresponding calculation formulae

View factor	Formula used for calculation
F_{T-S}	$\frac{1}{2}\left((2+(z_{TS}/Ri)^2) - \sqrt{((2+(z_{TS}/Ri)^2)^2 - 4)} \right)$
F_{B-S}	$\frac{1}{2}\left(\left(2+(z_{BS}/Ri)^2\right) - \sqrt{\left(\left(2+(z_{BS}/Ri)^2\right)^2 - 4\right)} \right)$
F_{1-2}	$1-\left(1-\left(2(z_{12}/Di)^3 + 3(z_{12}/Di)\right) \Big/ \left(2(z_{12}/Di)^2+1\right)^{1.5} \right) dz$
F_{1-T}, F_{1-B},	$((z_{1T}/Di)^2 + 0.5) \Big/ \sqrt{(z_{1T}/Di)^2+1} \; - \; z_{1T}/Di$
F_{1-S}	$((z_{1S}/Di)^2 + 0.5) \Big/ \sqrt{(z_{1S}/Di)^2+1} \; - \; z_{1S}/Di$

As mentioned, these view factors vary along the length of the gasifer. For example the view factors between a cylindrical wall surface of the gasifier control volume with the top (F_{1-T}) and bottom (F_{1-B}) ends of the gasifier are shown in Figure 3.4.

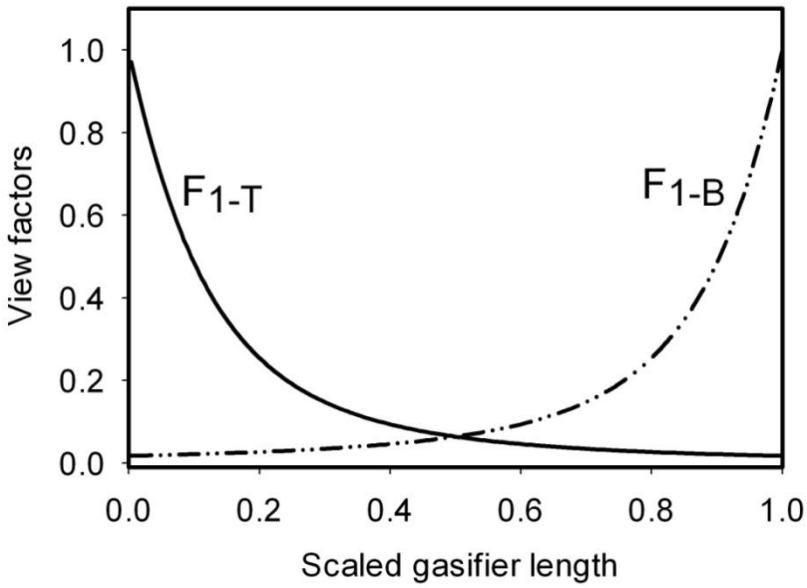

Figure 3.4: Sample view factors

The gasifier length can either be uniformly discretized into *n* control volumes of fixed length Δz or can have multiple sections each of a specified discretization spacing for example regions of steep gradients may have finer grid than those with mild gradient. At any given control volume (*i*), the mechanisms of heat transfer between gas-solid, side wall-top end (*T*), particles-side wall, particles-bottom end (*B*), etc., as shown in Figure 3.3, are considered. The radiation view factors between the various radiating surfaces, some of which are shown in Figure 3.3, are appropriately calculated with formulas shown in Table 3.1. Nevertheless, some simplifying assumptions are made to ensure a numerically tractable solution and these include the following:

- The gas phase was assumed to be transparent to the radiation from the wall temperature.

- The solid particles were assumed to be uniformly dispersed over the circular cross-section to aid in the calculation of view factors between solids and wall surfaces.
- The top and bottom ends of the gasifier were assumed to be flat circular surfaces and they see each other.
- The view factors between the gas and solid were assumed to be constant. The emissivities of the wall and solids were assumed to be constant with values of 0.78 and 0.9 respectively.

3.2.5 Reaction Kinetics

The mass and energy balance equations above(Equations 3.6, 3.7, 3.12, and 3.13) contain terms involving the rate of formation or consumption of the chemical species taking place in the gasifier reactions, and therefore, in order to close the mass balance equations, the reaction rates of the devolatilization, heterogeneous and homogeneous reactions need to be specified.

3.2.5.1 Devolatilization Reaction Kinetics

The evolution of volatile matter from solid fuels leads to a series of reactions during combustion and gasification, thus, a good model for the devolatilization process is essential for any reasonable modeling and simulation of combustion or gasification equipment (de Souza-Santos, 2004).

The various models that have been used were described in the literature review. In the current study, we use the devolatilization model developed by Syamlal et al., (1992). They used a phenomenological model that preserves a strict elemental balance to determine the stoichiometry of the volatile gas components. The model is based on data from certain lab-scale experiments that characterize the coal such as the ultimate and proximate analysis of the coal,

among others. In their model, the devolatilization process is modeled as a series of three different processes namely drying, devolatilization and tar cracking.

Drying:

$$\text{Moisture(coal)} \rightarrow H_2O \tag{3.20}$$

Devolatilization:

$$VM \rightarrow \alpha_d Tar + \beta_d^{CO} CO + \beta_d^{CO_2} CO_2 + \beta_d^{CH_4} CH_4 + \beta_d^{H_2} H_2 + \beta_d^{H_2O} H_2O \tag{3.21}$$

Tar cracking:

$$Tar \rightarrow \alpha_c FC + \beta_c^{CO} CO + \beta_c^{C_2O} CO2 + \beta_c^{CH_4} CH_4 + \beta_c^{H_2} H_2 + \beta_c^{H_2O} H_2O \tag{3.22}$$

where *VM* is the volatile matter obtained from the proximate analysis of the coal. However, because the entrained gasifier operates at relatively high temperatures, the tar cracking reaction is modeled as an instantaneous reaction. The kinetic parameters of the above reactions are given in the appendix. In the current study, the tar cracking reaction was considered to take place instantaneously and thus these kinetics were neglected. In addition, the higher molecular weight hydrocarbons that are released through the devolatilization and tar cracking reactions were partially lumped into the methane species.

3.2.5.2 Heterogeneous Reactions Kinetics

The four gasification reactions considered in most gasification studies, as well as in the current study, are:

Char combustion: $$2C + \frac{1}{\phi} O_2 \rightarrow \left(2 - \frac{2}{\phi}\right) CO + \left(\frac{2}{\phi} - 1\right) CO_2 \tag{3.23}$$

Steam gasification reaction: $$C + H_2O \leftrightarrow CO + H_2 \tag{3.24}$$

CO_2 gasification: $$C + CO_2 \leftrightarrow 2CO \tag{3.25}$$

H_2 gasification: $$C + 2H_2 \leftrightarrow CH_4 \tag{3.26}$$

In the above representation, only the main products are assumed; although in general, more than a single product is realized from each of the gasification reactions as shown in the detailed representation of Chapter 2. In particular, the char-combustion reaction, Equation (3.23), gives both CO_2 and CO as the main products whose ratio was reported to vary markedly with temperature of the reaction, with carbon monoxide favored at higher temperatures and carbon dioxide favored at lower temperatures (Tognotti et al., 1991).

The role played by char reactivity in these reactions is not trivial because a combination of chemical and physical processes occurring under the intense conditions of the entrained gasifier influences the conversion rate of coal char. These processes include diffusion of gas to the surface of the char particle and through the pores of the particle, surface reaction and diffusion of the products away from the reaction sites, which in turn can be related to the resulting changes in the pore structure and sometimes to the char composition resulting from the gasification of the carbonaceous material (Roberts and Harris, 2006). The rate of char conversion can be influenced by a range of factors including process conditions (temperature, heating rate, and pressure); char reactant properties, such as particle size, morphology and composition and gasifying environment (product composition) among others. It has been shown that the gasification of char by any of carbon dioxide, steam, or hydrogen is affected by the presence of carbon monoxide and the other gasifying gases. For example, Mann et al., (2004) showed the char-steam gasification is inhibited by CO and H_2 and enhanced by CO_2. The work of Luo et al., (2000) revealed the char reactivity dependencies on the pyrolysis conditions.

The char gasification reactions have been extensively studied, but many of these experiments were carried out at relatively low temperatures and at atmospheric pressure such that the results from such studies may not be appropriate for direct application to entrained gasification process. Although, considerable work has since been directed towards studying char gasification at elevated temperatures and pressures close to those in entrained gasifiers (Harris and Roberts, 2004;, Liu et al., 2006), in general, it is hard to replicate the harsh conditions in the entrained gasifiers.

In addition, there seem to be a wide variation in the available char gasification kinetic models such that selection of the appropriate model for a given study is itself a modeling problem. These variations are attributed in part to the different techniques or methods employed in the various studies and the experimental conditions. Many such studies have been carried out using equipment such as thermo-gravimetric analyzers (TGA), fixed beds, and drop tube reactors, among others. Each type of equipment has its own limitations for example the mass transfer in an entrained flow gasifier is very different from that in a cell of a TGA and the heating rate in a TGA is several orders of magnitude lower than in an entrained gasifier (Liu et al., 2006).

The nth-order power law is one of the common approaches used in modeling the char reaction rates. In this approach, a simple Arrhenius expression with a partial pressure term for each of the gasifying agent is used and represented as:

$$\mathrm{Rate_i} = A\exp(-E/RT).P_i^n \tag{3.27}$$

The temperature dependence is expressed by the activation energy. However, this simple nth-order approach does not account for the independent influences of intrinsic chemistry, transport, pore evolution, and deactivation and as such, cannot remain accurate over a broad domain of

operating conditions. There are also problems associated with the fractional pressure orders. In general, these expressions have been applied successfully to low pressure studies without an inhibitant.

Another approach in modeling char gasification reactions has been the use of Langmuir-Hinshelwood type rate expressions of varying complexities. They have gained increasing applicability and have been used in many studies (Muhlen et al., 1985; Liu et al., 2000; Roberts and Harris, 2000). These are multiple reactant exponential expressions with experimentally determined exponential constants and activation energies. They are an improvement over the simple Arrhenius expression as, in addition to accounting for the temperature and pressure dependencies, they also account for inhibitions from other gasifying agents and are applicable to a wider range of operating conditions. However, there is an excessive degree of variability in the number of terms included as well as the experimental values of the *k* terms in these expressions. This can be attributed to the fact that some of these expressions were developed when researchers considered only reacting gas pairs such as carbon dioxide-carbon monoxide, steam-hydrogen, in contrast, only a few workers considered reaction rates in gas mixtures containing all species, in addition to different conditions such as low/high pressures or temperatures (Mann et al., 2004; Muhlen et al. 1985; Liu et al., 2000; Roberts and Harris, 2000). The major limitation of these types of rate expressions is the relatively large number of experimentally determined constants (as high as 24, for example see Bearth, 1995) that means the values for the different constants are not unique and extrapolation outside the range of experimental conditions is dangerous. Moreover, a large amount of experimental data, over a wide range of conditions, is needed to ensure suitability and accuracy of expression constants (Bearth, 1996).

The shrinking-core model (Wen ,1968; Levenspiel, 1972; Doraiswamy and Sharma, 1984) adopted in the current study is one of the most widely used (Wen and Chaung, 1979; Govind and Shah,1984; Choi et al., 2001; Deng et al. 2008) structural (phenomenological) models developed to explain the kinetics of non-catalytic heterogeneous char gasification reactions. It is also known as the sharp-interface model because the reaction is assumed to take place at a sharp interface between the exhausted outer shell and the unreacted core of the solid. In this model, it is assumed that the particle is a nonporous, spherical solid whose size remains constant but as it reacts with the gaseous reactants, the unreacted core shrinks in size leaving behind a porous ash layer.

In its formulation, it is also assumed that the temperature is uniform throughout the particle. This solid-gas model considers three types of resistances that the reacting gas *A*, encounters; diffusion through the gas film surrounding the particle, diffusion through the ash layer, and the chemical reaction at the surface of the solid. According to this model, the overall reaction rate, can then be written as:

$$R_A = k_{overall}.(P_i - P_i^*) \tag{3.28}$$

$$k_{overall} = \frac{1}{\frac{1}{k_{diff}} + \frac{1}{k_{ash}}\left(1 - \frac{1}{Y}\right) + \frac{1}{k_s Y^2}} \tag{3.29}$$

where,

$Y = \frac{r_c}{R}$; r_c is the radius of the unreacted core and *R* the original size of the particle,

k_{diff}, k_{ash}, k_s are the gas film diffusion coefficient, ash diffusion coefficient, and the surface reaction constants respectively all in (*g/cm*^{2} *atm s*). The ash diffusion constant is obtained by the following correlation (Syamlal *et al.* (1992);

$k_{ash} = k_{diff}(\varepsilon_{ash}^{2.5})$; ε_{ash} is the voidage of the ash layer.

$P_i - P_i^*$, is the effective partial pressure of the ith-component in the gas (O_2, H_2, H_2O or CO_2) participating in the gasification reactions and takes into account the reverse reaction effect where P_i is the partial pressure of ith-component in the gas. The kinetic parameters for each of the gasification reactions are given in Table 3.2.

Table 3.2: Solid phase reactions kinetic parameters (Wen and Chaung, 1979)

Reaction/ Stoichiometry	Reaction Parameters
$2C + \frac{1}{\phi}O_2 \rightarrow \left(2 - \frac{2}{\phi}\right)CO + \left(\frac{2}{\phi} - 1\right)CO_2$	$K_{diff} = 0.292\phi\left(\frac{4.26}{T_\infty}\right)\left(\frac{T_\infty}{1800}\right)^{1.75} / (P_t d_p)$, $K_r = 8710\exp(-17967/T_s)$, $P_i - P_i^* = P_{O_2}$ $K_{ash} = K_{diff}\varepsilon^{2.5}$
$C + H_2O \leftrightarrow CO + H_2$	$K_{diff} = 0.001\left(\frac{T}{2000}\right)^{0.75} / \left(P_t d_p\right)$ $K_r = 247\exp(-21060/T_s)$ $P_i - P_i^* = P_{H_2O} - \frac{P_{H_2} - P_{CO}}{\exp(17.644 - 16811/T_s)}$
$C + CO_2 \leftrightarrow 2CO$	$K_{diff} = 7.45e-4\left(\frac{T}{2000}\right)^{0.75} / (P_t d_p)$, $P_i - P_i^* = P_{CO_2}$ $K_r = 247\exp(-21060/T_s)$,
$C + 2H_2 \leftrightarrow CH_4$	$K_{diff} = 1.33e-3\left(\frac{T}{2000}\right)^{0.75} / (P_t d_p)$, $P_i - P_i^* = P_{H_2} - \sqrt{P_{CH4}/K_{eq}}$ $K_r = 0.12\exp(-17921/T_s)$,

In the char-combustion reaction, ϕ is a mechanism factor that gives the ratio of CO_2 to CO in the reaction products. It is roughly estimated by the following equations (Wen and Dutta, 1979):

$$\phi = (2Z+2)/(Z+2) \text{ for } d_p \le 0.005\text{cm}$$

$$\phi = \left[(2Z+2) - Z(d_p - 0.005)/0.095\right]/(Z+2) \text{ for } 0.005\text{cm} \le d_p \le 0.1\text{cm} \tag{3.30}$$

$$\phi = 1.0 \text{ for } d_p > 0.1\text{cm}$$

where,

$$Z = [\text{CO}]/[\text{CO}_2] = 2500\exp(-6249/T);\ d_p \text{ in cm and } T = (T_s + T_g)/2 \text{ in K} \tag{3.31}$$

Other related kinetic parameters in the above relations are obtainable from (Wen and Chaung, 1979).

3.2.5.3 Homogeneous Reactions Kinetics

As mentioned previously, a number of homogeneous reactions are possible in the gasifier but the current study is limited to the following set of homogeneous reactions:

$$CO + 1/2O_2 \longrightarrow CO_2 \tag{3.32}$$

$$CH_4 + 2O_2 \longrightarrow CO_2 + 2H_2O \tag{3.33}$$

$$H_2 + 1/2\,O_2 \longrightarrow H_2O \tag{3.34}$$

$$CO + H_2O \longleftrightarrow CO_2 + H_2 \tag{3.35}$$

$$CO + 3H_2 \longleftrightarrow CH_4 + H_2O \tag{3.36}$$

$$CH_4 + H_2O \longrightarrow CO + 3H_2 \tag{3.37}$$

$$1/2N_2 + 3/2H_2 \longrightarrow NH_3 \tag{3.38}$$

$$NH_3 \longrightarrow 1/2N_2 + 3/2H_2 \tag{3.39}$$

In the early stages of gasification when the concentration of oxygen is still high, the combustion reactions dominate due to the rapid reaction of oxygen with the reactive volatile

gases. The water-gas shift reaction is considered the most important reaction among the equilibrium reactions as it determines the composition of the product gases. It also determines the ratio of carbon monoxide to hydrogen in the syngas product. On the other hand, at high pressures, the methanation reaction (3.36) becomes more important as it produces methane, a more desired product in hydrogasifiers.

Table 3.3 Gaseous reactions kinetic parameters

Reaction	**Rate/kinetic parameters**
$CO + \frac{1}{2}O_2 \xrightarrow{k_4} CO_2$	$\text{Rate} = 3.98e14 \exp(-40,000/RT_g)\varepsilon C_{O_2}^{0.25} C_{CO} C_{H_2O}^{0.5}$ [Westbrook & Dryer,(1981)]
$CH_4 + 2O_2 \xrightarrow{k_5} CO_2 + 2H_2O$	$\text{Rate} = 6.7e12 \exp(-48,400/RT_g)\varepsilon C_{O_2}^{1.3} C_{CH_4}$ [Westbrook & Dryer,(1981)]
$H_2 + \frac{1}{2}O_2 \xrightarrow{k_6} H_2O$	$\text{Rate} = 1.08e6 \exp(-30,000/RT_g)\varepsilon C_{O_2} C_{H_2}$ [Peters,(1979)]
$CO + H_2O \xrightleftharpoons{Keq} CO_2 + H_2$	$\text{Rate} = 2.877e10\, w_{g3} f_3 P^{(0.5-P/250)} \exp(-27760/RT_g) \cdot$ $(x_{CO}x_{H_2O} - x_{CO_2}x_{H_2} / Keq)$ [Wen et al.(1982)]
$CH_4 + H_2O \underset{k_b}{\overset{k_f}{\rightleftharpoons}} CO + 3H_2$	$\text{Rate} = 3.00e8 \exp(-15105/T_g) C_{CH_4} C_{H_2O}$ [Wen and Chaung,(1979)]
$\frac{1}{2}N_2 + \frac{3}{2}H_2 \underset{k_b}{\overset{k_f}{\rightleftharpoons}} NH_3$	$k_f = 1053,\ E_{a,f} = 5970$ $k_b = 46607, E_{a,b} = 11225$ [Fredrichs & Wagner,(2000)]

The kinetics of these homogeneous reactions have been studied for a long time (Jones and Lindstedt, 1988); Westbrook and Dryer, 1988). The chemistry is described by simple global reaction kinetics of the form:

$$\text{Rate} = A_i T_g^n \exp(-\frac{E_i}{RT_g})[X]^a[Y]^b \tag{3.40}$$

where A_i is the frequency factor, T_g is the gas temperature, E_i is the activation energy, a and b are the global reaction exponents for the species X and Y participating in the homogeneous reactions, n is the temperature order assumed to be zero for most reactions. The kinetic parameters used for the above reactions are given in Table 3.3

The kinetics for the water-gas shift reaction (WGS) were modeled as a combination of a catalytic rate (Wen et al., 1982) and a non-catalytic rate (Karan et al., 1999). The latter was in a slightly modified form suggested by Karan et al. (1999).

3.3.0 Solution Methodology

The above system of time-dependent partial differential and algebraic equations was solved in Aspen Custom Modeler® using the well-known method of lines approach; whereby, the PDEs in the spartial domain are discretized using a first order backward finite difference scheme and the resulting differential algebraic equations (DAEs) are then integrated over time using a dynamic integrator. A steady-state solution was obtained first by neglecting the transient terms in the model equations. The steady state solution was then used as a starting point for obtaining the dynamic model solution. A Newton-based solver is used for solving the equations and the variable step Gear's integrator was used when obtaining the dynamic solution.

3.3.1 Solution approach

The process is broadly divided into two major stages, the first involves obtaining a steady-state model and the second stage involves an extension of the steady-state model to obtain the dynamic model solution.

A very good initial guess was necessary in order to obtain a converged solution of the model. This was achieved by solving the model through a number of steps, starting with a fairly

simple model to which details are gradually added until a dynamic solution is obtained. These steps are described below:

a) The first step was to solve a simplified isothermal model with no chemical reactions in the system. This was essentially equivalent to solving overall mass and momentum equations for the gas and solid phases flowing in the reactor/gasifier for which the unknowns were the pressure, voidage, solid and gas velocities. The momentum transfer is thus the main process between the two phases.

b) Following this step the introduction of simplified chemical reactions was implemented to the model before a full kinetic model involving devolatilization, and other gasification reactions defined in the earlier chapters. This has been completed successfully.

c) With a fully defined kinetic model, mass and momentum equations are then solved in which the unknowns are the phase species mass fractions, pressure, voidage and densities.

d) The final step in accomplishing the first stage is adapting the model for nonisothermal conditions and thus, incorporation of energy balances.

Finally, the fully detailed model with all the major desired components is solved for four different coal types whose properties are shown in Table 3.4

Table 3.4: Proximate .and ultimate analysis (as received) of the various coal feeds

	Proximate				Ultimate				
Coal	Moisture	VM	FC	Ash	C	H	O	N	S
Pitt #8	1.00	33.52	57.69	7.79	76.83	5.49	6.03	1.40	1.46
Illinois #6	11.12	34.70	44.19	9.99	63.75	4.50	6.88	1.25	2.51
PRB	17.89	36.24	40.27	5.60	58.37	3.85	13.20	0.80	0.29
Lignite	14.20	43.40	41.40	1.00	62.07	4.49	17.55	0.68	0.08

Table 3.5 gives some additional model input parameters that were selected to closely match the feed conditions in the IGCC study of Bhattacharrya et al. (2011) and correspond to the feed conditions given in a U.S. Department of Energy report (TECO, Final Technical Report; 2002) on the Tampa Electric Company (TECO) gasifier. The results are then compared to the TECO data and to other results in the literature.

The feed conditions (Table 3.5) to the gasifier indicate that the slurry make-up water enters the gasifier in the liquid state and that this water must be evaporated from the coal before any gasification can take place. Other model parameters such as the heat capacities for the solid and gas phases are obtained from the METC Gasifier Advanced Simulation (MGAS) model (Syamlal and Bissett, (1992)). The wall thermal properties including the thickness of the refractory, insulation, and outer steel layers are obtained from Monaghan et al. (2009). A schematic diagram of the GEE/Texaco gasifier including the radiant syngas cooler was shown in Figure 3.1.

Table 3.5: Additional sample model parameters and input conditions used in the simulation

Parameter	*Value*
Gasifier length (cm)	350
Gasifier inside diameter (cm)	152
Particle diameter (µm)	100
Emissivity of gas, particle	0.9
Emissivity of wall	0.78
Gas-wall heat transfer coefficient (kcal/hr.m^2.^{o}C)	122
Input condition	
Gasifier pressure (atm)	54
Coal feed rate (g/s)	60000
Particle diameter (µm)	100
All feed temperature (K)	303
Oxidant composition	95% O_2, 5% N_2

Chapter 4

Steady-State Results and Discussion

4.1 Introduction

In this section results from the steady-state and dynamic models outlined previously are presented. These results broadly include the validation results, profiles of the key model variables along the length of the gasifier, sensitivity or parametric study results that evaluated the effect of changing key model parameters and the dynamic responses of model variables as the feed conditions were changed. The change in feed conditions may include change in coal type, flow rates and inlet stream temperatures among others.

4.2 Steady-State Results

The steady-state results were obtained by neglecting the temporal or accumulation terms of the mass, momentum and energy balance equations. This resulted in a system of ordinary differential equations (ODEs) for example; the gas continuity equation is changed from

$$\frac{\partial(\rho_s(1-\varepsilon))}{\partial t}+\frac{\partial(\rho_s(1-\varepsilon)U_s)}{\partial x}=-(1-\varepsilon)\Gamma_{s-g} \tag{3.3}$$

to

$$\frac{d(\rho_s(1-\varepsilon)U_s)}{dx}=-(1-\varepsilon)\Gamma_{s-g} \tag{4.1}$$

Other balance equations are similarly modified and then discretized and solved as described in Section 3.3.. The results of which are reported in the subsequent sections.

4.2.1 Model Validation

As is the standard practice, validation of the model results is an important step in any modeling work. Using Illinois #6 coal type, the gasifier model results are validated by comparing with two sets of experimental data:, Texaco pilot plant data (EPRI Final Report, EPRI AP-5029, 1987), and industrial data from the Tampa Electric Company (TECO) (Final Technical Report, 2002). The validation runs were carried out with gasifier dimensions and operating conditions shown in Table 4.1.

Table 4.1: Conditions for the Validation runs

Conditions	Texaco Pilot plant	TECO
Gasifier configuration		
Outer diameter (cm)	152	400
Internal diameter (cm)	15.8	179
Length (cm)	330	662
Operating conditions		
Coal feed rate (kg/s)	0.1875	40
Oxygen/coal ratio	0.90	0.82806
Water/coal ratio	0.61	0.4108
Pressure(atm.)	24	26

The Texaco pilot plant gasifier is divided internally into two sections; a partial oxidation zone and a quench section for cooling the syngas stream. During the validation run, only the partial oxidation zone was considered and its length (Govind and Shah, 1984) was taken to be 330 cm as shown in Table 4.1. The inner diameter could not be found in the open literature but was back-calculated based on the assumption that the residence time in the pilot gasifier is similar to that of the TECO gasifier whose dimensions were available (TECO Final Technical Report, 2002; Slezak et al., 2010). The validation results are shown in Figure 4.1.

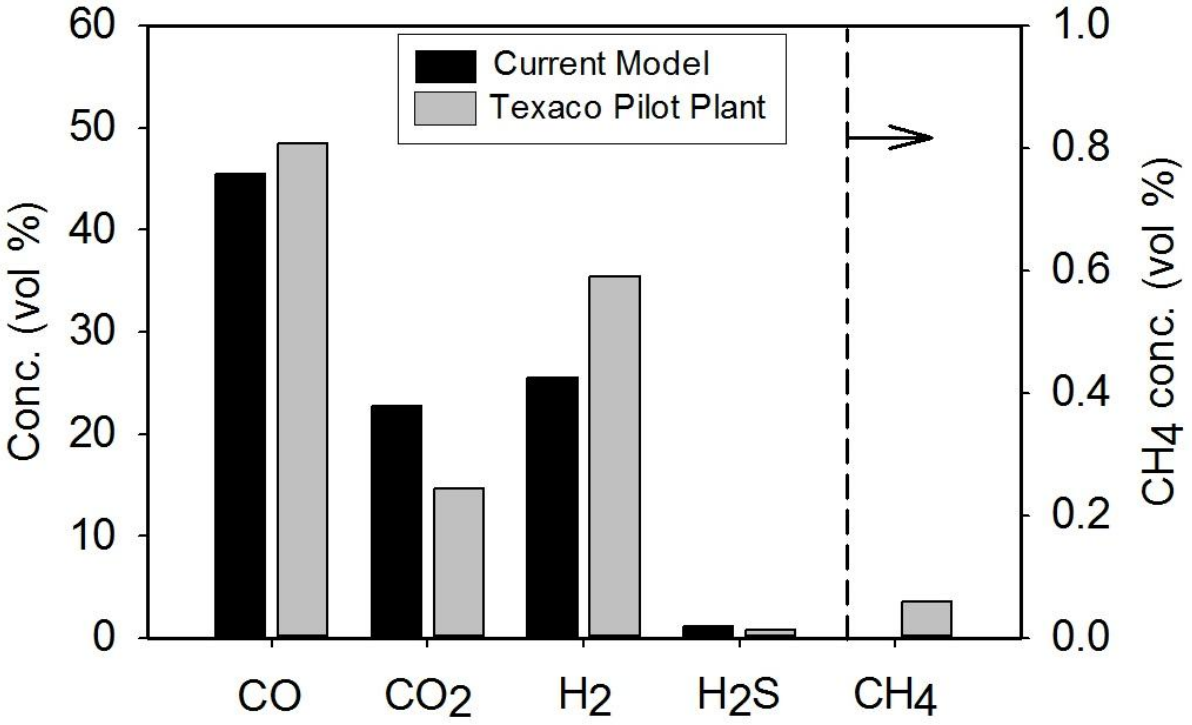

Figure 4.1: Comparison of current model with pilot plant data (dry basis)

The comparison shows a general qualitative agreement of the model's results with the pilot data. Quantitatively, the model's results compare fairly well with the pilot data. The methane concentration shows some mismatch but the two values are very low and are well within generally acceptable values. The under-prediction in the methane is attributed to the faster kinetics of the methane destruction reactions. Slower kinetics rate schemes are also available[6] that usually over-predict the methane concentration. Tuning of the reaction kinetics could have been done to match the pilot plant data, but no such attempt was made in this study. Other apparent mismatches in species concentration may be possibly attributed to the differences in the temperature profiles in the two gasifiers and consequently the carbon conversion. In addition, the residence time in the gasifier is assumed and is not known. However, even without any tuning of

the kinetic parameters, the model predictions showed reasonable agreement with the pilot plant data.

When comparing the current results with those from TECO, it should be noted that these industrial data are from the clean syngas stream downstream of the radiant syngas cooler (RSC), while the current model gives results for conditions exiting the gasifier prior to entering the RSC. Moreover, it is reported by Bhattacharrya et al. (2011) that certain reactions, most importantly the WGS, continue to take place within the RSC. In order to reconcile this inconsistency, the operation of the RSC was also accounted for in this work as illustrated in Figure 3.1.

The RSC was modeled as a plug flow reactor in Aspen Plus® with the inlet conditions identical to those exiting the gasifier. The dimensions and configuration of the RSC were obtained from Robinson and Luyben, (2008). As in their study, a multiple tube reactor configuration with a constant coolant temperature (336°C) was used and only the WGS reaction was modeled in the RSC. The exclusion of other reactions in the RSC is reasonable because other gas species, such as CH_4, have very low partial pressures and the rates for reactions such as methane reforming are low and will have minimal impact on the gas concentration leaving the RSC. In fact, the results remained unchanged when both the WGS and methane reforming reactions were modeled within the RSC.

The results from the RSC modeling are shown in Figure 4.2 and it is clearly seen that the WGS reaction continues to take place within the initial 20-25% length of the RSC before being quenched by the cooling fluid.

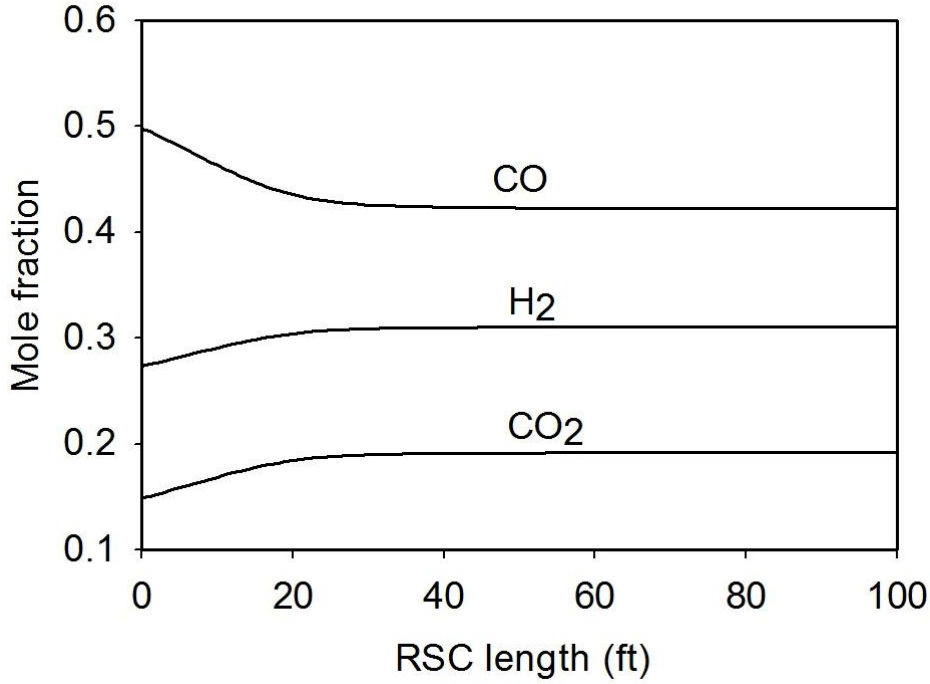

Figure 4.2: Species composition profile along the RSC

The RSC exit compositions are then compared to the TECO data as shown in Figure 4.3.

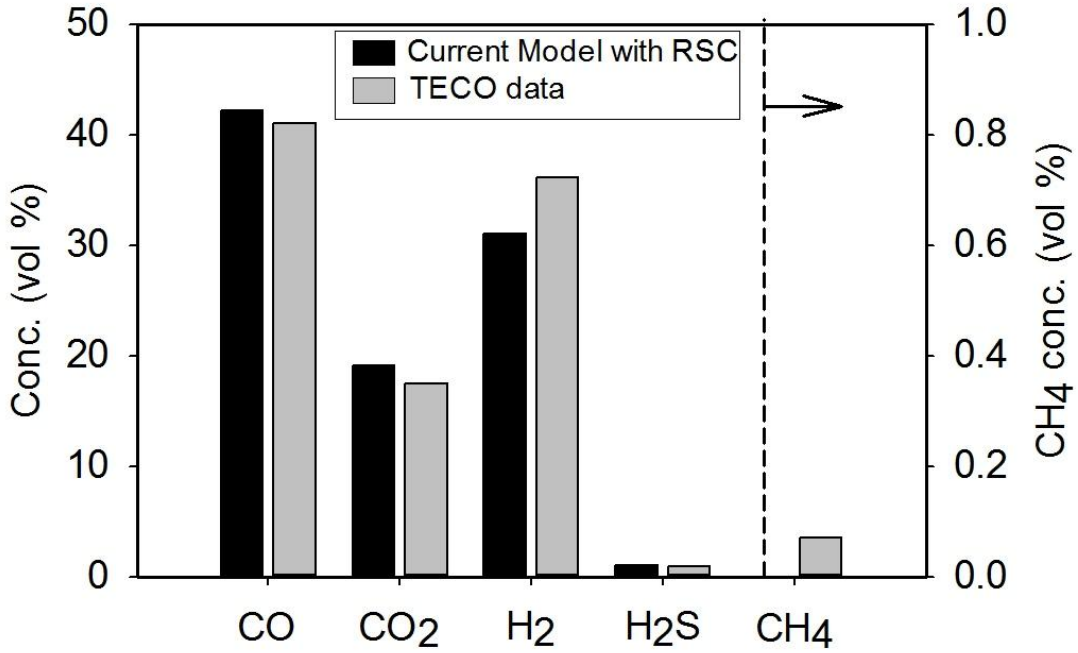

Figure 4.3: Comparison of the TECO data with the current model results at RSC exit (dry basis).

Figure 4.3 shows good qualitative and quantitative general agreement of the model predictions with the industrial data. The CO and CO_2 concentrations are slightly higher in the current model than in the industrial data and this is attributed to the higher carbon conversion in the current study (almost complete conversion for the conditions considered) than in the industrial case (~98%). The lower methane concentration as explained previously, is attributed to the faster methane destruction kinetics. Again, no tuning of reaction kinetics was carried out in the current study other than using reaction schemes obtained from the open literature.

4.2.2 General Model Predictions

This section presents general model predictions in the form of temperature profiles, species concentration, and carbon conversion profiles and the effect of coal types on the exit gasifier product distribution. These runs were obtained with gasifier configuration and operating conditions shown in Table 4.1.

When using Pittsburgh #8 coal, Figure 4.4 shows the gas and solids temperature profiles along the reactor length. At the beginning of the gasifier, the solids temperature gradually increases and then levels-off slightly at the point when the water starts to evaporate (at a scaled reactor length of approximately 0.05). Following another gradual increase, the solids temperature increases rapidly as the volatile matter, consisting of CO, H_2, and CH_4, evolves and is subsequently combusted releasing additional energy. This temperature behavior is further illustrated in Figure 4.5. The corresponding carbon conversion profile shows that there is no significant consumption of carbon until all the devolatilization takes place and the temperature rapidly increases due to the combustion of volatiles. However, after the volatile products have

combusted, there is appreciable carbon conversion mainly due to the carbon gasification reactions.

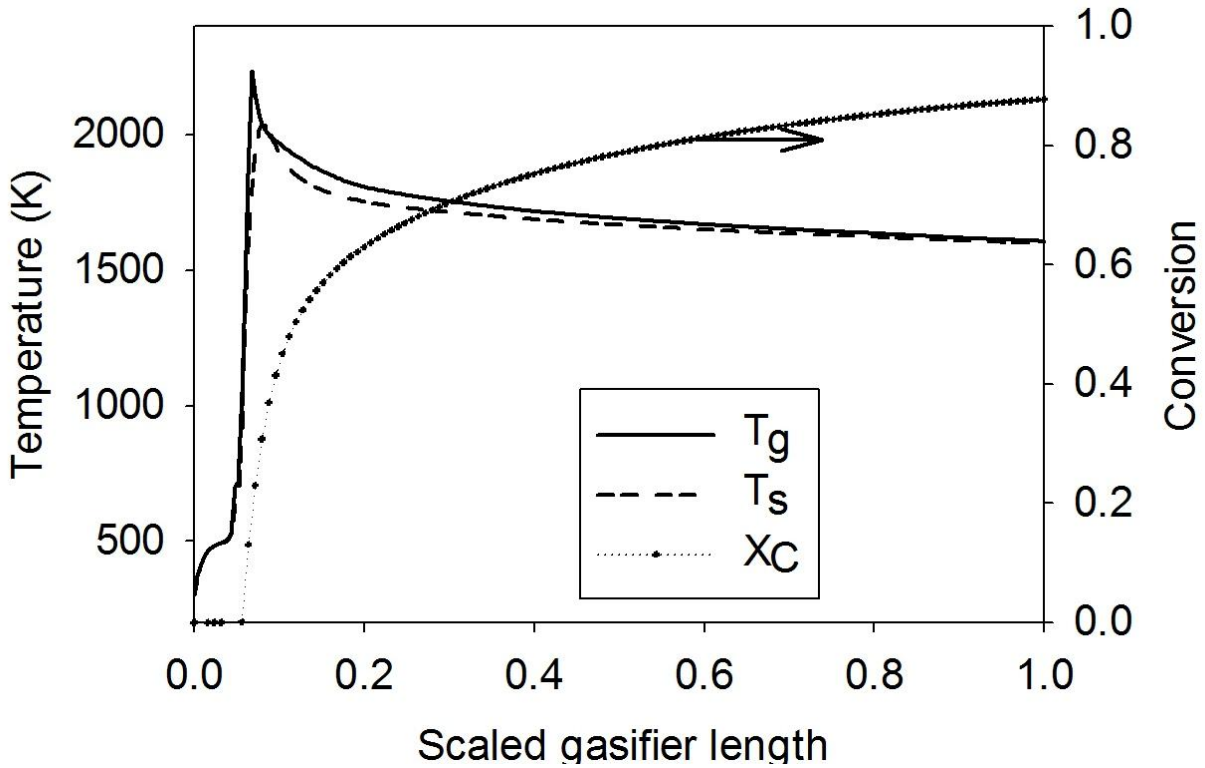

Figure 4.4: Temperature profile and carbon conversion along the gasifier length (water/coal: 0.4 oxygen/coal ratio: 0.8, Pittsburgh #8 coal)

Figure 4.5 shows the profile of the mass fraction of the slurry water and volatile matter (VM) of the Pittsburgh #8 coal and the solid temperature profile. As the water starts to evaporate with the initial increase in temperature, the mass fraction of the volatile matter increases in the solid phase before slightly leveling off at the point when the entire water is evaporated but the temperature is still below the devolatilization temperature. The volatile matter is then released almost instantaneously as the temperature reaches the devolatilization temperature.

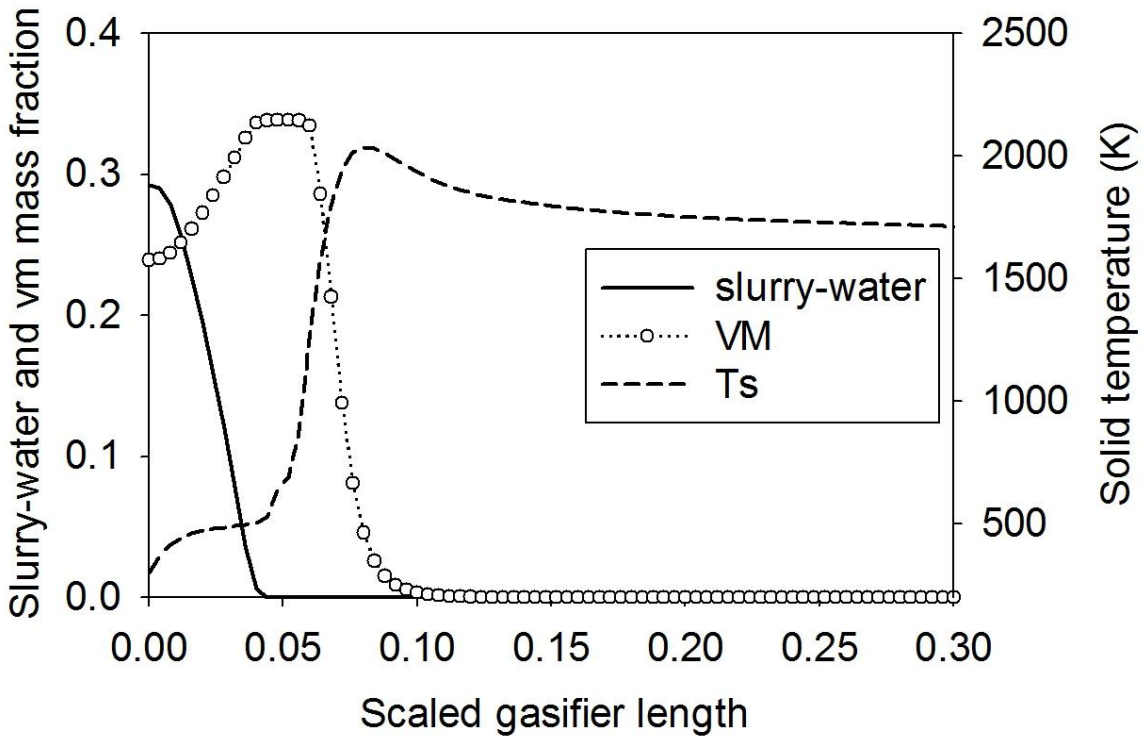

Figure 4.5: Profiles of volatile matter, moisture content, and temperature of the solids along the gasifier length (water/coal: 0.4 oxygen/coal ratio: 0.8, Pittsburgh #8 coal)

Figure 4.6 shows the profiles of the major gas species along the length of the gasifier. Previous studies (Wen and Chaung, 1979; Govind and Shah, 1984; Vamvuka et al. 1995a) have shown that there is no co-existence of the combustible gas species components such as CO and H_2 when sufficient oxygen is present. This is also observed in the current study. The small accumulation of CO and H_2 at the front of the reactor is due to recirculation. However, this occurs at locations before the combustion temperature is reached in the gasifier. The results also show peaks in the CO_2 and H_2O concentration profiles at the point when the maximum temperature occurs in the gasifier. This is also consistent with previous results (Wen and Chaung, 1979; Govind and Shah, 1984; Vamvuka et al., 1995a).

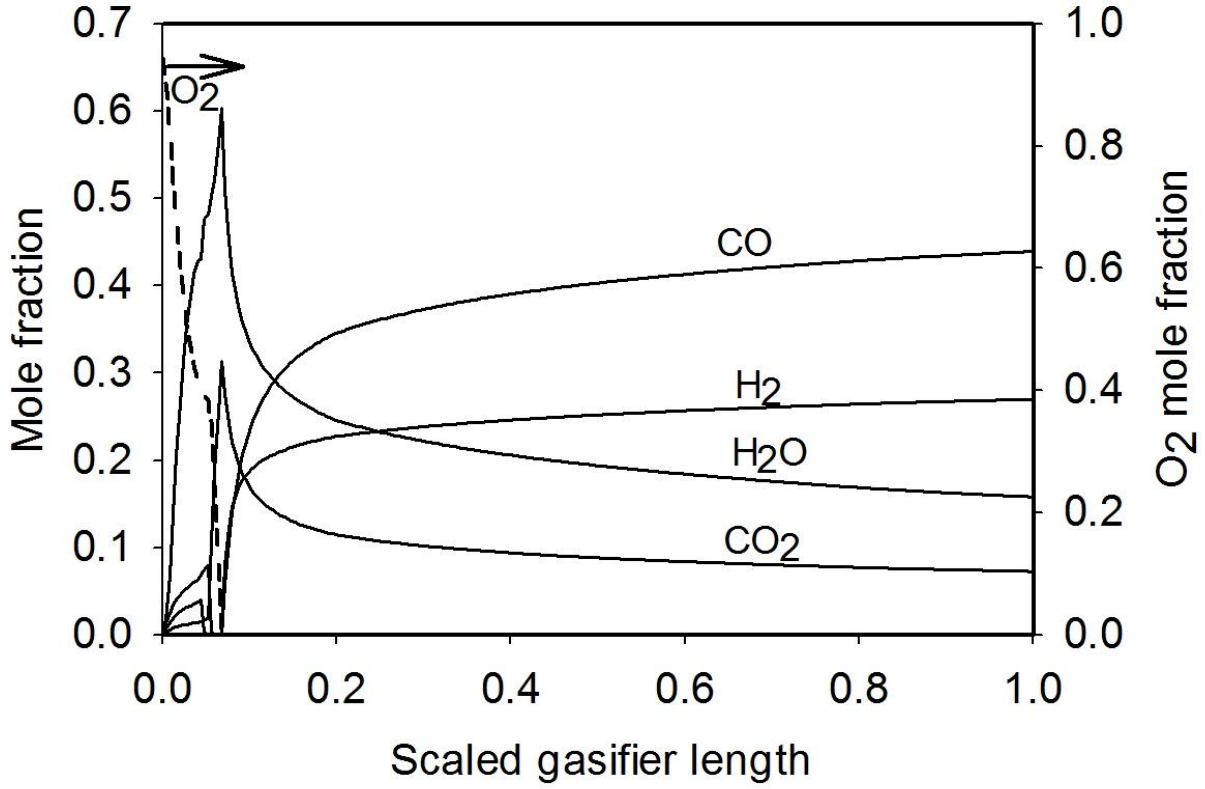

Figure 4.6: Major gas species concentration profiles along the dimensionless gasifier length (water/coal: 0.4 oxygen/coal ratio: 0.8, Pittsburgh #8 coal)

As discussed previously, the current model assumes no *a priori* wall temperature profile. The temperature of the wall is calculated and its profile is shown in Figure 4.7. It should be mentioned that apart from the commonly assumed linear wall temperature profile (Wen and Chaung, 1979; Govind and Shah, 1984), which is also plotted in Figure 4.7, there is no other known temperature profile in the literature to which the current profile could be compared. The wall is seen to experience an initial increase in temperature attaining a maximum value and then steadily decreasing. This characteristic is remarkably different than the assumed linear temperature profile. In addition, the temperature gradient along the wall is calculated to be much less steep than the assumed slope of the linear temperature profile.

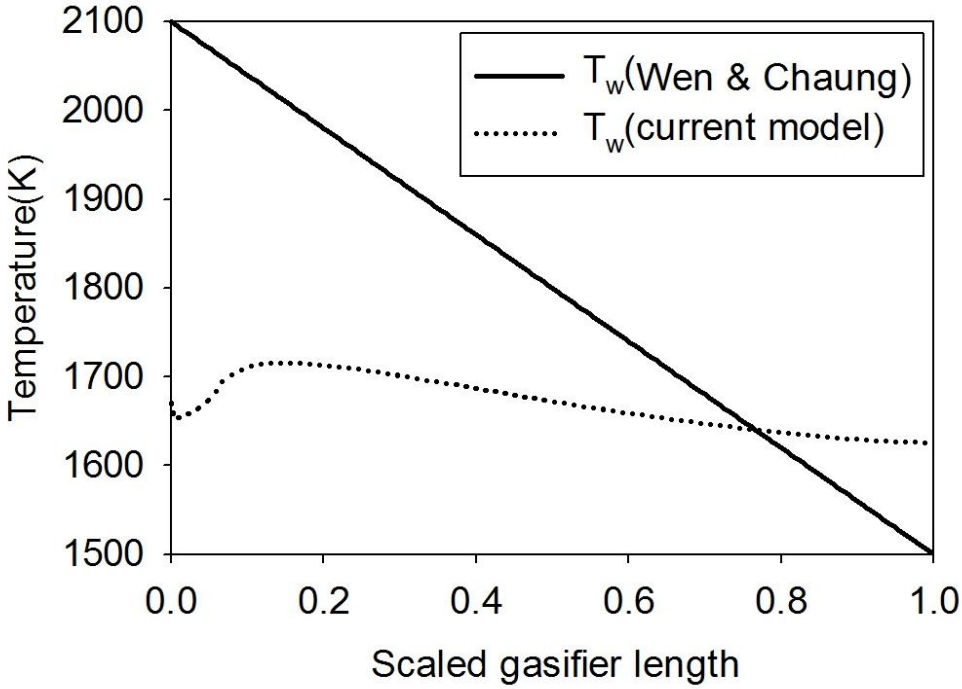

Figure 4.7: Calculated wall temperature profile (T_w) compared to the linear wall temperature profile (Wen and Chaung, 1979)

4.2.3 Steady-State Sensitivity Studies

A series of sensitivity studies was performed to gain more insight into the response of the gasifier to changes in certain key parameters. The studies include the effect of coal feed properties on the product distribution, the effect of water-to-coal and oxygen-to-coal ratios on the maximum temperature attained in the reactor, the effect of the recirculation ratio on temperature, and the effect of the water-to-coal and the oxygen-to-coal ratios on coal conversion.

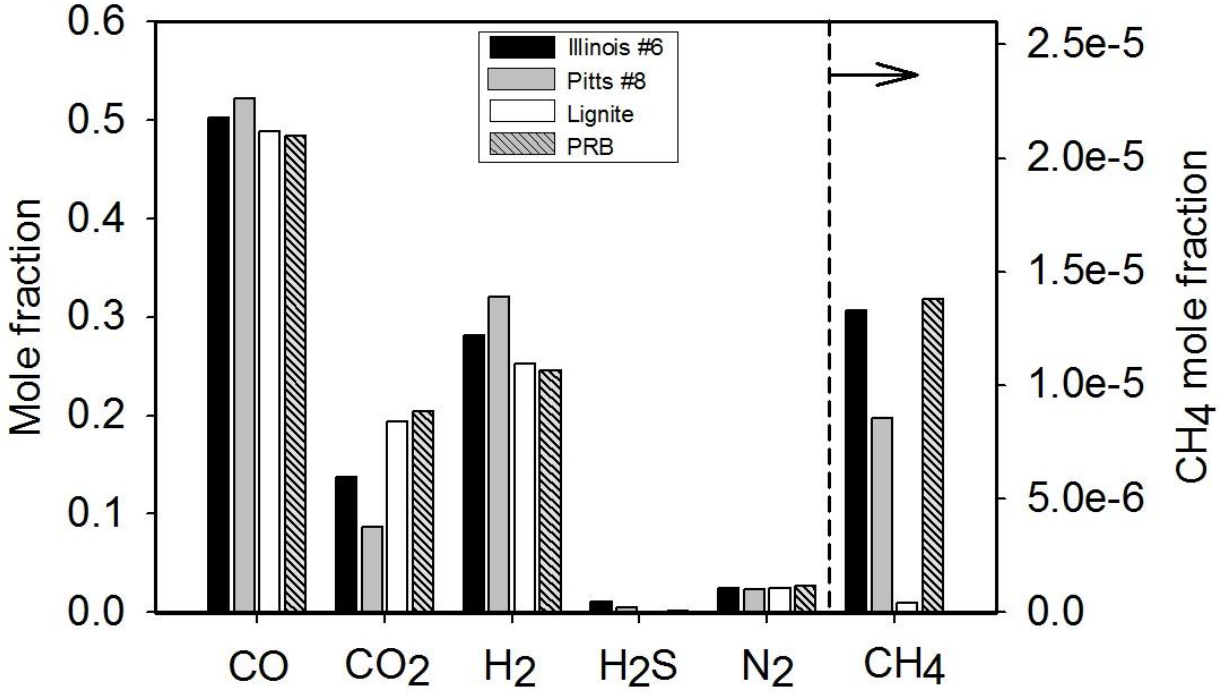

Figure 4.8: Product distribution of exit gas for different coal feeds (water/coal: 0.4 oxygen/coal ratio: 0.8).

Figure 4.8 shows the product distributions obtained when different coal feeds are used at the same feed conditions. The results show a marked variation in the gaseous products distribution but with CO, CO_2 and H_2 consistently produced as the major dominant species and CO having the highest composition in all cases. It is also interesting to note that the maximum phase temperature, particularly that of the solid phase varies markedly with coal type as seen in Figure 4.9. These results highlight the strong dependence of the gasifier response on the coal type.

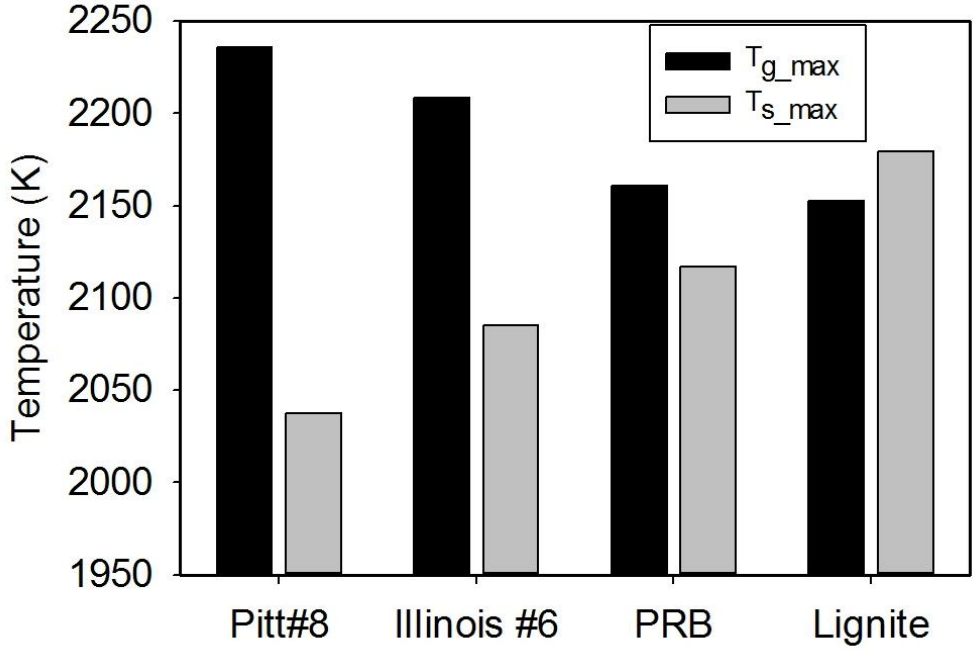

Figure 4.9: Maximum gas and solid temperatures for different coal feed types

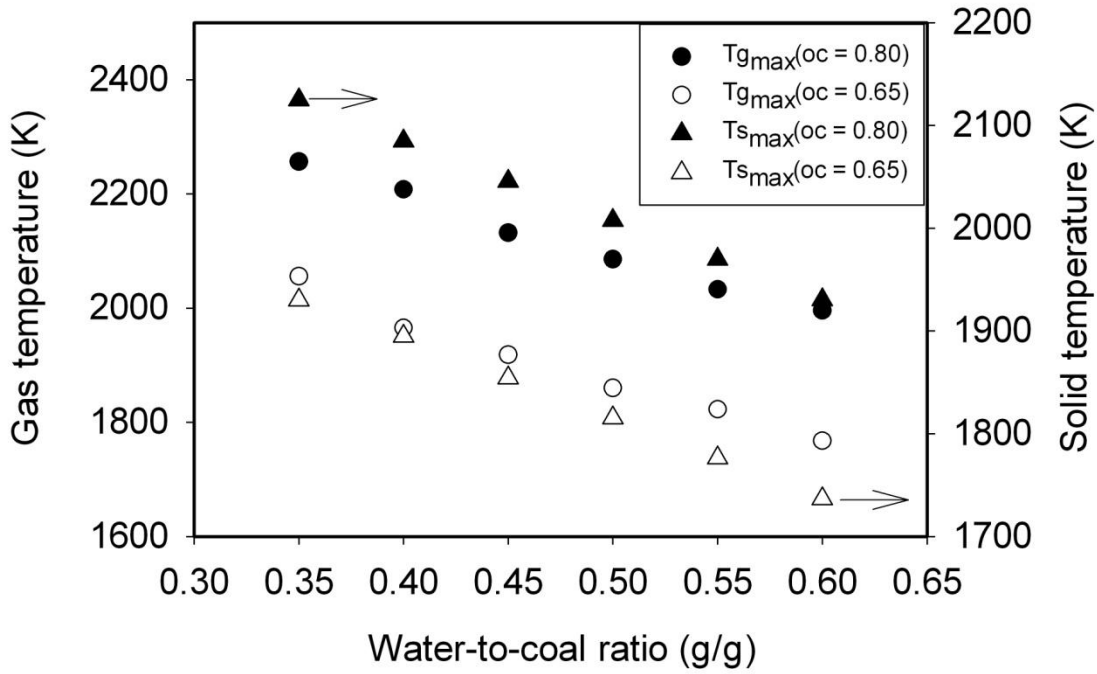

Figure 4.10: Effect of water-to-coal ratio on the maximum phase temperatures at oxygen/coal ratios (oc) of 0.65 and 0.8 (Illinois #6 coal)

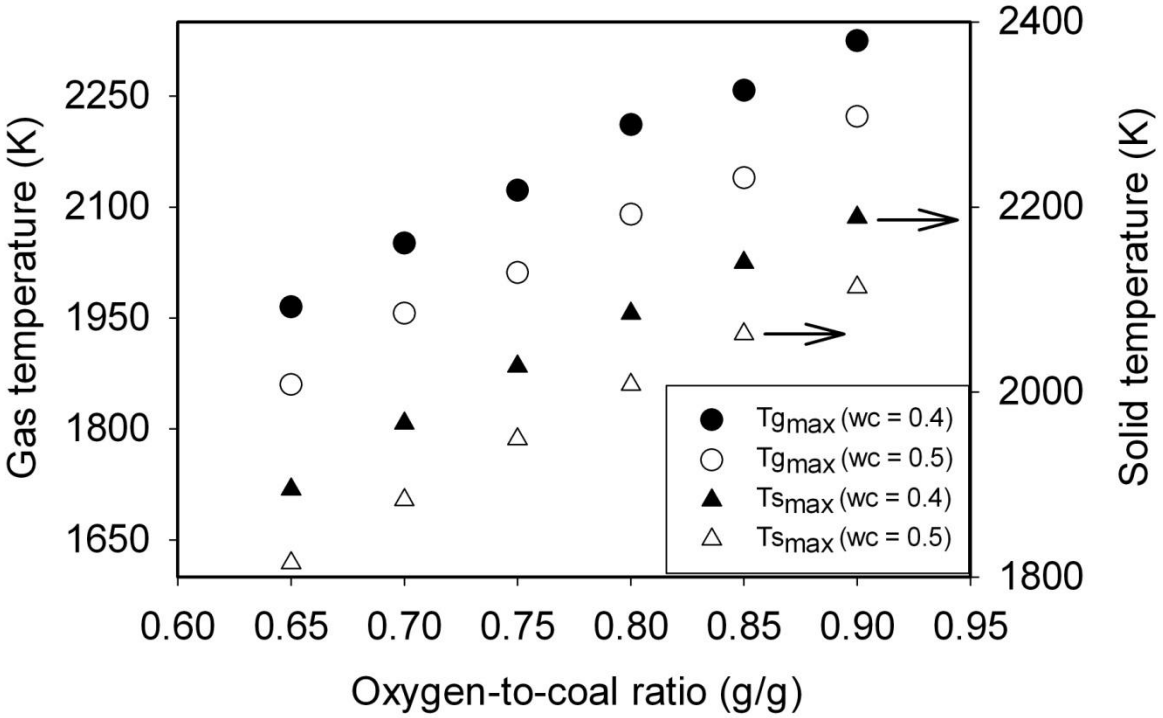

Figure 4.11: Effect of oxygen-to-coal ratio on the maximum phase temperatures at water/coal (wc) ratios of 0.4 and 0.5 (Illinois #6 coal)

Figures 4.10 and 4.11 show the co-effect of the water-to-coal and oxygen-to-coal ratios on the maximum temperatures attained by the solid and gas phases inside the gasifier for Illinois #6 coal. In Figure 4.10, as the water-to-coal ratio increases, the maximum temperatures for both solid and gas phases decrease at any fixed oxygen-to-coal ratio. In addition, by increasing the oxygen-to-coal ratio (for example from 0.65 to 0.8) the maximum temperature of each phase increases. This is further illustrated in Figure 4.11 in which the maximum phase temperatures increases with increasing oxygen-to-coal ratio. However, at a fixed oxygen-to-coal ratio, the maximum temperatures decreased as the water-to-coal ratio increased from 0.4 to 0.5. As expected, increasing the water-to-coal ratio decreases the maximum temperatures while increasing the oxygen-to-coal ratio increases the maximum temperatures.

In addition to the above observations, the position of the maximum temperature is seen to shift downstream from the inlet of the gasifier with increasing water-to-coal ratio. This result is similar to that shown by Vamvuka et al. (1995b). The higher this ratio is the longer it takes to evaporate the water and hence the ignition point tends to drift away from the gasifier inlet as seen in Figure 4.12.

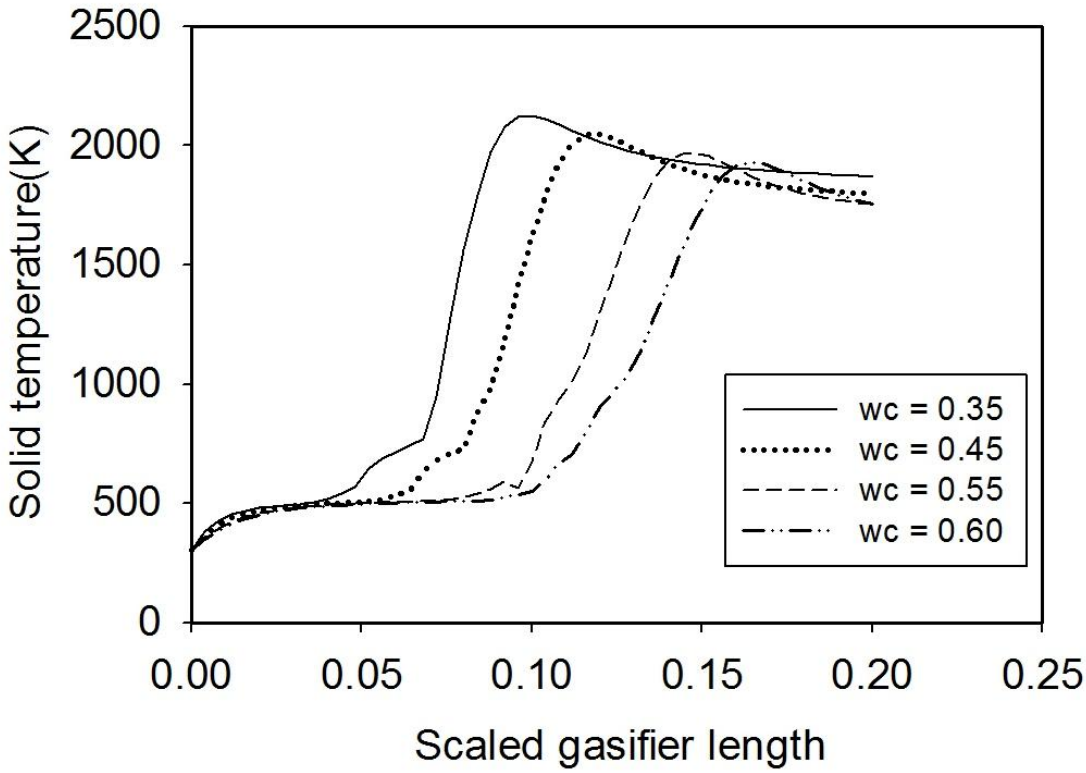

Figure 4.12: Effect of water-to-coal ratio (wc) on solid temperature (oxygen/coal: 0.8; coal: Illinois #6)

A shift in the position of the maximum temperature seen in Figure 4.12 is similarly observed when the model is run at different recirculation ratios as seen in Figure 4.13. However, the recirculation ratio has no appreciable effect on the maximum values of the temperature.

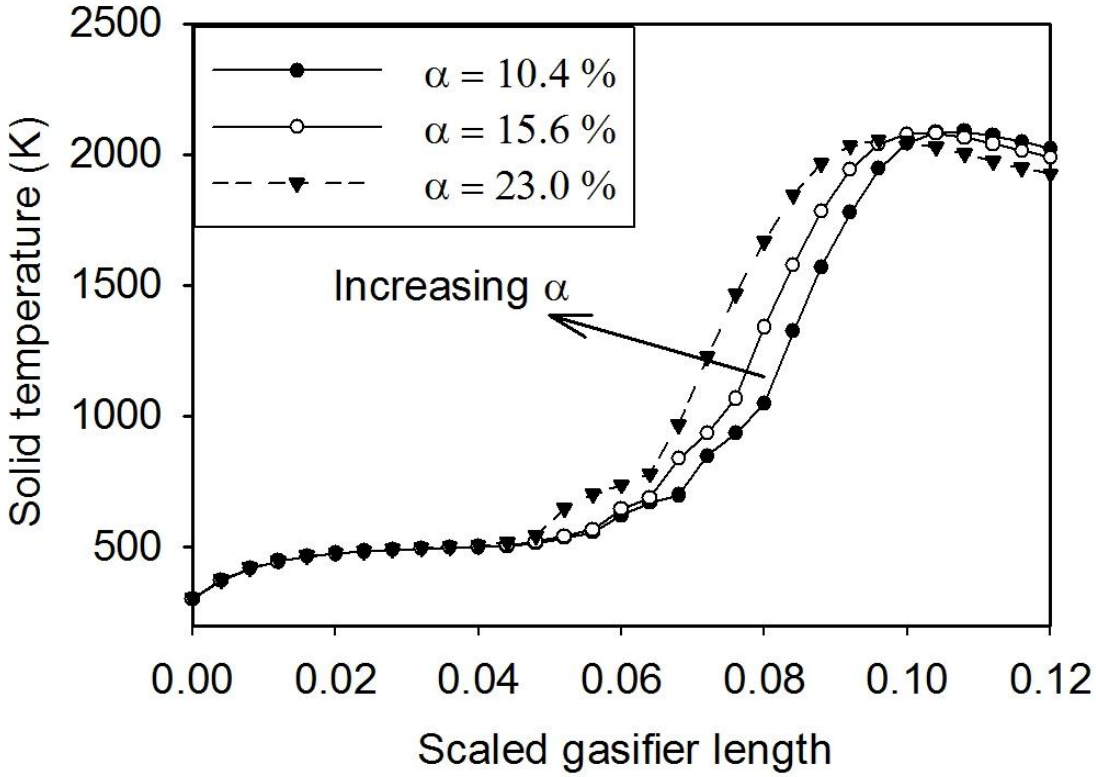

Figure 4.13: Effect of recirculation ratio (α) on solid temperature

Additionally, the effect of the recirculation ratio on the composition of the exit gas species is shown in Figure 4.14. The results show that this ratio has a negligible effect on the gas composition.

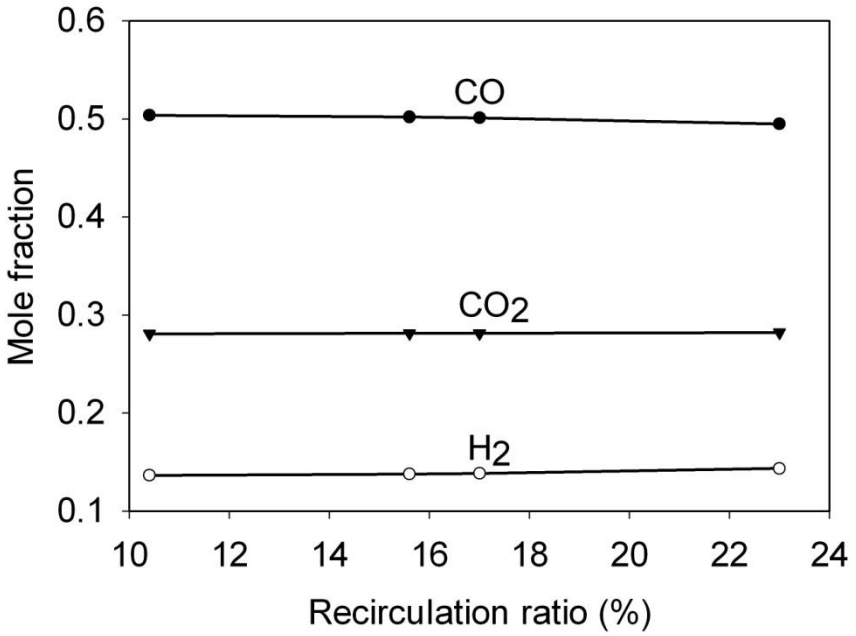

Figure 4.14: Effect of the recirculation ratio on the main gas composition

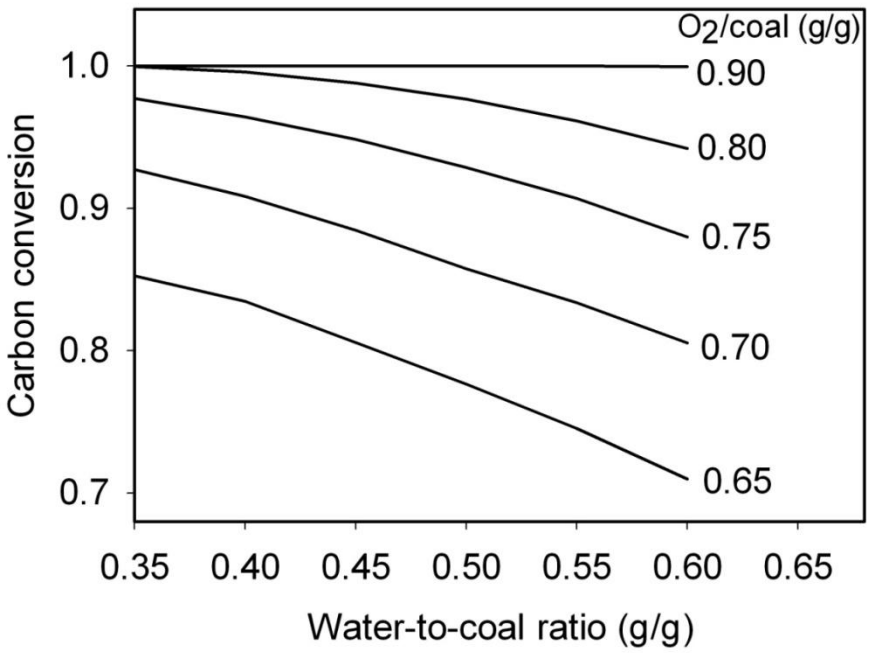

Figure 4.15: Effect of water-to-coal feed ratio on carbon conversion as a function of oxygen-to-coal ratio.

Figure 4.15 shows the effect of the water-to-coal and oxygen-to-coal feed ratios on carbon conversion. At a fixed oxygen-to-coal ratio, the carbon conversion is seen to decrease

with increasing water-to-coal feed ratio. This is attributed to the decrease in temperature as the water-to-coal ratio is increased. Conversely, conversion significantly increases with increasing oxygen-to-coal feed ratio. This is due to the increase in temperature as a result of the additional energy added from the exothermic combustion reactions. With the water-to-coal and oxygen-to-coal ratios used in the model, carbon conversion of at least 99% is achieved with an oxygen-to-coal ratio of 0.8 and water-to-coal ratio of less than 0.4. It is evident that the oxygen-to-coal ratio significantly affects the carbon conversion more than the water-to-coal ratio.

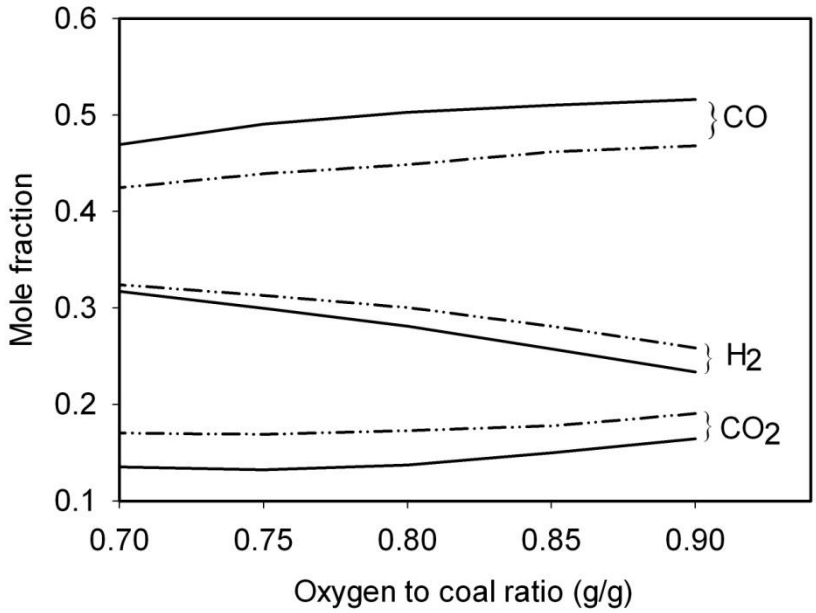

Figure 4.16: Product gas composition as a function of oxygen-to-coal ratio (broken line: water-to-coal = 0.55, solid line: water-to-coal = 0.4)

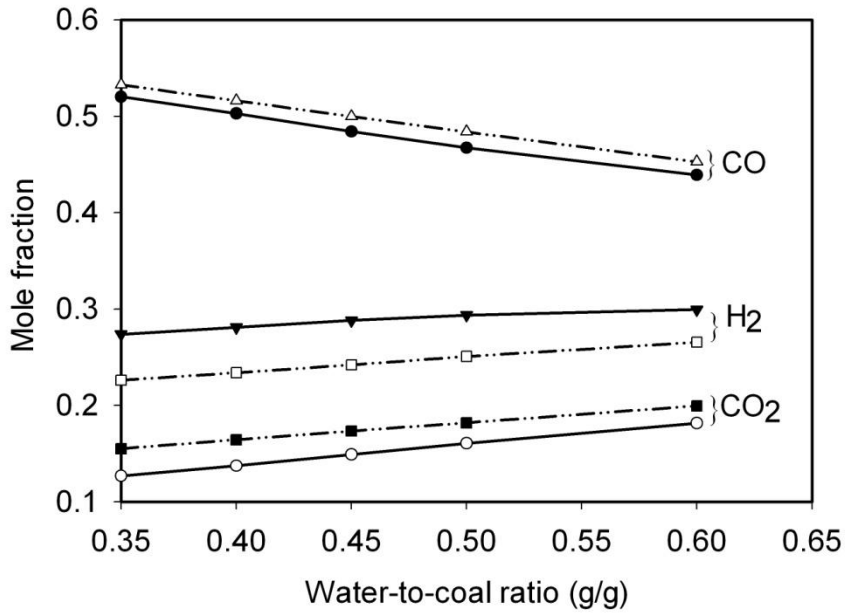

Figure 4.17: Product gas composition and carbon conversion as a function of water-to-coal ratio (solid line: oxygen-to-coal = 0.8, broken line: oxygen-to-coal = 0.9)

Figures 4.16-4.17 show the co-effects of water-to-coal and oxygen-to-coal ratios on the composition of the major gas products. In Figure 4.16, CO and CO_2 concentrations are seen to increase while H_2 concentration decreases with increasing oxygen-to-coal ratio. However, at any fixed oxygen-to-coal ratio, the concentrations of CO_2 and H_2 increase while that of CO decreases with increasing water-to-coal ratio as shown by the two plots with water-to-coal ratio values of 0.55 and 0.4. This result is mainly due to the competing char-gasification and the WGS reactions. The decrease in CO and increases in H_2 and CO_2 is consistent with the direction of the WGS reaction equilibrium. In Figure 4.17, increasing the water-to-coal ratio at fixed oxygen-to-coal ratio leads to an increase in H_2 and CO_2 concentrations and a decrease in CO concentration. Again this is consistent with the direction of the WGS reaction equilibrium. Increasing the oxygen-to-coal ratio (for example from 0.80 to 0.90) at any fixed water-to-coal ratio shows a decrease in H_2 and an increase in CO_2 and CO concentrations. An increase in oxygen content

leads to in more combustion of H_2 and carbon and causes the observed reduction in H_2 and increase in CO and CO_2, which are the major products of the char-combustion reaction. These results are due to the competing reactions (mainly char-combustion, char-gasification and WGS), taking place in the gasifier as reported in Wen and Chaung, (1979) and Govind and Shah, (1984). It is also apparent that the water-to-coal ratio has a larger effect on the gas product composition than the oxygen-to-coal ratio.

In the last of these sensitivity studies, it was also observed that the cold gas efficiency of the gasifier (which is calculated from Equation 4.2) is strongly influenced by both the water-to-coal and oxygen-to-coal ratios as shown in Figure 4.18.

$$\eta_{cg} = \frac{product\ gas\,(mass\ flow * LHV) - additional\ \ fuel\,(mass\ flow * LHV)}{coal\,(mass\ flow * LHV_{coal})} \qquad (4.2)$$

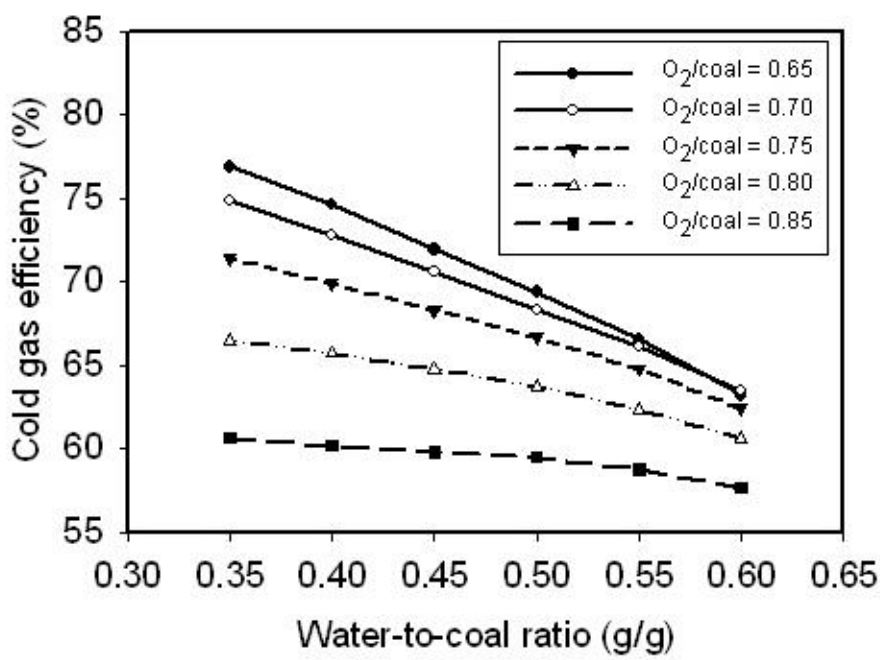

Figure 4.18: Effect of water-to-coal and oxygen-to-coal ratios on the cold gas efficiency of the gasifier

As seen in Figure 4.18, the cold gas efficiency, calculated based on the lower heating values of coal and the gas products, decreases with increasing water-to-coal ratio at any given oxygen-to-coal ratio. At the same time, the maximum values of the cold gas efficiencies are obtained at the smallest oxygen-to-coal ratios. These results are consistent with those reported in the literature (Ni and Williams, 1994).

4.3 Conclusion for Steady-State Studies

A steady-state model of an entrained, GEE/Texaco type, downward-flow gasifier is presented. In addition to mass, momentum, and energy balance equations for the solid and gas phases, the gasifier model includes heterogeneous char-gas and homogeneous gas-gas reactions and equations describing the drying and devolatilization processes for the slurry feed. The gasifier wall temperature profile is not assumed *a priori*, but rather is calculated from the detailed multi-surface, multi-mechanism energy balance model. A heuristic recirculation model is considered to capture the initial energy transfer to the slurry feed within the "mixing" zone at the gasifier entrance.

For validating the gasifier model, results are compared with the pilot plant data as well as the available industrial data from the TECO IGCC plant. The model predictions compared appreciably with the pilot plant data even without any tuning of the reaction kinetics. The model results compare satisfactorily to the TECO results when an RSC model is included at the gasifier outlet. The residual mismatch in the syngas composition is attributed to the higher carbon conversion in the current model.

The gasifier model is also used to simulate the gasification of different coal types. The results show a strong dependence of the product composition and maximum phase temperatures on the type of the coal fed to the gasifier.

A recirculation ratio of greater than 10.4% affects only the position at which the ignition occurs in the gasifier without having any major effect on the maximum phase temperature and the product gas composition in the gasifier.

The optimum range for the water-to-coal and oxygen-to-coal ratios necessary for achieving at least 99% carbon conversion for the cases considered in the study is 0.3-0.4 and 0.8-0.9, respectively.

The cold gas efficiency was observed to have a strong dependency on both the water-to-coaland oxygen-to-coal ratios; the maximum cold gas efficiency occurred at the smallest oxygen-to-coal ratio at any water-to-coal ratio, and increasing the water-to-coal ratio resulted in a decrease in the cold gas efficiency for a given oxygen-to-coal ratio.

Chapter 5

Dynamic Model Study Results

5.1 Introduction

In this section, the results obtained from the transient model are reported. The steady state-model in the previous section was extended to the dynamic model by solving the partial differential equations (PDEs) reported in Chapter 3. However, in order to extend the steady state model to a transient one, a number of modifications had to be made.

Unlike in the steady-state study in which the accumulation terms were neglected, the balance equations were solved as they appear in Chapter 3. In addition, the boundary conditions in the single gasifier block of the steady-state model were modified in such a way that instead of being fixed as in the steady-state solution, they are variables whose values are obtained from the feed streams that are now connected to the gasifier through ports as shown in Figure 5.1. A Port is a connection terminal through which a stream is connected to a given model or through which any two models are connected via a stream. The port contains variables similar to those in the connecting stream and their values are inherited from the feed stream values while the exit stream values are inherited from the port values.

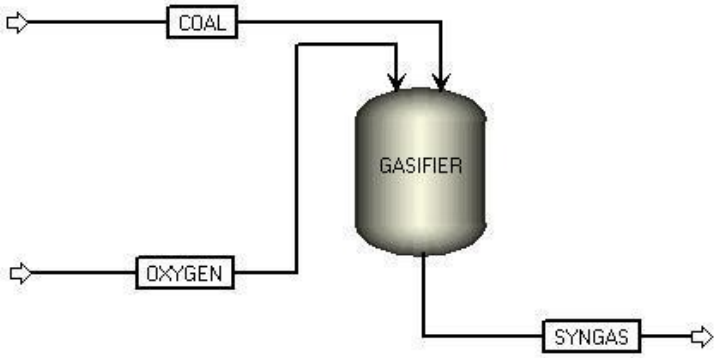

Figure 5.1 Block diagram of gasifier with connected feed streams

Figure 5.1 shows two feed streams; the coal slurry feed and the oxygen feed streams and the mixed exit stream connected to the gasifier block (B1).

5.2 Dynamic Run Set-up

In order to complete the dynamic set-up for the model, valve models must be connected to the streams (Figure 5.2) in order to ensure that a pressure-flow relationship is established for the pressure-driven flow dynamics, targeted in the current study. This flow relationship is modeled through a valve equation and the stream flow rate is calculated through this relationship (Equation 5.1).

$$F = C_0 \, (Pos/100) \, \left(\Delta p \, \rho\right)^{1/2} \tag{5.1}$$

where, F is the stream flow rate, C_0, is the valve constant, Pos is the percent valve opening, Δp is the pressure drop across the valve, and ρ is the density of the flowing materials in the stream. The block diagram with valves is shown in Figure 5.2, in which valves V_01, V_02 and V_03 were added to the coal slurry, oxygen and mixed exit streams, respectively. The configuration is such that the upstream pressures of the two feed stream valves (V_01 and V_02) are fixed while the downstream pressures are calculated. On the other hand, the downstream pressure of the exit valve (V_03) is fixed while its upstream pressure is a free calculated variable.

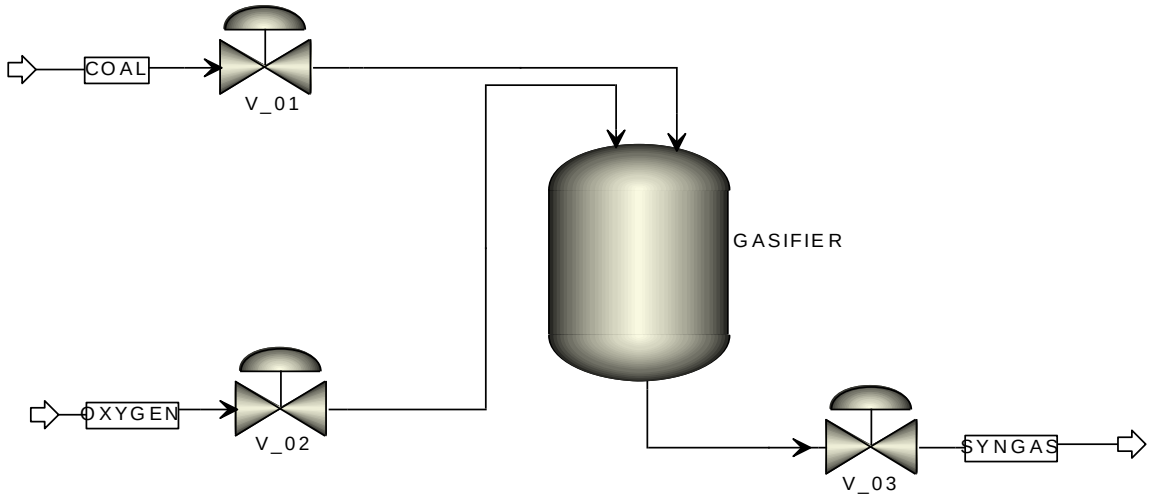

Figure 5.2 Block diagram of gasifier with flow valves

With the pressure-flow dynamics fully defined, the dynamic runs were then performed. These dynamic simulations may be performed in either a closed-loop mode (with controllers) or in an open-loop mode (with no controllers or with controllers in MANUAL mode). This is explained more fully in the next section.

5.3 Open Loop Dynamic Run

As mentioned previously, for open-loop dynamics, the model is run with no controller action. Figure 5.2 shows a configuration for an open-loop run with no controllers connected to the model. Although the normal gasifier operation is not open loop in nature, this run was necessary to establish the response of the model to any dynamic disturbances.

5.3.1 Open Loop Dynamic Responses

In this section the responses of selected key gasifier variables to dynamic disturbances are reported. During the run, a step change or ramp change to the coal slurry flow rate or oxygen flow rate were introduced in the model and the responses noted.

5.3.1.1 Responses to a step change input in coal slurry flow

In Figures 5.3-5.6 responses to a step change increase in coal slurry flow are presented. This was introduced through a 5% step change input to the coal slurry flow stream valve (V_01) position opening (from a value of 50 to 52.5) as shown in Figure 5.3.

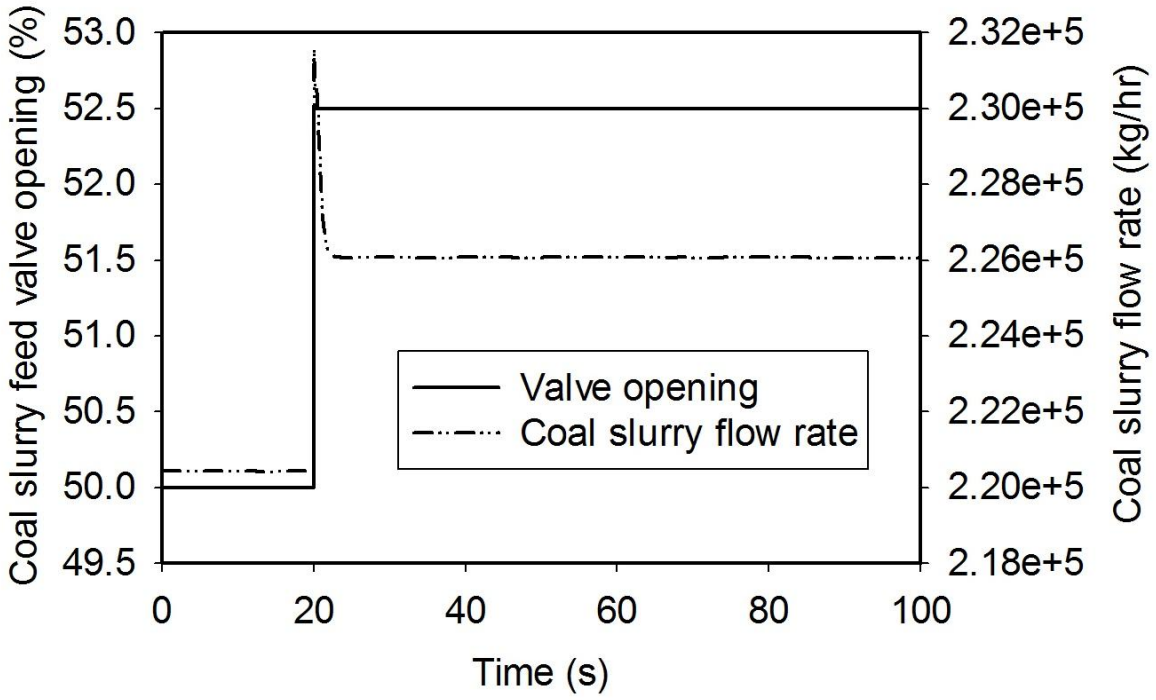

Figure 5.3 Coal slurry valve position % opening and the coal slurry flow rate

Figure 5.3 shows that a 5% step input increase in the valve opening results in an overshoot in the slurry flowrate before the slurry flowrate settles down to the final value.

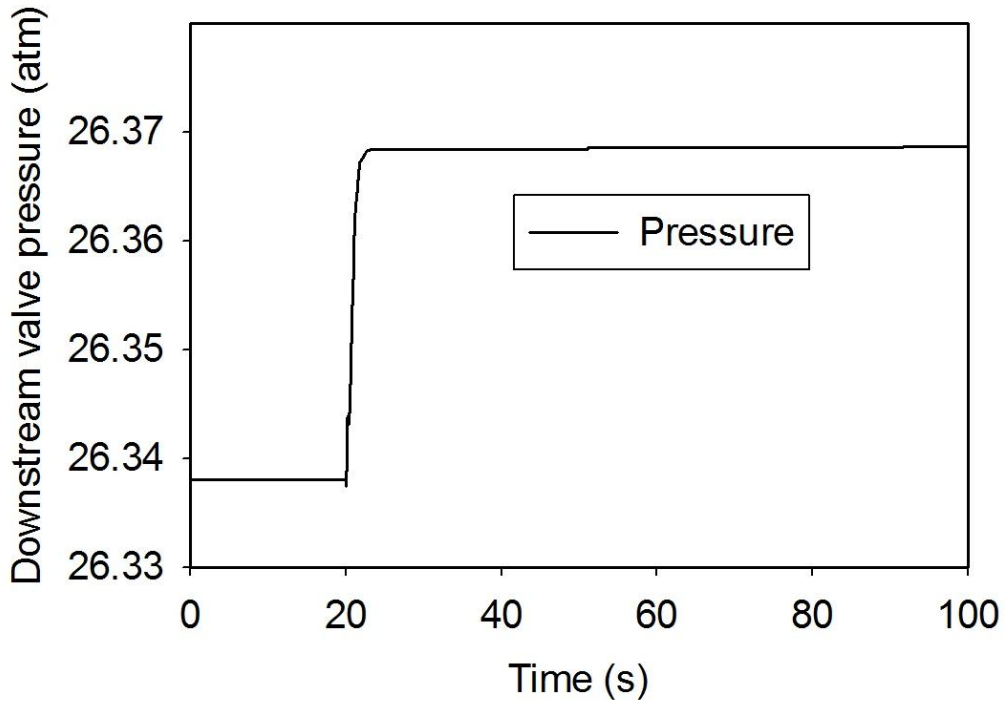

Figure 5.4: The downstream valve pressure response.

The transient response of the pressure at the outlet of the feed valve is shown in Figure 5.4 in which the pressure is seen to increase with the step increase in the valve position. This is expected as it results in an increase in the pressure drop consistent with the increased flow rate. However, this results in a decrease in the oxygen flow rate as seen in Figure 5.5. This is because the pressure at the outlet of the oxygen feed valve is the same as the pressure at the outlet of the coal feed valve and an increase in this pressure is expected to result in a decrease in the flow of oxygen as the opening of the oxygen valve is kept constant. The impact of these flow rate changes on some key model variables are shown in Figures 5.6-5.9.

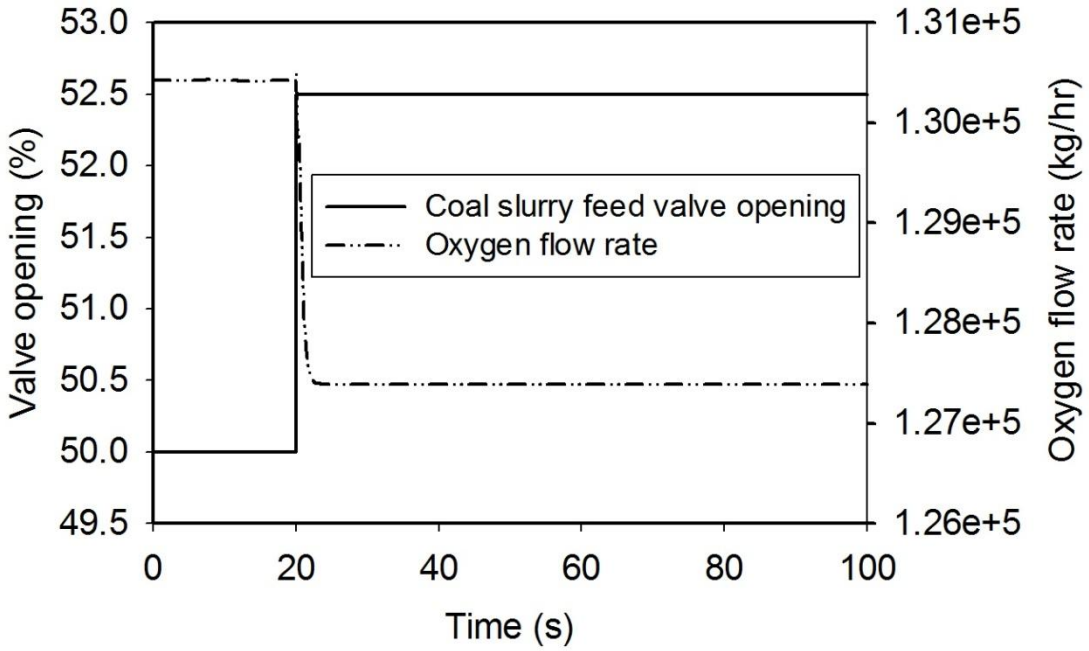

Figure 5.5 Coal slurry valve position % opening and the oxygen flow rate response

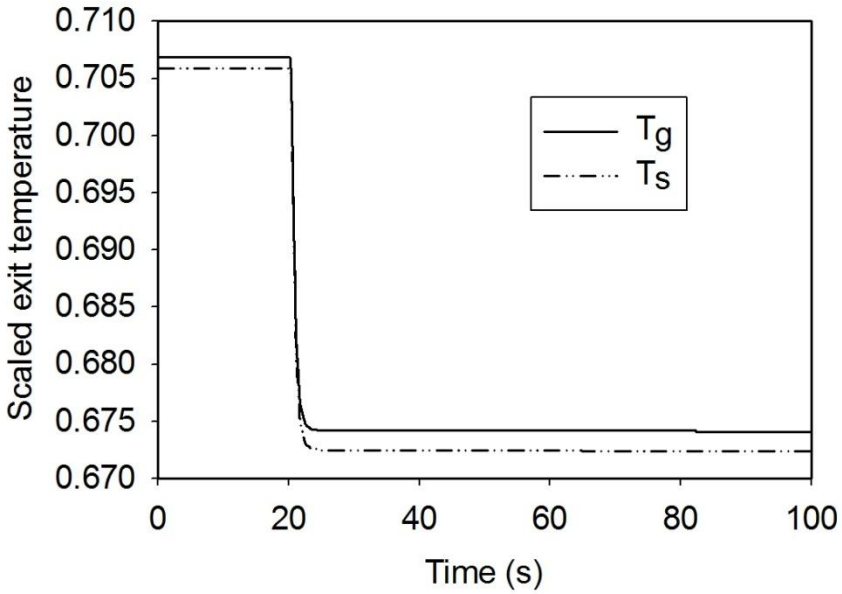

Figure 5.6 Scaled exit phase temperature (leaving the gasifier) response profiles to a 5% step change increase in coal slurry feed stream valve position opening

Figure 5.6 shows that a step decrease in the exit gas and solid temperatures results from a step change increase in the coal slurry flow rate. A similar result is observed in Figure 5.7 which shows a step decrease in the carbon conversion. The decrease in temperature and conversion is consistent with the increased coal slurry flow rate and reduced oxygen flow rate as the extent of the exothermic combustion reactions gets decreased. Also the reduced temperatures are attributed to the increase in the fraction of water in the overall gasifier feed as the slurry flow rate is increased.

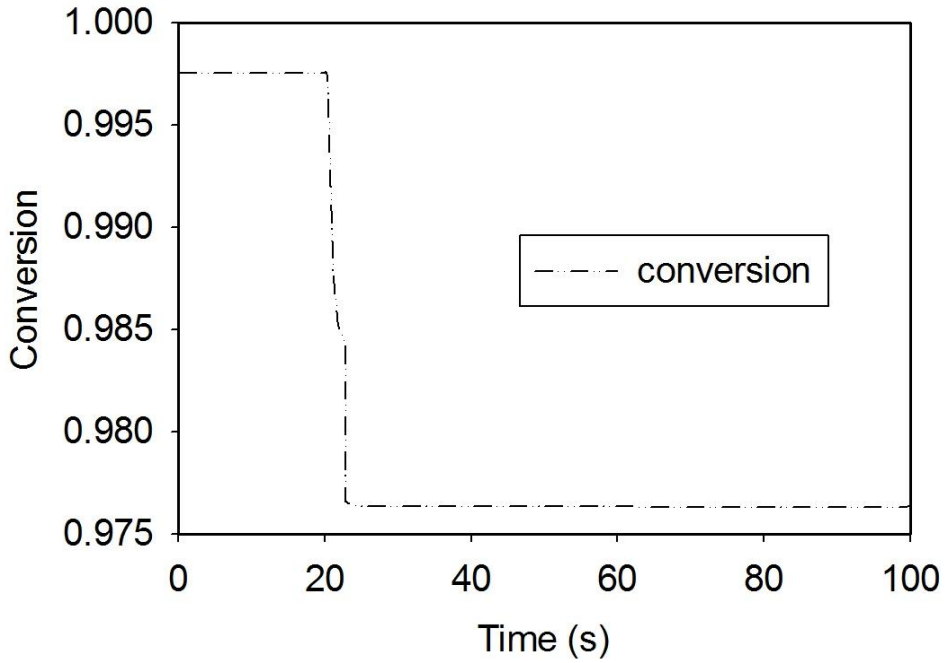

Figure 5.7 Carbon conversion response profile to a step change increase in coal slurry feed stream valve position opening.

The reduction in the exit temperature is an indication of the general reduction of maximum temperature within the gasifier that results in the reduction in the extents of the gasification reactions and thus the reduction in overall conversion.

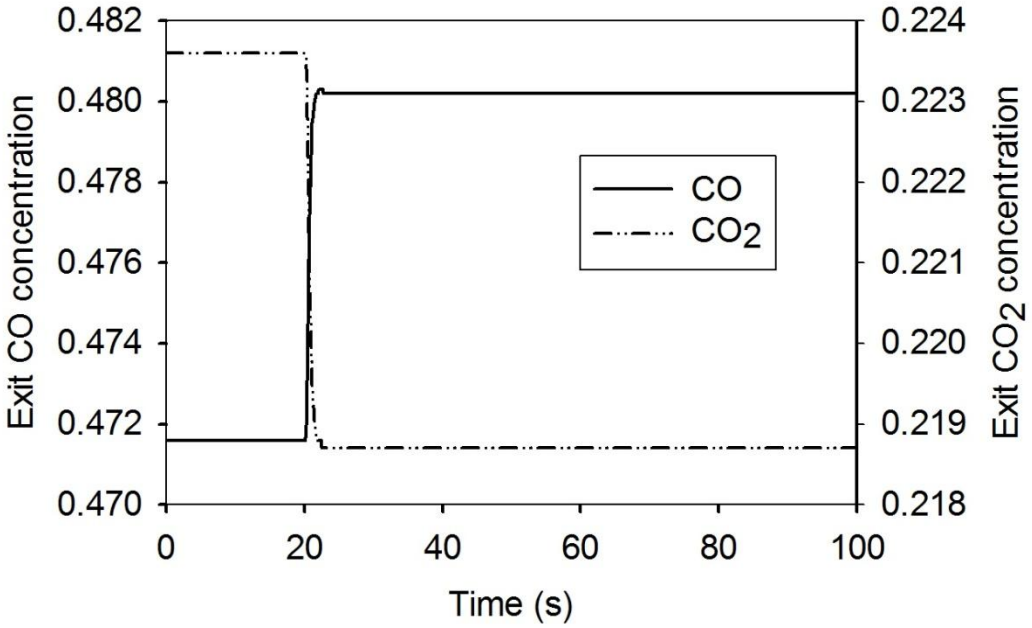

Figure 5.8 Exit CO and CO_2 response profiles to a 5% step change increase in in coal slurry feed stream value position opening

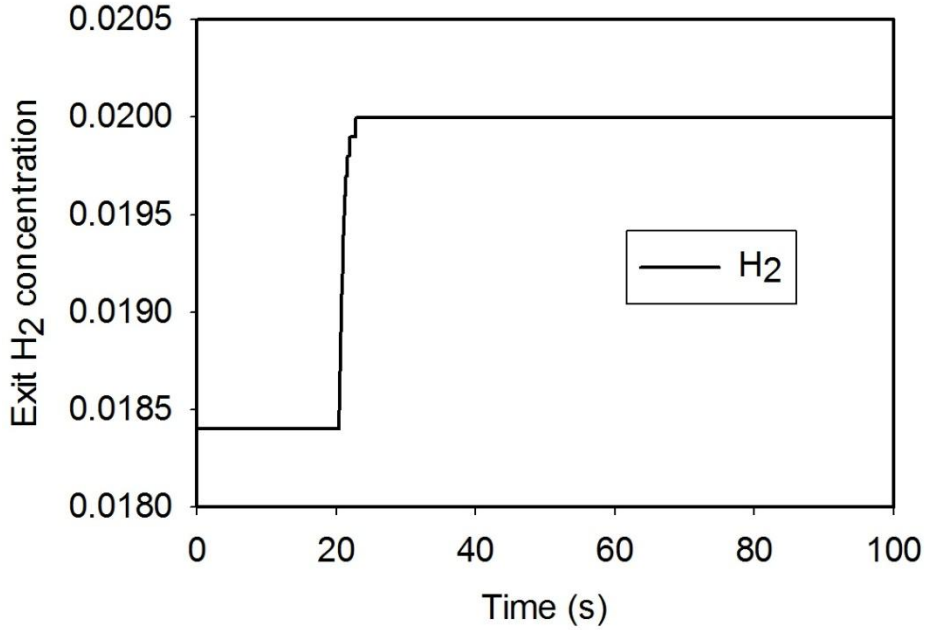

Figure 5.9 Exit Hydrogen concentration response profile to a 5% step change increase in coal slurry feed stream valve position opening

Figures 5.8 and 5.9 show the responses of the main syngas gas components. A step increase in CO and H_2 and a step decrease in CO_2 in the exit streams are observed. The increase in the combustible gases of CO and H_2 is due to the reduction in oxygen flow rate resulting in limited combustion and thus a decrease in CO_2 that is a combustion product.

5.3.1.2 Responses to a step change input in Oxygen flow

Another open loop disturbance introduced in the model was a step change in the oxygen flow rate. Responses to a 5 % step change decrease in the oxygen valve opening (from 50 to 47.5%) are presented in this section.

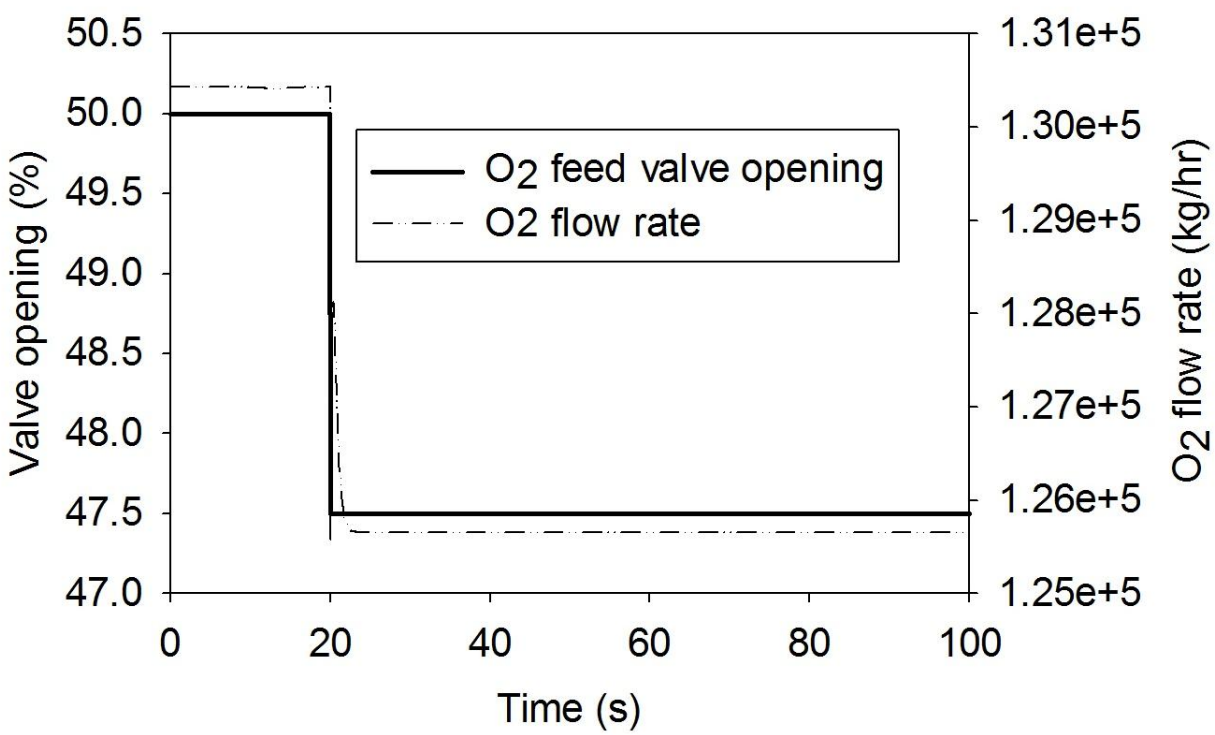

Figure 5.10 Oxygen valve opening step change and oxygen flow rate response

Figure 5.10 shows the step decrease in the opening of the oxygen valve and the response of the oxygen flow rate. A step decrease in the valve opening results in a decrease in the oxygen flow rate. This in turn results in an increase in the coal slurry flow rate as seen in Figure 5.11.

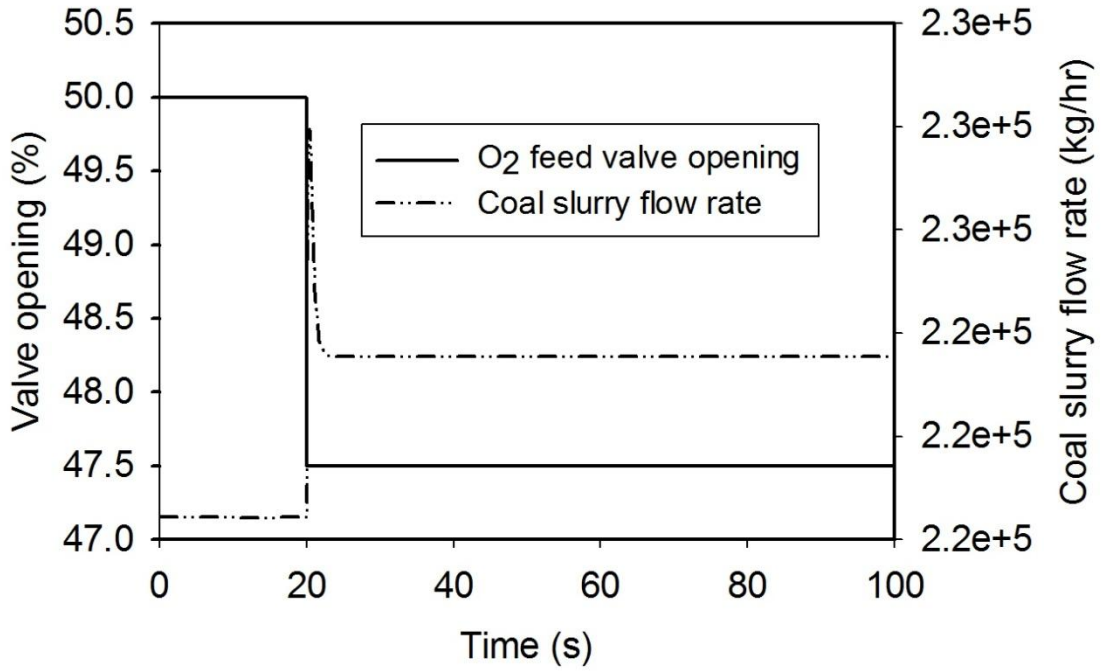

Figure 5.11 Oxygen valve position % opening and coal slurry flow rate

The responses in the flow rates can be explained by similar reasoning based on the pressure-flow relationships presented before.

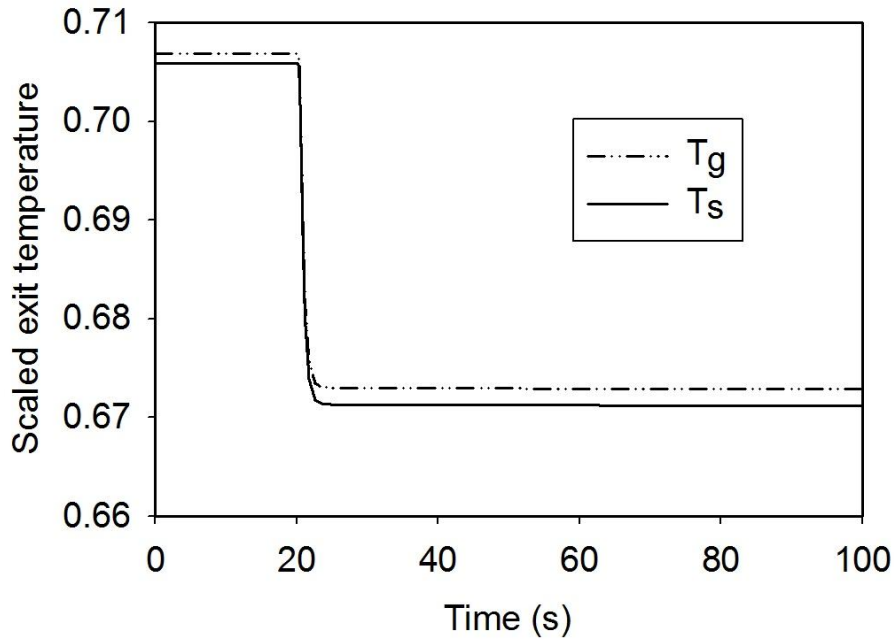

Figure 5.12 Scaled exit phase temperature profiles response to a 5% step change decrease in oxygen feed stream valve position opening

The temperature response is shown in Figure 5.12 which shows a step decrease in the scaled exit gas and solid temperatures. This is due to the reduction in the oxygen flow rate and an increase in the coal slurry flow rate which results in a reduced oxygen-to-coal ratio (at constant water-to-coal ratio) a consequence of which is reduced levels of combustion in the gasifier. The corresponding key syngas species profiles are given in Figures 5.13 and 5.14 that show a step reduction in CO_2 a combustion product and a step increase in combustible gases CO and H_2, which is consistent with the above observations. Although not shown, this change resulted in a reduction in the carbon conversion.

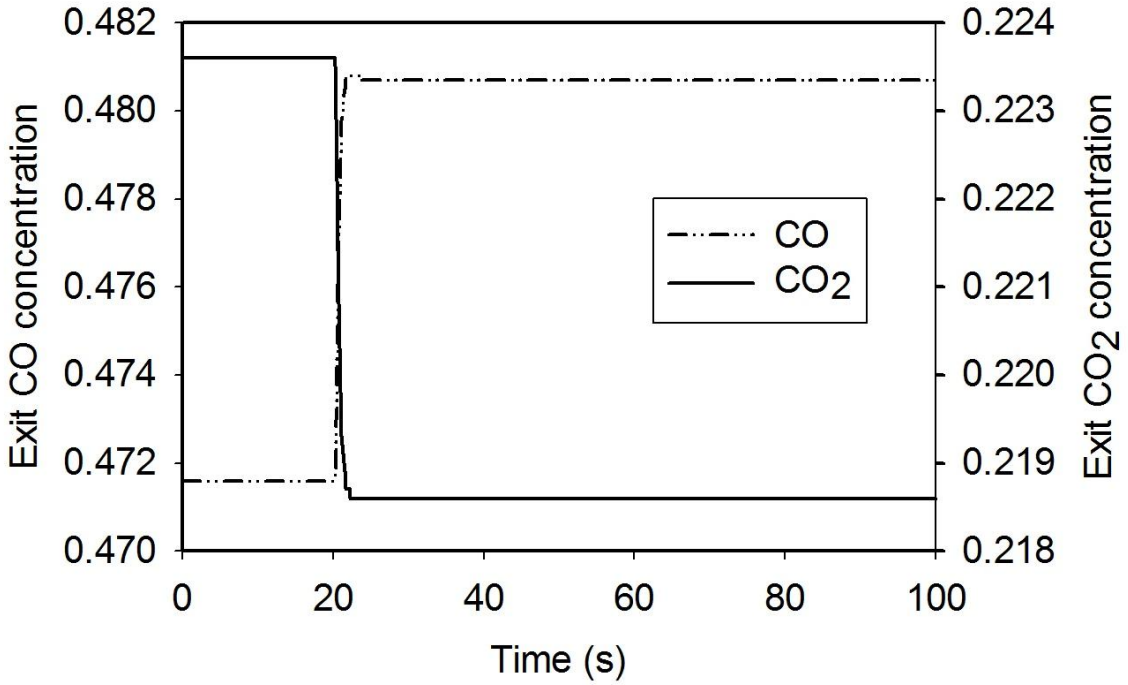

Figure 5.13 Exit CO and CO_2 response profiles due to a 5% step change decrease in oxygen feed stream valve position opening

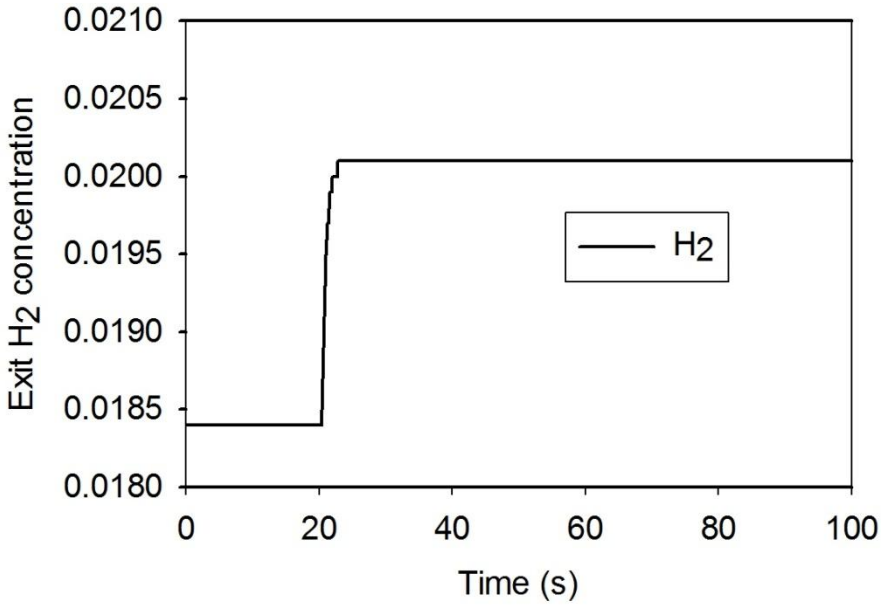

Figure 5.14 Exit Hydrogen response profile to a 5% step change decrease in oxygen feed stream valve position opening

In practical gasifier operation, it is common practice for the oxygen-to-coal ratio to be maintained at a desired value or the exit temperature to be maintained at a certain value or range, which requires inclusion of controllers to achieve this purpose. This closed loop dynamic gasifier operation was performed and the results presented in the next section.

5.4 Closed Loop Dynamic Run

In the closed loop dynamic run, controllers are added to the model to achieve a given control objective. The controllers are added to control certain key variables such as flow rates, the oxygen-to-coal ratio, water-to-coal ratio and the exit gasifier temperature among others. In gasifier operation, one of the main operating objectives is to achieve a certain level of carbon conversion. As reported before, conversion strongly depends on the gasifier temperature, oxygen-to-coal and water-to-coal ratios. Thus, any of these key parameters or variables is a potential control variable for achieving a selected conversion level. In the current study, the control strategy was based on two control variables namely the oxygen-to-coal ratio and the exit gasifier temperature and this is considered further in the “Control Schemes” section below.

5.4.1 Control Schemes

Two control schemes (I and II) were considered to test the dynamic model's closed loop response.

5.4.2 Control Scheme I

In the first control scheme shown in Figure 5.4.1, the oxygen-to-coal ratio was the key control variables in the dynamic simulation.

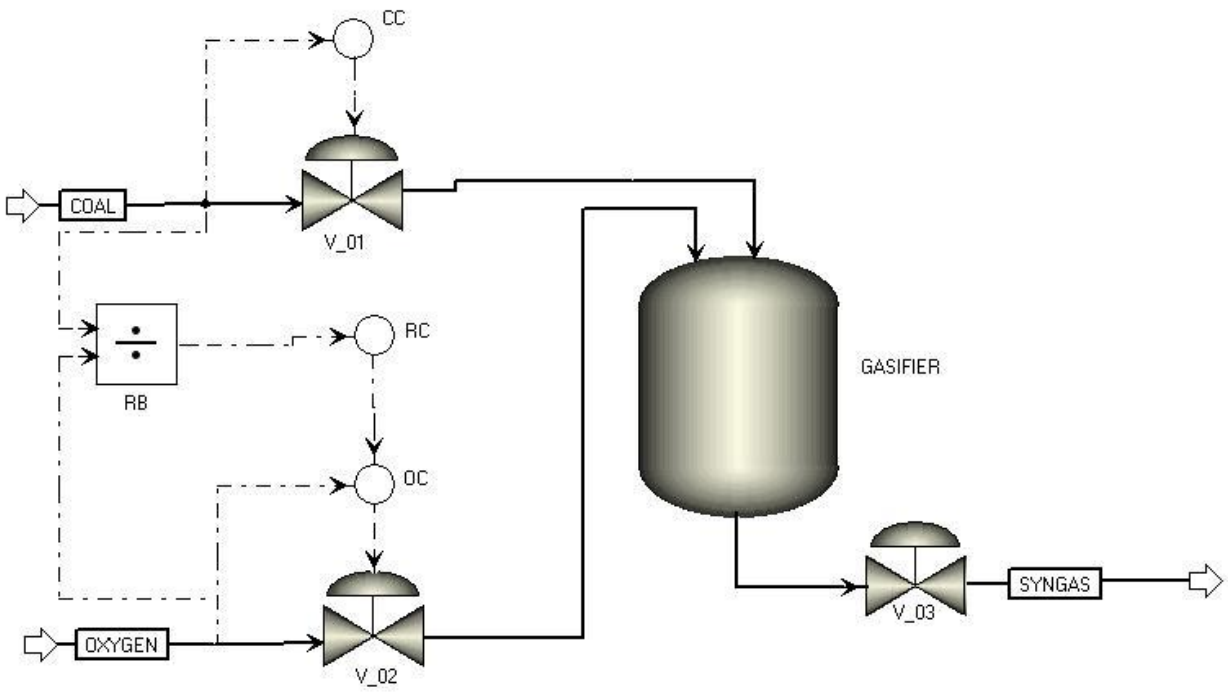

Figure 5.15 Gasifier dynamic Control Scheme I

In Figure 5.15, flow controllers CC and OC control the coal slurry and oxygen flow rates respectively while controller RC controls the oxygen-to-coal ratio. RB is a ratio block added to calculate the oxygen-to-coal ratio, which is the process variable (PV) that is sent to controller RC. The output of RC is the remote set point to the oxygen controller (OC). In other words the

flow rate of oxygen is controlled in such a way that the desired oxygen-to-coal ratio set point (SP) of OC is maintained.

5.4.3 Control Scheme II

In the second control strategy, shown in Figure 5.16, the exit gasifier temperature is the key control variable. As a disturbance is introduced into the process, the control objective is to reject the disturbance by manipulating the oxygen flowrate.

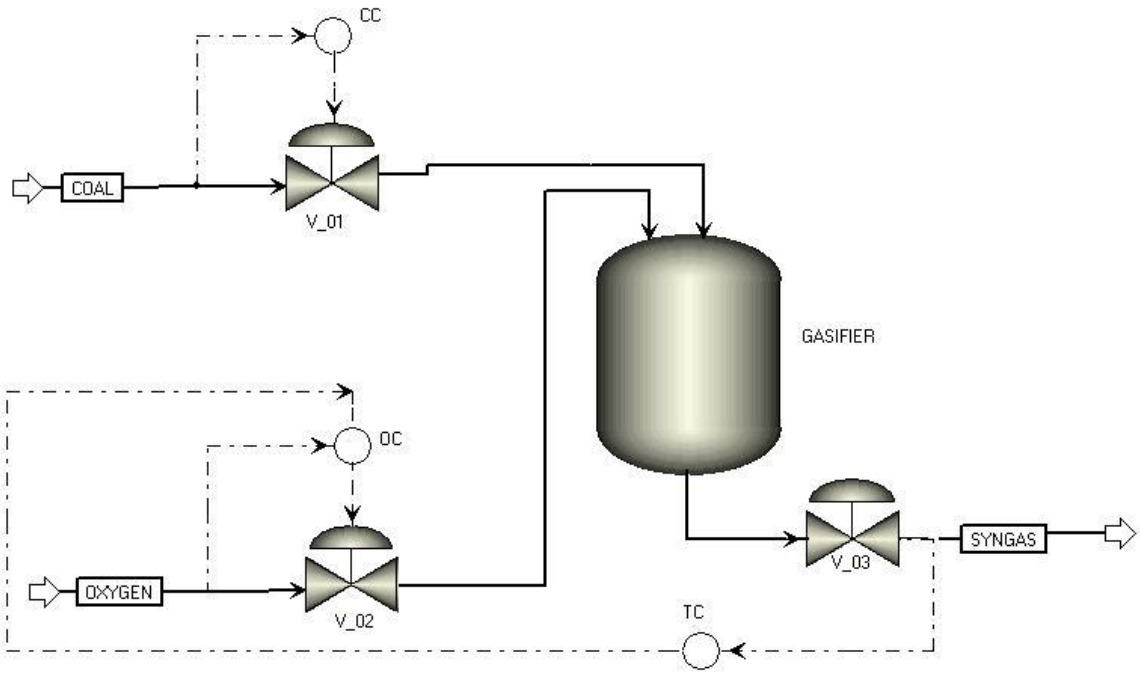

Figure 5.16: Gasifier dynamic control scheme II

In Figure 5.16, controllers CC and OC control the coal slurry and oxygen flow rates respectively. A third controller, TC is introduced to control the exit gasifier temperature as explained above. The set point (SP) of TC is the desired gasifier temperature and the TC output is the remote set point input to the OC. In other-words, as disturbances are introduced to the coal flow rate, the oxygen controller responds by adjusting the oxygen flow rate in order to maintain the exit temperature SP.

In both control schemes, satisfactory control performance for servo as well as regulatory control is desired and thus a careful tuning of the controllers is an important step. The tuning of these controllers is briefly discussed in the next section.

5.4.4 Controller Tuning

The performance of the above controllers depends on, among other factors, the controller tuning parameters that are established through standard tuning procedures using various tuning rules/laws. This is generally a trial-and-error procedure, which can lead to different values depending on which tuning rules are used.

In the current study, the controllers were tuned by both the trial and error approach and the in-built step test method in ACM. The step test method is used to obtain the open loop gain, time constant and time delay values that are then used to calculate the approximate tuning parameters using the desired tuning rules. Details can be obtained in standard control text-books.

Example sample tuning parameters calculated from one of the step test methods for the temperature controller are given in Table 5.2. The open loop gain, integral time and time-delay values obtained while tuning the temperature controller (TC) using a 1% change step are given in Table 5.1.

Table 5.1 Open loop tuning parameters for TC (PID)

Open loop parameter	***Value***
Gain (K)	1.33246
Time constant (*I*)	0.03643
Time-Delay (T_d)	0.02164

Table 5.2 Step test Controller Tuning Parameters for TC (PID)

Tuning rule/Parameter	***Ziegler-Nichols***	***Cohen-Coon***	***IMC***	***IAE***	***ISE***	***ITAE***
K	1.518895	1.868146	0.748742	1.740088	1.835652	1.667944
I	0.04328	0.043353	0.047254	0.028091	0.022358	0.029493
T_d	0.01082	0.007102	0.008342	0.009712	0.012081	0.008266

The Ziegler-Nichols based tuning parameters were used in all the dynamic studies performed in the current study. In the next section, dynamic response results to dynamic disturbances introduced in each of the above control schemes are presented.

In what follows, some of the dynamic responses to disturbances in the coal flow rate and oxygen-to-coal set points are presented.

5.4.5 Control Scheme I (Ratio Controller) Responses

As illustrated above, in this scheme the coal flow or oxygen flow rates are adjusted while maintaining a given oxygen-to-coal ratio which is controlled by a ratio controller.

5.4.5.1Responses to a ramp increase in the coal slurry flow rate

With both the oxygen and coal controllers in cascade mode, a ramp increase in the coal flow rate was introduced at a rate of 5% per minute, which is typical ramp change in practical gasifier operation [EPRI, Final Report, RP 1459, 1990].

Figure 5.17 shows the coal slurry flow controller process variable (PV) response to a set point (SP) ramp change. As the ramp change is introduced to the set point, the process variable starts to track the increasing flow rate. In the figure, the PV takes approximately 450 s before finally reaching the new set-point.

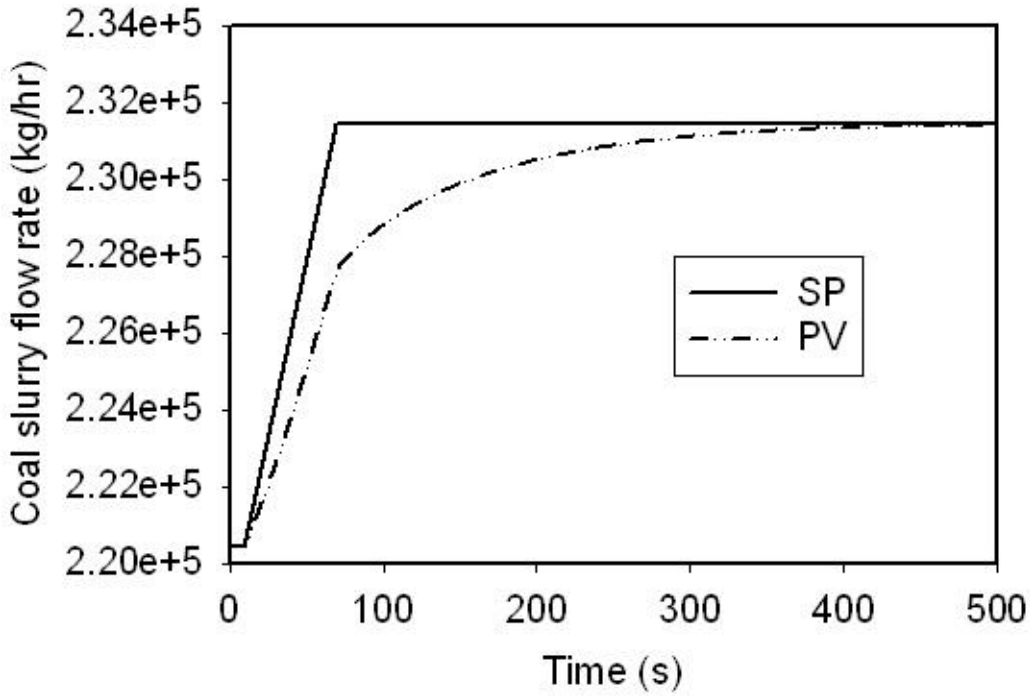

Figure 5.17 Coal slurry controller (CC) process variable (PV) response to set point (SP) ramp

While the PV tracks the SP, the oxygen controller's response is to increase the oxygen flow rate (Figure 5.19) in such a way that the oxygen-to-coal ratio, which initially decreases as the coal flow rate increases, is restored to the desired set point as shown in Figure 5.18.

Figure 5.19 shows the responses of the oxygen flow and the exit gas temperature. After an initial delay, the oxygen flow gradually increases so as to restore the oxygen-to-coal ratio set point. On the other hand, the temperature initially decreases due to the increasing coal flow rate,

and then gradually increasing as the oxygen flow rate increases and then finally leveling off as the oxygen-to-coal ratio is restored.

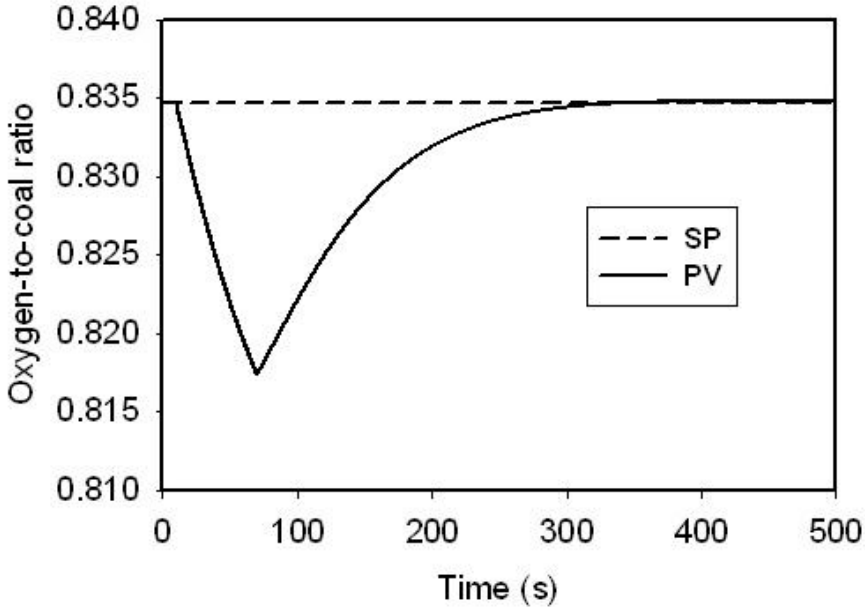

Figure 5.18 Ratio controller PV and SP response profiles to a ramp increase in coal flow.

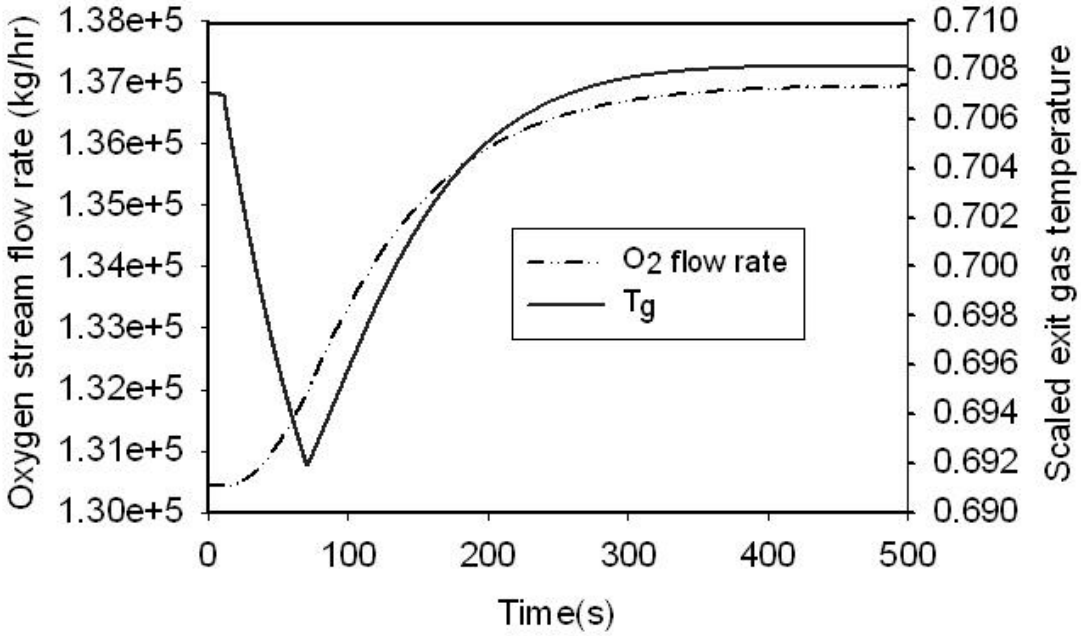

Figure 5.19 Oxygen flow and scaled exit gas temperature response profiles to a ramp increase in the coal slurry flow

The gas species responses are shown in Figure 5.20 and 5.21. In Figure 5.20 there is an initial increase in CO as the increasing coal flow rate reduces the temperature and hence reduces the extent of the combustion reactions, this results in an observed initial drop in CO_2 a product of carbon or CO combustion. As the oxygen flow increases, the CO decreases and the CO_2 increases, and then level off at values similar to their starting values.

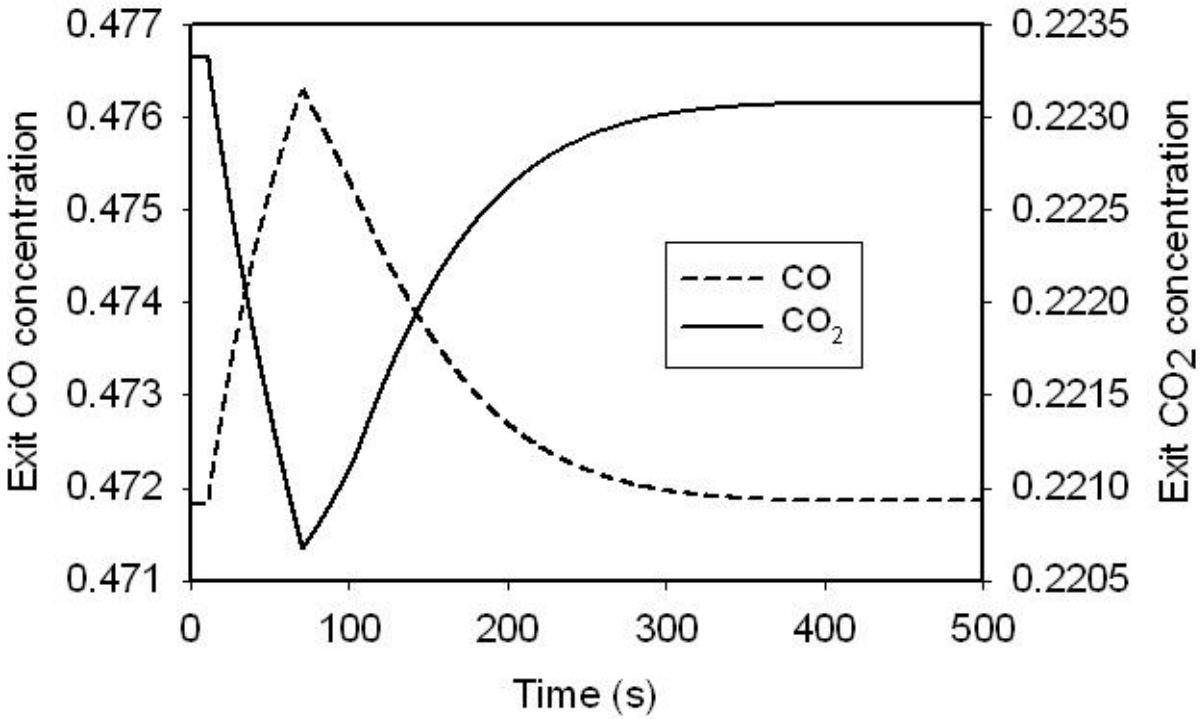

Figure 5.20 CO and CO_2 exit concentration (mass fractions) responses to a ramp increase in coal slurry flow

As expected the hydrogen response is similar to that of CO as shown in Figure 5.21 and can be explained by similar reasoning to the CO response profile.

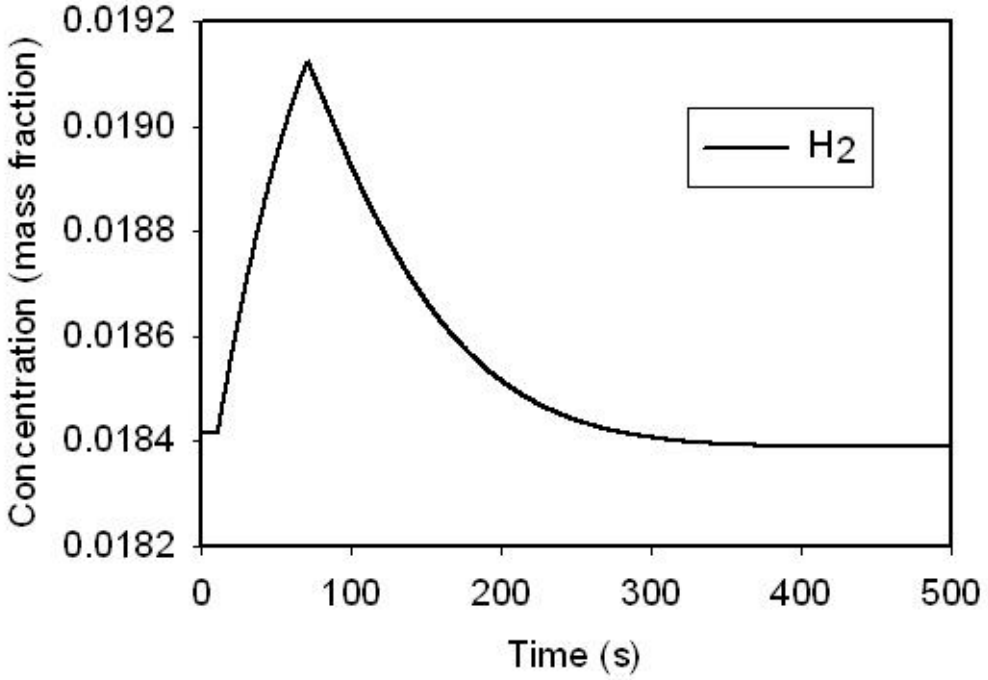

Figure 5.21 H_2 Response profile to the ramp increase in the coal slurry flow rate

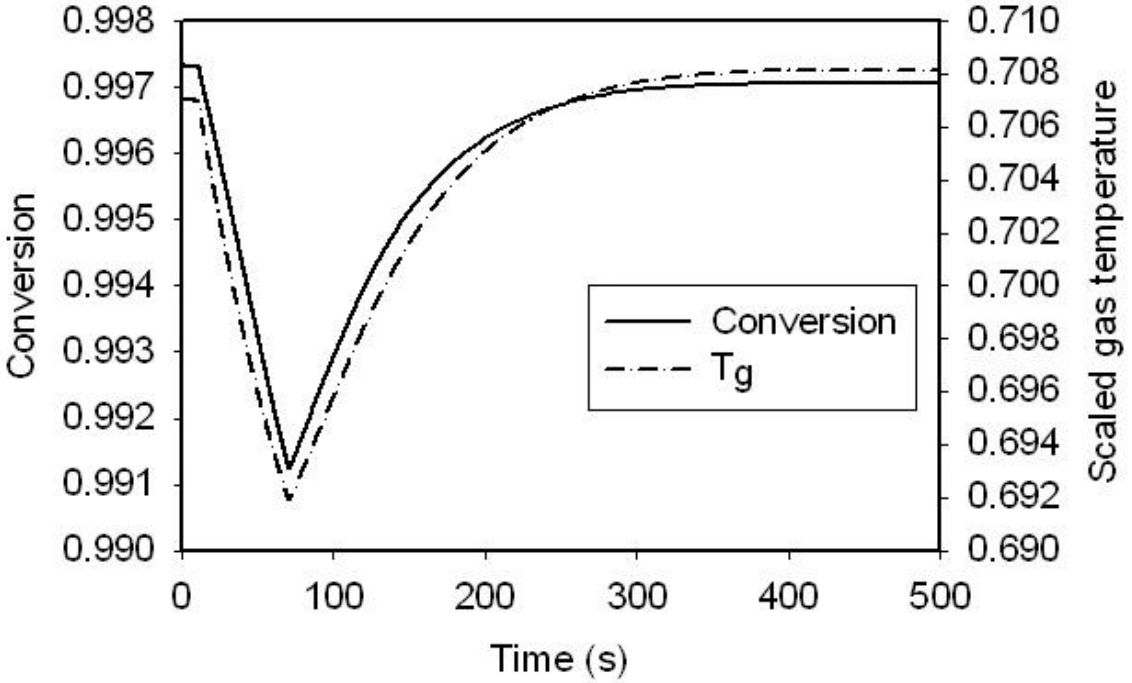

Figure 5.22 Conversion and scaled exit temperature response to ramp increase in coal slurry flow rate

In Figure 5.22, the carbon conversion response is shown together with the scaled exit gas temperature. Because the carbon conversion is a strong function of temperature, its response mirrors that of temperature; decreasing with a decrease in temperature and then increasing as the temperature starts to increase and finally then leveling off as the temperature reaches a new steady-state value.

5.4.5.2 Responses to a step and ramp change in the oxygen-to-coal ratio

In this section, responses to a ramp increase and a step decrease in the oxygen-to-coal ratio are presented. Figures 5.23 -5.26 show the responses to a ramp increase in the oxygen-to-coal ratio. The change was introduced in the model (at time = 20s) by ramping the set point (SP) variable value of the ratio controller from 0.835 to 0.862 as shown in Figure 5.23.

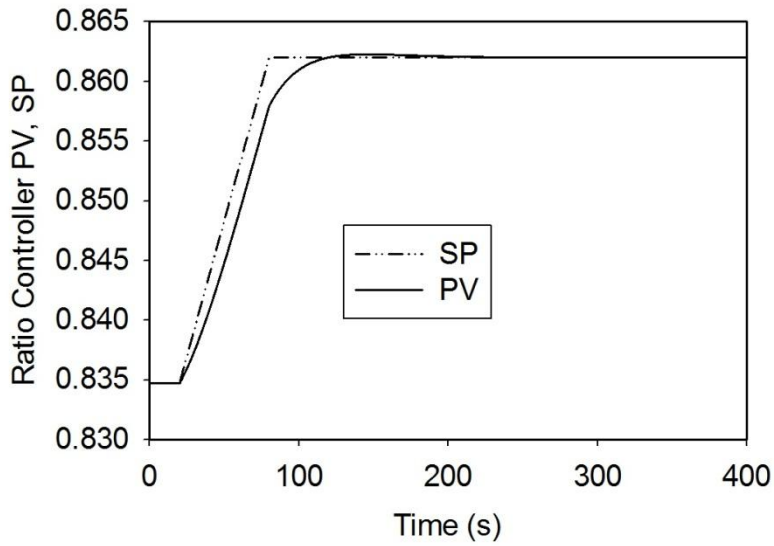

Figure 5.23: Ratio controller set point (SP) ramp change and process variable (PV) response

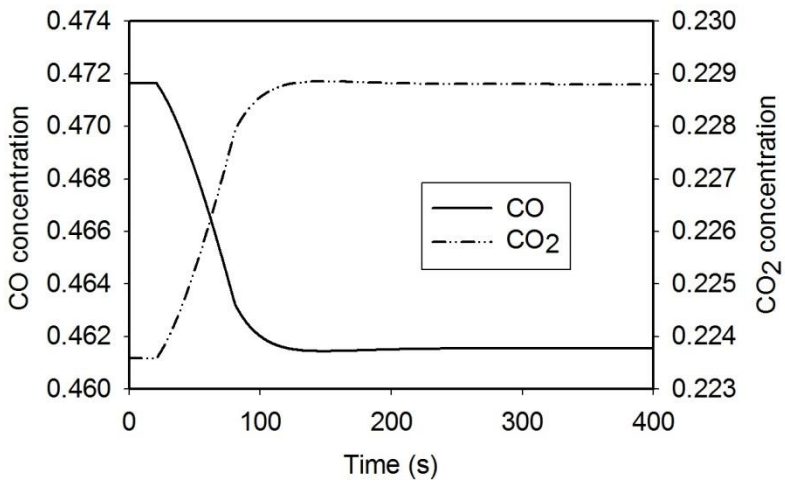

Figure 5.24: Exit CO and CO_2 concentration response to a ramp increase in oxygen-to-coal ratio

In Figures 5.24 and 5.25, the transient responses of the exit gasifier CO, CO_2 and H_2 concentration to an increase in the oxygen-to-coal ratio are shown. As expected, an increase in this ratio leads to an increase in the combustion level within the gasifier and as a result the concentration of the combustible gases (CO and H_2) decreases while that of CO_2, a combustion product increases.

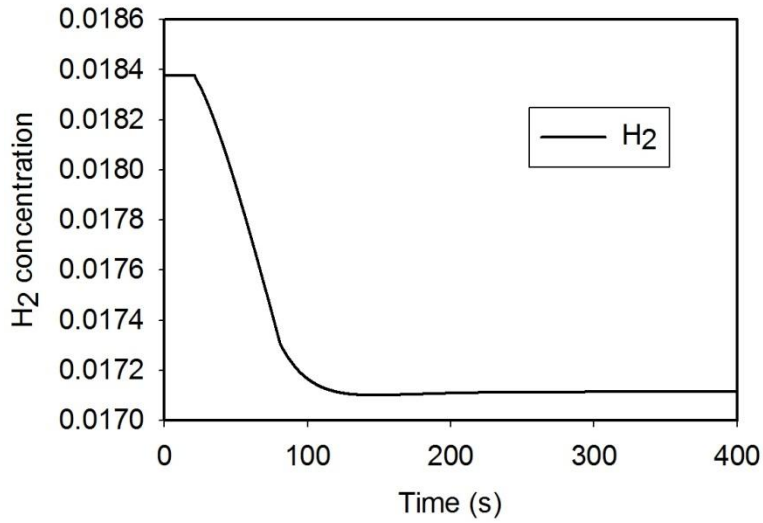

Figure 5.25: Exit H_2 concentration response to a ramp increase in oxygen-to-coal ratio

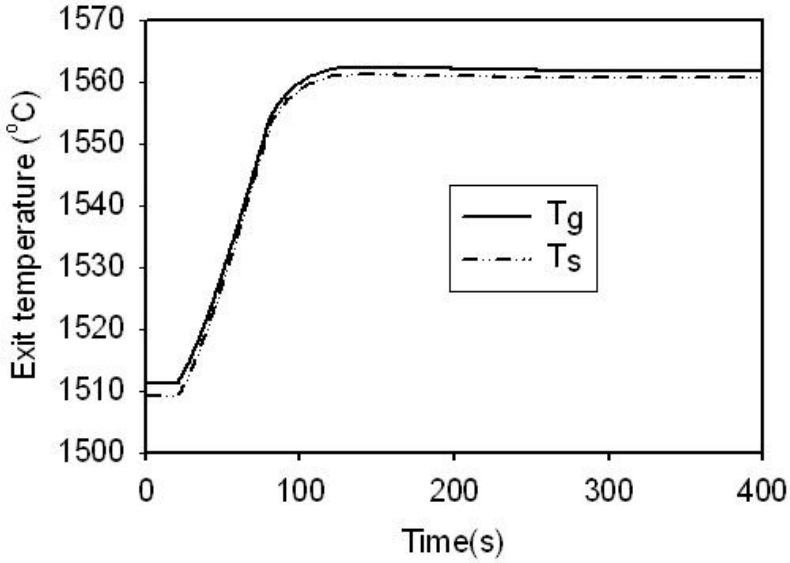

Figure 5.26: Exit gas (T_g) and solid (T_s) phase temperature responses to a ramp increase in oxygen-to-coal ratio

Lastly, in Figure 5.26, the response of the exit temperatures of the gas and solid phases are plotted and as expected, these temperatures increase with an increase in the oxygen-to-coal ratio as previously observed in the steady-state results of Chapter 4.

On the other hand, directionally reverse responses are expected if the oxygen-to-coal ratio is ramped down or decreased through a step decrease. Some of the responses to a step decrease from 0.835 to 0.80 in the oxygen-to-coal ratio (Figure 5.27) are shown in Figures 5.28-5.30. The set point of the oxygen-to-coal ratio controller was changed from 0.835 to 0.8. This change results in a reduction in the extent of the combustion reactions within the gasifier leading to a step increase in the exit combustible gases H_2 and CO (Figure 5.28) and a decrease in the exit temperatures of the gas and solid (Figure 5.29). It also leads to a decrease in the exit CO_2 concentration and carbon conversion as shown in Figure 5.30.

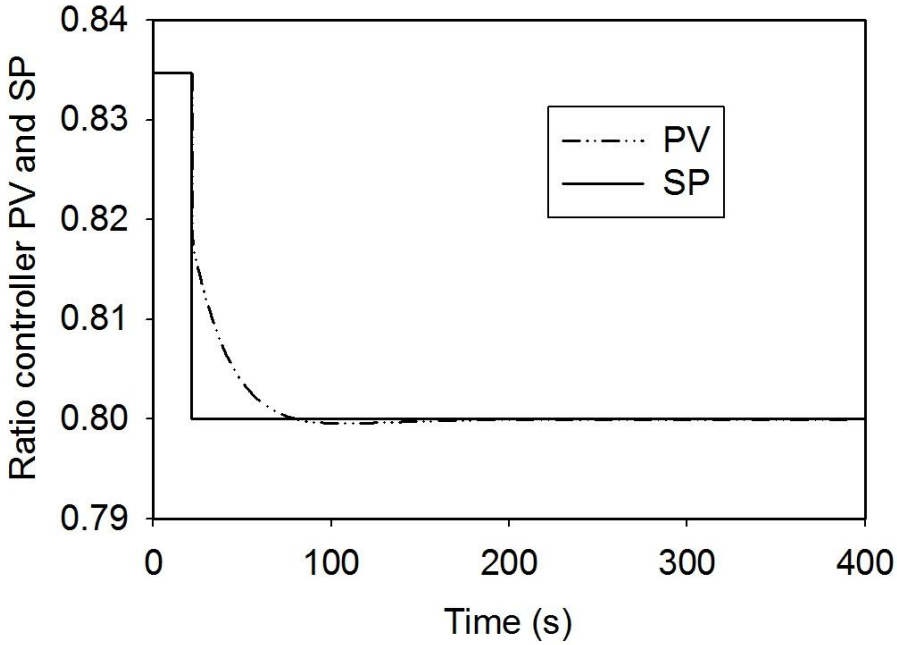

Figure 5.27 Step change decrease (0.835 to 0.8) input in the oxygen-to-coal ratio

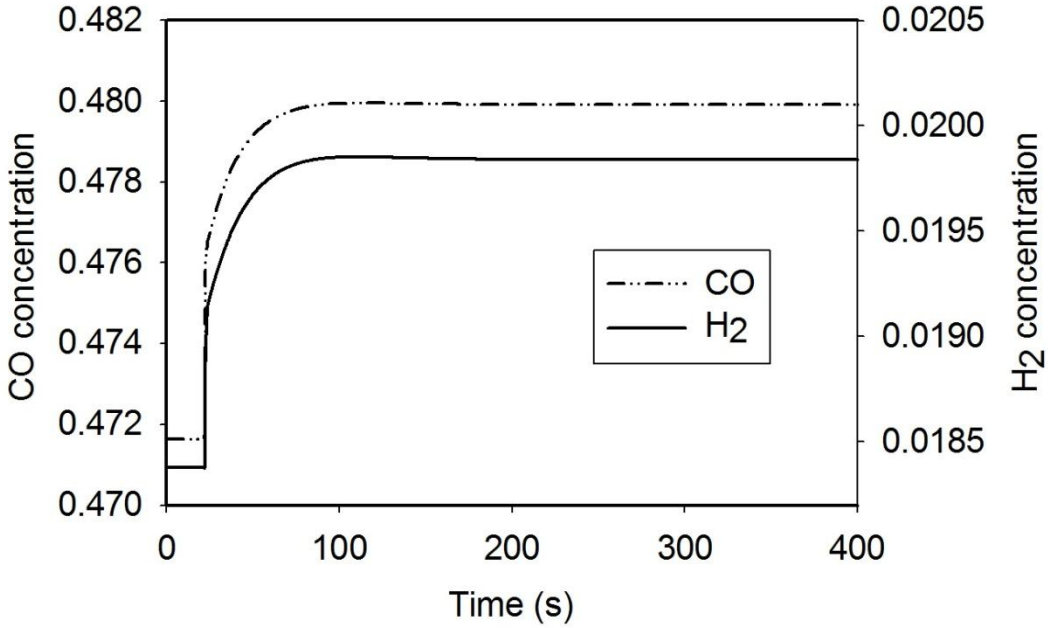

Figure 5.28 Exit CO and H_2 responses to a step change decrease in the oxygen-to-coal ratio

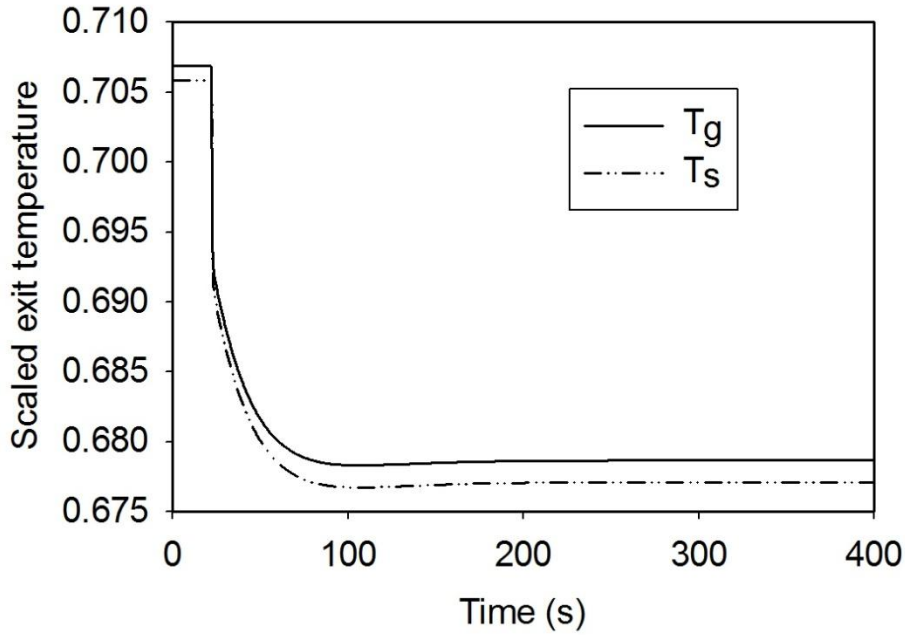

Figure 5.29 Scaled exit temperature response to a step change decrease in the oxygen-to-coal ratio

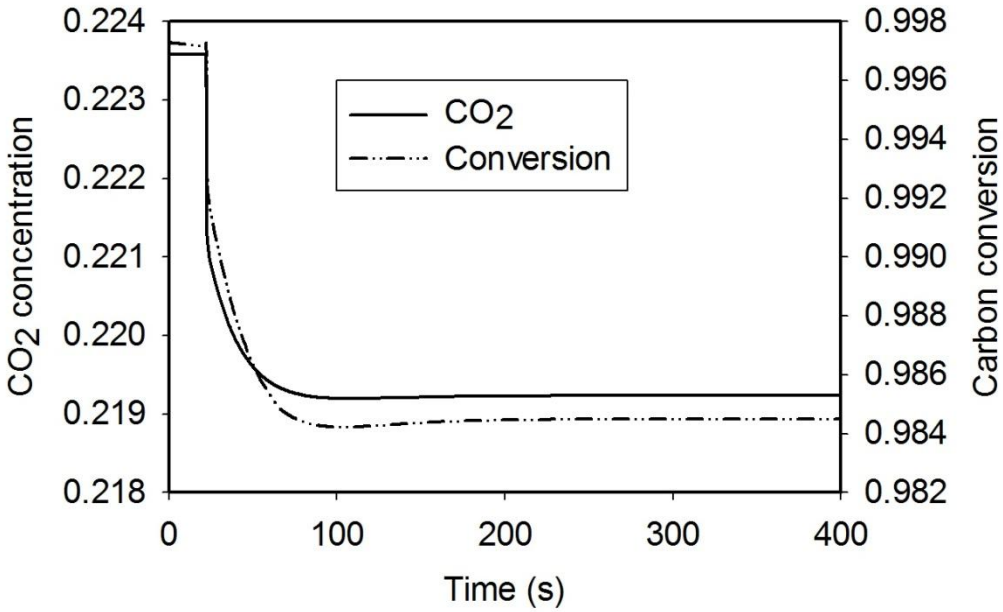

Figure 5.30 Exit CO_2 concentration and Carbon conversion response to a step change decrease in the oxygen-to-coal ratio

5.4.6 Control Scheme II (Temperature Controller) Responses

In this section, dynamic disturbances are introduced in the model while maintaining the exit gasifier temperature at a given set point value using a temperature controller as explained in section 5.4.3. The responses to a 5% ramp increase in the coal slurry flow rate (Figure 5.31) are presented in Figures 5.32-5.34.

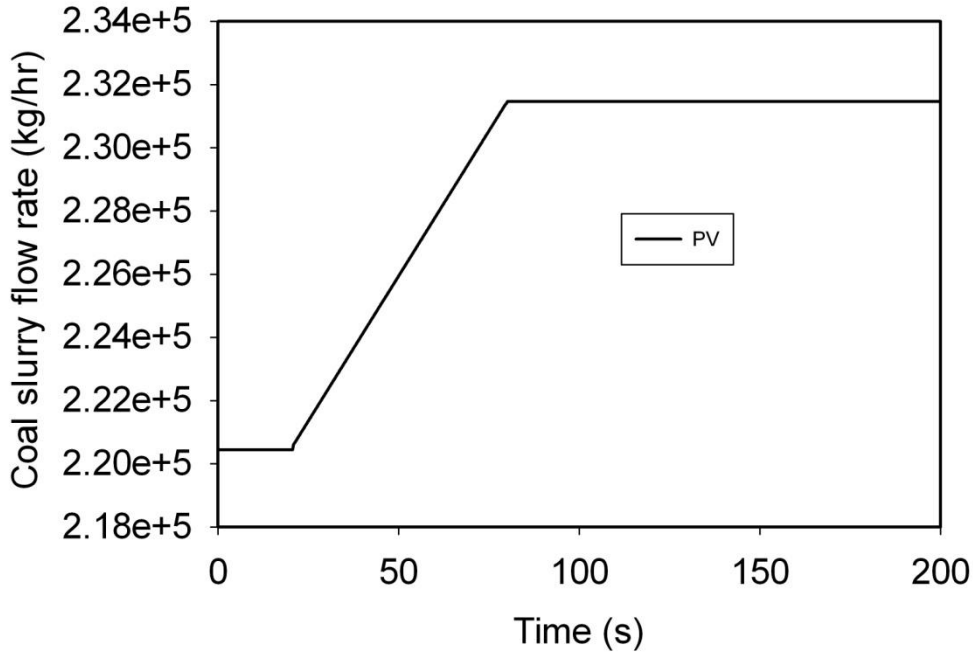

Figure 5.31 Coal slurry flow ramp increase input

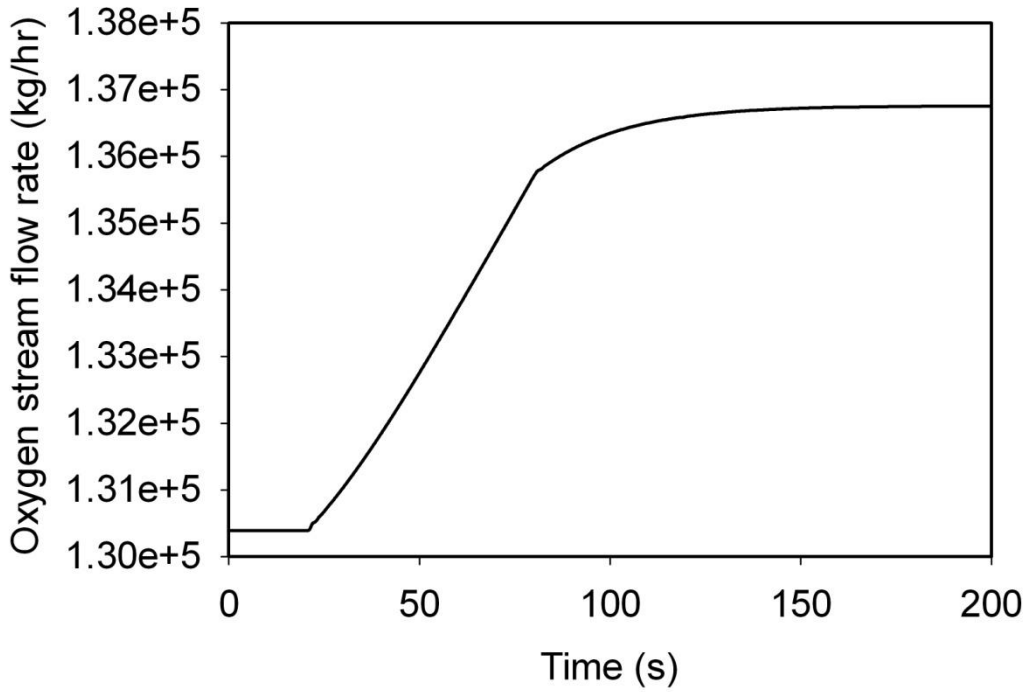

Figure 5.32 Oxygen flow response to a ramp increase input in coal flow rate

Figure 5.32 shows the process variable (PV) response of the oxygen flow controller. The oxygen flow increases when the slurry flow rate is increased in order to maintain the exit gasifier temperature to the set point value of the temperature controller which is shown in Figure 5.33.

In Figure 5.33, the temperature controller process variable (PV) and set point (SP) profiles are plotted. The temperature PV initially decreases up to the end of the coal slurry ramp and then gradually increases untill it matches the temperature set point. Similar responses are observed with the exit solid temperature as shown in Figure 5.34.

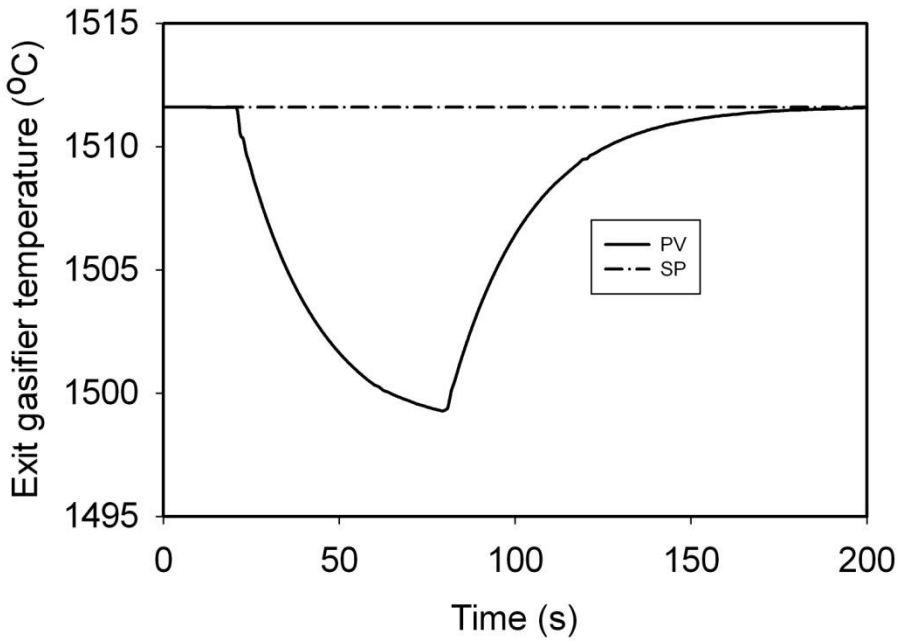

Figure 5.33 Controlled exit gasifier temperature response to ramp increase in coal slurry flow

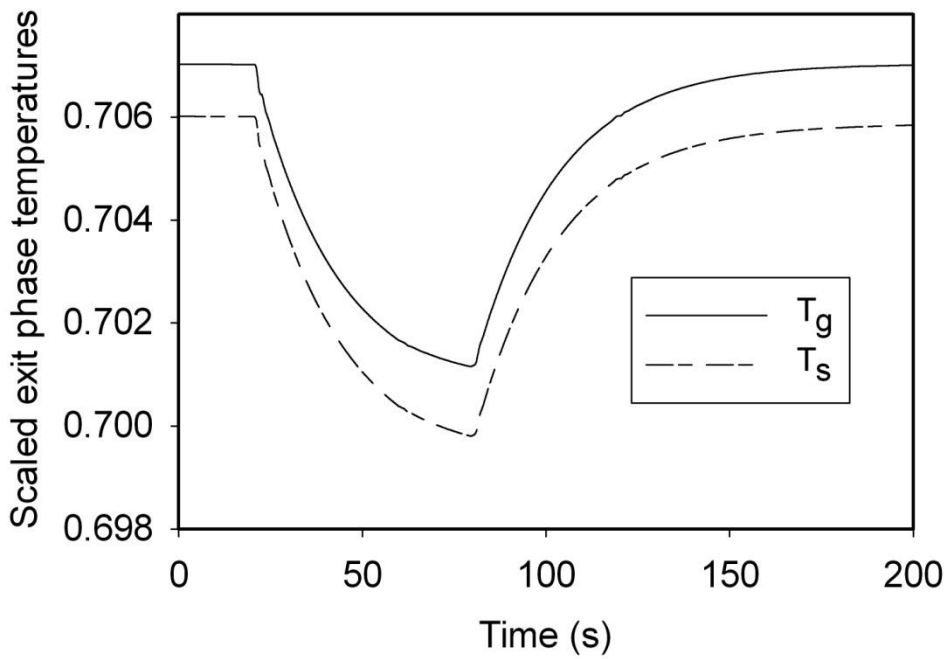

Figure 5.34 Scaled exit gas (T_g) and solid (T_s) temperature response to ramp increase in coal slurry flow rate in control scheme II

5.4.7 Dynamic Model Validation

Similar to the steady-state model, the results from the dynamic model are compared with the available experimental dynamic data from the operating industrial gasifiers or/and with the previous dynamic studies. Scarcity of dynamic data in the open literature makes it difficult to validate the model in a wide operating range. However, some experimental data have been reported by certain research groups in academia, industry and government laboratories that may be used for this purpose.

An EPRI report [EPRI, Final Report, RP 1459, 1990] presented some data from dynamic studies of the Cool Water gasification project, which was the first commercial-scale prototype of an integrated gasification combined cycle (IGCC) power plant. Results from the load-following studies on the plant were reported. The tests was performed in two parts; the first was to change the plant load from approximately 100% to approximately 50 % load, and the second part was to return the plant load from 50% to 100%. In both cases, transient responses of the key gasifier variables such as the exit gasifier temperature were plotted. A control structure analogous to Control Structure I of this study was employed. It was also reported that a plant fuel feed change from 65% to 100% corresponded to a change in power output of 50% to 100%.

One way to validate the current model predictions was to implement the coal feed turndown from 100% to 65% to mimic the 100% to 50% plant load change and then compare the exit temperature profile to that in the report.

To achieve this objective, it was necessary to modify Control Scheme I, which was used for this study as shown in Figure 5.35. In the Cool Water project, a time-delay was used while ramping the gasifier feed flow. While ramping down the feed flow, the oxygen flow is decreased first followed by the decrease in the slurry flow. A reverse strategy is used while ramping up the

slurry flow. This strategy avoids temperature excursions in the gasifier during ramping. Control Scheme I is accordingly modified as shown in Figure 5.35 by including a time-delay in the loop

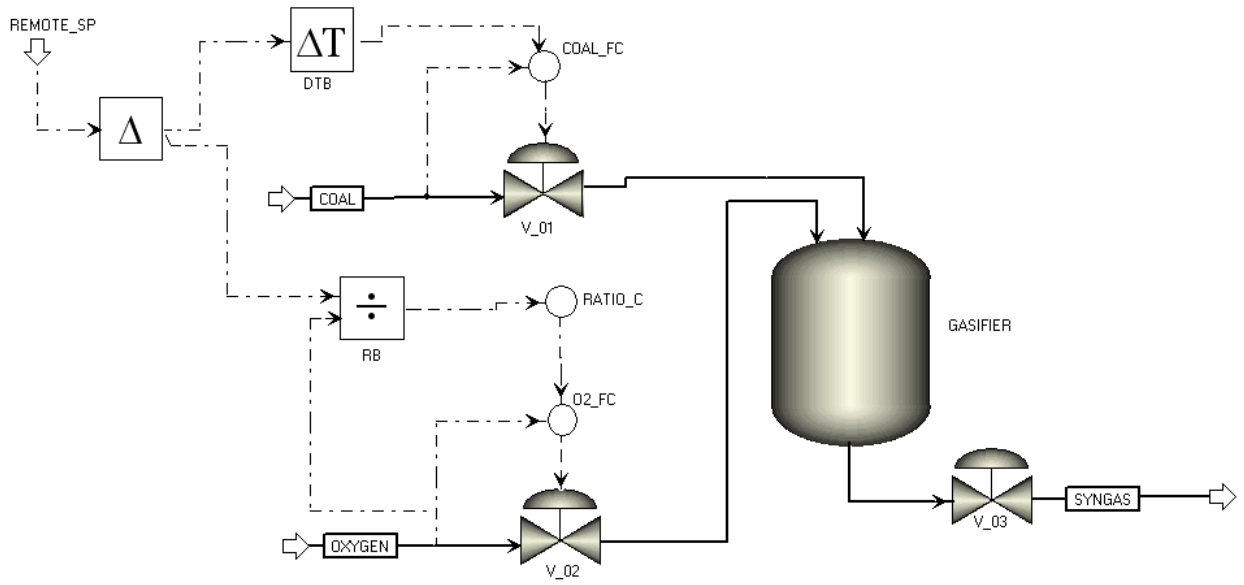

Figure 5.35: Modified Control Scheme I

In this modified Control Scheme I, in addition to the ratio controller, (RATIO_C) and the oxygen (O2_FC) and coal slurry (COAL_FC) flow controllers (previously denoted as RC, OC and CC respectively), as well as the Ratio block (RB) , and a dead-time/time delay block (**ΔT** or DTB) were added. However, the addition of the dead-time block resulted in the introduction of a lag time, which is an additional tuning parameter. The set-point of the COAL_FC is introduced into a comparator block (denoted by Δ) and sent to the coal flow controller via the time-delay block. By using a flowsheet script, the gasifier throughput is then ramped down to 65% at 5% change/min as shown in Figure 5.36.

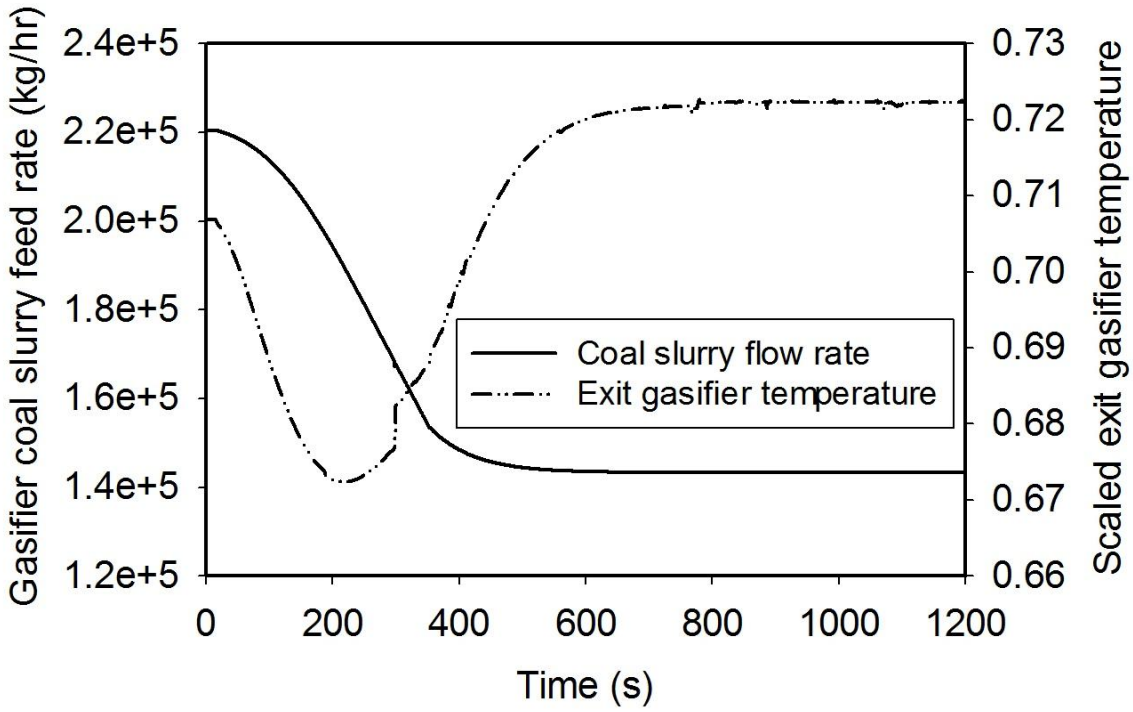

Figure 5.36: Exit gasifier temperature response to a 65% turndown (TD) in the coal feed rate

In Figure 5.36, there is an initial decrease in the gasifier exit temperature before the temperature gradually increases and leveling off. The initial decrease in temperature is attributed to the controller tuning parameters used in the model. However, the eventual increase and leveling off of the exit gasifier temperature is qualitatively similar to the response of the Cool Water temperature profile. Thus the current model predictions are qualitatively consistent with the data from the commercial gasifier.

The modified Control Scheme I was further tested to see if lower turndowns could be achieved with it. In one of the cases examined, a 50% turndown in the coal flow rate at 5% change/min was implemented. The results which are plotted together with those from the 65% turndown are shown in Figure 5.37.

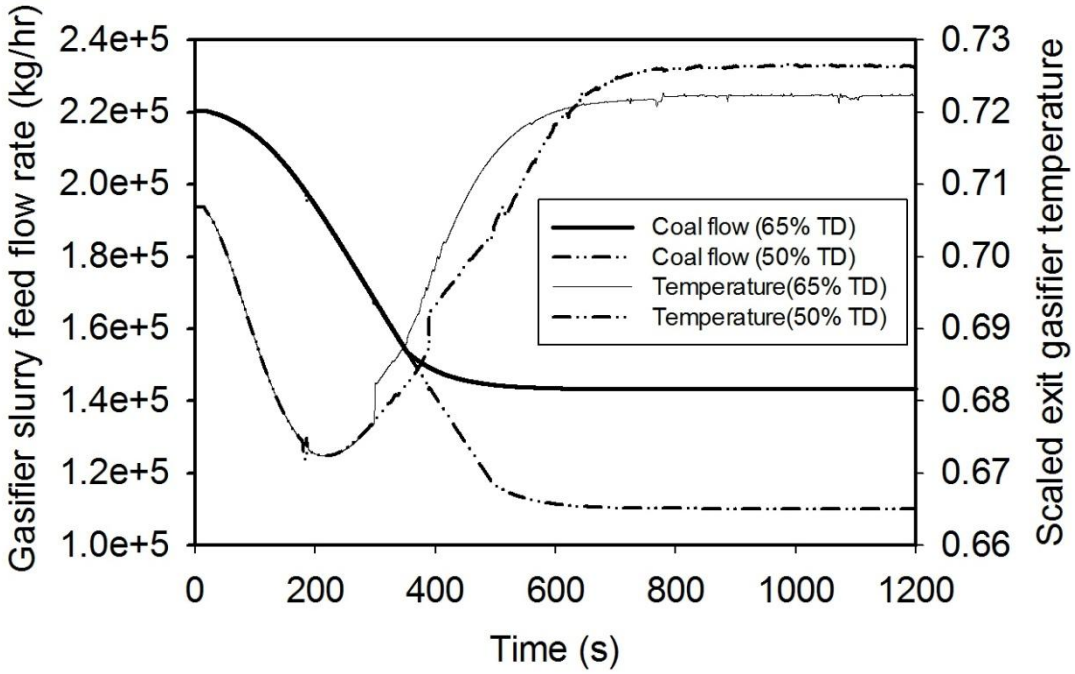

Figure 5.37: Temperature responses to both 50% and 65% turndown (TD) in coal flow rates

Results of Figure 5.37 show that the final exit gasifier temperature is higher for the higher turndown (50%) in the coal flow than for the lower turndown (65%) in the coal flow rate as would be expected. Overall the results of the model predictions are consistent with the observed industrial/practical gasifier operation.

Additionally, some dynamic data has been recently obtained for gasifier related studies (Robinson and Luyben, 2008; Monaghan et al., 2010; Yang et al., 2011]. Although these studies are for entrained gasfier type, they are significantly different from the current study. No direct comparison can be made with our dynamic responses with Monaghan et al.'s study, and although Yang et al.'s model is for an oxygen-staged slagging entrained gasifier, they report responses in temperature and some gas species profiles to a step input change in the gasifier oxygen feed flow rate. Qualitatively, the current model responses to such changes are similar to those in Yang et al. (2011). In the simple dynamic gasifier model of Robinson and Luyben, (2008) some

responses to disturbances in feed streams flow rates are presented. Although the control structure in the model is in somewhat different from the current study, the temperature response to the increase/decreases in key flow streams is similar to those obtained in the current study.

In conclusion to the model validation, the dynamic model simulation results are consistent with the dynamic run results of an industrial commercial-size gasifier. However, it should be recognized that as a one-dimensional model, it may not be possible to capture all aspects of the industrial gasifier.

Chapter 6

Conclusions and Recommendation for Future work

Results from the mathematical modeling of a single stage downward-firing GEE/Texaco type gasifier have been presented and the general conclusions and recommended future work are presented below:

- The steady-state model results of chapter 4 are consistent with previous studies and theoretical understanding of the gasification process and were validated with Texaco pilot plant data as well as the industrial data from the Tampa Electric Company (TECO). Appreciable agreement of the model prediction with the experimental data was obtained.
- The steady-state parametric studies performed with the model showed that the oxygen-to-coal ratio had a stronger effect on the carbon conversion than the water-to-coal while at the same time the water-to-coal ratio had a stronger effect on the product gas distribution of the exit syngas than the oxygen-to-coal ratio. The parametric studies of the model are consistent with previous studies.
- Unlike in most of the previous one-dimensional models in which simplified energy balances have been considered, the current study incorporated a detailed radiation model which considered energy transfer between the various gasifier surfaces using variable radiation view factors.
- The study assumed no a *priori* wall temperature profile and the wall temperature was calculated as one of the solution output. No such results exist in the literature and thus no verification of the observed wall temperature could be performed due to absence of such data in the open literature.

- The steady-state model was extended to obtain a dynamic model by inclusion of temporal terms in the model balance equations. Dynamic model studies were performed to obtain the model responses to dynamic disturbances input to the model. Both ramp and step change inputs were introduced in the model in both open loop (no control action) and closed loop (with controllers) and the responses were consistent with industrial operations observations.
- Even though qualitative comparisons of the model results with the industrial data are found satisfactory, some modifications would be needed including changes in the gasifier size, plant throughput and feed composition for direct comparison of the model results with such data

However, the model shortcomings present some opportunities for future work which may include the following recommendations:

- As a simplification in the model, the ash was assumed to come out of the gasifier with the mixed stream but in reality the high temperatures in the gasifier may lead to slagging of the ash and inclusion of slag model would be an appropriate extension of the current model.
- Although the dynamic responses of the model are consistent with the industrial operation of the gasifier, the actual simulation times are about an order of magnitude slower than the real time responses. Development of reduced-order models (ROM) of the gasifier would certainly help the model run in real-time simulation.

Finally, it would be interesting to know at what turndown the gasifier model would fail to solve as a result of failure to sustain the temperature requirements at the exit of the gasifier.

References

Anthony B. D.; Howard, B. J.; Hottel, C. H.; Meissner, P. H. Rapid devolatilization and hydrogasification of bituminous coal. *Fuel.* **1976**a. *55*, 121-128

Anthony, B. D.; Howard, B. J. Coal devolatilization and hydrogasification. *AIChE Journal.* **1976**, *22* (4), 625-656.

Arastoopour, H.; Gidaspow, D. Vertical pneumatic conveying using four hydrodynamics models. *Ind. Eng. Chem. Fund.* **1979**, *18* (2), 123

Badzioch, S.; Hawksley, W. G. P. Kinetics of thermal decomposition of pulverized coal particles. *Ind. Eng. Chem. Process Des. Develop.* **1970**, *9* (4), 521-530.

Bautista, J. R.; Russel, W. B.; Saville, D. A. Time –resolved pyrolysis product distributions of softening coals. *Ind. Eng. Chem. Fund.* **1986**, 25, 536-544

Bearth, C. Mathematical modeling of entrained flow coal gasification. PhD. Thesis, Department of chemical engineering, University of Newcastle, Australia, **1996**.

Benyahia, S.; Syamlal, M.; O'Brien, T. J. Summary of MFIX Equations, **2005-4.** URL http://www.mfix.org/documentation/MfixEquations2005-4-3.pdf .

Bhattacharyya, D.; Turton, R.; Zitney, S. E. Steady-state simulation and optimization of an integrated gasification combined cycle power plant with CO_2 capture. *Ind. Eng. Chem. Res.* **2011,** 1674-1690.

Bird, B. R.; Stewart, E. W.; Lightfoot, N. E. Transport phenomena, second edition, *John Wiley & Sons, Inc.* **2002.**

Brown, B. W.; Smoot, D. L. Smith, J. P.; Hedman, O. P. Measurement and prediction of entrained-flow gasification processes. *AIChE.* **1988**, *34* (3), 435-446.

Chen, C.; Horio, M.; Kojima, T. Numerical simulation of entrained flow gasifiers. 1: modeling of coal gasification in an entrained flow gasifier. *Chemical engineering Science.* **2000,** *55*, 3861-3874.

Chen, C.; Horio, M.; Kojima, T. Use of numerical modeling in the design and scale-up of entrained flow coal gasifiers. *Fuel*. **2001**, *80*, 1513-1523.

Choi, Y. C; Li, X. Y; Park, T. J; Kim, J. H; Lee, J. G. Numerical study on the coal gasification characteristics in an entrained flow coal gasifier. *Fuel*. **2001**, *80*, 2193-2201.

de Souza-Santos, L. M. Solid Fuels Combustion and Gasification: Modeling, Simulation, and Equipment operation. *Marcel Dekker Inc.* **2004.**

Deng, Z.; Xiao, R.; Jin, B.; Huang, H.; Shen, L.; Song, Q.; Li, Q. Computational fluid dynamics modeling of coal gasification in a pressurized spout-fluid bed. *Energy Fuels*, **2008**, *22*(3), 1560-1569.

Doraiswamy, L. K.; Sharma, M. M. Heterogeneous Reactions: Analysis, Examples, and Reactor Design. 1: Gas-solid and solid-solid reactions, *John Wiley & Sons, New York*, **1984.**

EPRI, Cool water coal gasification, Final Report, RP 1459, **1990**

Fan, L–S.; Zhu, C. Principles of Gas-Solid Flows, *Cambridge University Press*, New York, **1998**.

Friedrichs, G.; Wagner, H. Direct Measurements of the reaction NH2+H2→NH3+H at temperatures from 1360 to 2130 K. *Zeitschrift für Physikalische Chemie.* **2000**, 214(8), 115-1160.

Gavalas, G. R.; Cheong, P. H.; Jain, R. Model of coal pyrolysis. 1. Qualitative development. *Ind. Eng. Chem. Fundam.* **1981a**, *20*, 113-122.

Gavalas, G. R.; Cheong, P. H.; Jain, R. Model of coal pyrolysis. 2. Quantitative formulation and results. *Ind. Eng. Chem. Fundam.* **1981b**, *20*, 122-132.

Gidaspow, D. Multiphase Flow and Fluidization, Continuum and Kinetic Theory descriptions. *Academic Press*. **1994.**

Govind, R.; Shah, J. Modeling and simulation of an entrained flow gasifier. *AIChE Journal.* **1984,** *30* (1), 79-92.

Holt, H. A. N.; Alpert, B. S. Integrated combined-cycle power plants. *Encyclopedia of Physical Science and Technology*, **2004,** *18*, 897-924.

Hottel, H. C.; Sarafim, A. F. Radiative Transfer, *McGraw-Hill Book Company*, New York, **1967**.

Howard. B. J.; Essenhigh, H. T. Pyrolysis of coal particles in pulverized fuel flames. *I&EC Process Design and Development*. **1967**, *6* (1), 74-84.

Jones, W. P.; Lindstedt, R. P. Global reaction schemes for hydrocarbon combustion. *Combustion and Flame*. **1988**, *73*, 233-249.

Karan, K.; Mehrotra, K. A.; Behie, A. L. A high-temperature and modeling study of homogeneous gas-phase COS reactions applied to Claus plants. *Chemical Engineering Science.* **1999,** 54, 2999-3006.

Kobayashi, H.; Howard, J. B.; Sarofim, A. F. Coal devolatilization at high temperatures. In *Proc. 16th International Symposium on Combustion*, The Combustion Institute, Pittsburgh, **1977,** 411-425

Lee, W. C.; Scaroni, W.A.; Jenkins, G. R. Effect of pressure on the devolatilzation and swelling behavior of a softening coal during rapid heating. *Fuel*. **1991**, *70*, 957-965.

Levenspiel, O. Chemical Reaction Engineering. 2nd ed., *John Wiley & Sons, New York*, **1972.**

Liu, H.; Luo, C.; Kato, S.; Uemiya, S.; Kaneko, M.; Kojima, T. Kinetics of CO_2/char gasification at elevated temperatures, 1: Experimental results. *Fuel.* **2006**, *87*, 775-781.

Liu, S. G.; Rezaei, H. R.; Lucas, A. J.; Harris, J. D.; Wall, F. T. Modelling of a pressurized entrained flow coal gasifier; the effect of reaction kinetics and char structure. *Fuel*. **2000,** 1767-1779.

Loison, R.; Chauvin, R. Pyrolyse rapid du charbon. *Chimie et Industrie.* **1964,** *91*, 3.

Mann, D. M.; Knutson, Z. R.; Erjavec, J.; Jacobsen, P. J. Modeling reaction kinetics of steam gasification for a transport gasifier. *Fuel.* **2004,** *83*, 1643-1650.

Maurstad, O. An overview of coal based integrated gasification combined cycle (IGCC) technology. *MIT Institute of Technology Laboratory and the Environment. LFEE 2005-003 WP*, **2005.**

Minchener, J. A. Coal gasification for advanced power generation. *Fuel.* **2005**, *84*, 2222-2235.

Monaghan, D. Rory F.; Kumar, M.; Singer, L. S.; Zhang, C.; Ghoniem, F. A. Reduced order modeling of entrained flow solid fuel gasification. *Proceedings of the ASME International Mechanical Engineering Congress & Exposition.* IMECE2009-12985.

Neoh, G. K.; Gannon, E. R. Coal volatile yield and element partition in rapid pyrolysis. *Fuel.* **1984**, *63*, 1347-1352.

Ni, Q.; Williams, A. A simulation study on the performance of an entrained-flow coal gasifier. *Fuel*. **1995**, 74 (1), 102-110

Niksa, S. Rapid coal devolatilization as an equilibrium flash distillation. *AIChE Journal*. **1988**, *34*,790-802.

Niksa, S.; Kerstein, A. R. FLASHCHAIN theory for rapid coal devolatilization kinetics, 1. Formulation. *Energy and Fuels.* **1991**,*5*, 647-665

Niksa, S.; Kerstein, A. R. FLASHCHAIN theory for rapid coal devolatilization kinetics, 2.Impact of operating conditions. *Energy and Fuels.* **1991**, *5*, 665-673.

PC Coal Lab Version 4.0, User's Guide and Tutorial, Niksa Energy Associates LLC. **2004**

Pilot Plant Evaluation of Illinois No.6 and Pittsburgh No.8 coal for the Texaco Coal Gasification Process, EPRI Final Report, EPRI AP-5029, **1987**, Texaco Inc. South EL Monte, California.

Ranz, W. E; Marshall, W. R. Evaporation from drops. *Chem. Eng. Prog.* **1952**, 48, 141.

Rao, R. M.; Bhattacharyya, D.; Rengaswamy, R.; Choudhury, R. S. A two-dimensional steady state model including the effect of liquid water for a PEM fuel cell cathode. *Journal of Power Sources*. **2007,** 173, 375-393.

Roberts, G. D.; Harris, J. D. A kinetic analysis of coal char gasification reactions at high pressures. *Energy and Fuels.* **2006**, *20*, 2314-2320.

Robinson, P. J; William, L. L. Simple dynamic gasifier model that runs in Aspen Dynamics. *Ind. Eng. Chem. Res.* **2008**, 47, 7784-7792.

Rowe, P. N.; Henwood, G. A. Drag forces in Hydraulic Model of Fluidized Bed. *Trans. Chem. Eng.* **1961**, 39, 43.

Shamlal, M.; Bissett, L. A. METC gasifier advanced simulation (MGAS) model, *Technical Note, NITS report No. DOE/METC-92/4108 (DE92001111)*, **1992.**

Shi, P. S.; Zitney, E. S.; Shahnam, M.; Syamlal, M.; Rogers, A. W. Modelling coal gasification with CFD and discrete method. *Journal of the Energy Institute,* **2006,** 79(4), 217-221.

Siegel, R.; Howell, R.J. Thermal Radiation Heat Transfer, *McGraw-Hill Book Company*, New York, **1981**.

Slezak, A; Kuhlman, M. J; Shadle, J. L; Shi. S. CFD simulation of entrained-flow gasification: Coal particle density/size fraction effects. *Powder Technology*. **2010,** 203, 98-108.

Solomon, P. R.; Hamblen, D. G.; Carangelo, R. M.; Serio, M. A.; Deshpande, G. Y. General Model of Coal Devolatilization. *Energy and Fuels.* **1988,** *2*, 323-360.

Spenik, D. NETL, DOE, Morgantown, Personal communication.

Tampa Electric POLK power Station Integrated Gasification Combined Cycle Project, Final Technical Report; 2002, Tampa Electric Company, Tampa, FL, *http://www.netl.doe.gov/technologies/coalpower/cctc/cctdp/bibliography*.

Tognotti, L.; Longwell, J. P.; Sarofim, A. F. The products of high temperature oxidation of a single char particle in an electrodynamic balance. *Symposium (International) on combustion,* **1991**, 23 (1), 1207-1213.

Ubhayakar, K. S.; Stickler, B. D.; Gannon, E. R. Modeling of entrained-bed pulverized coal gasifiers. *Fuel*. **1977**, *56*, 281-291.

Vamvuka, D.; Woodburn, E. T; Senior, P. R. Modeling of an entrained flow coal gasifier, 1. Development of the model and general predictions. *Fuel*. **1995**, *74*, 1452-1460.

Vamvuka, D.; Woodburn, E. T; Senior, P. R. Modeling of an entrained flow coal gasifier, 2. Effect of operating conditions on reactor performance. *Fuel*. **1995**, *74*, 1461-1465.

Wagner, R.; Wanzl, W.; van Heek, K. H.; Influence of transport effects of pyrolysis reaction of coal at high heating rates. *Fuel.* **1985**, *64*, 571-573.

Wanatabe, H.; Otaka, M. Numerical simulation of coal gasification in entrained flow gasifier, *Fuel.* **2006**, *85*, 1935-1943.

Wen, C. Y.; Chaung, T. Z. Entrained coal gasification modeling. *Ind. Eng. Chem. Process Des. Dev.* **1979,** *18* (4), 684-695.

Wen, C. Y.; Chen, H.; Onozaki, M. C. User's manual for computer simulation and design of the moving-bed coal gasifier. *DOE/MC*/16474-1390, *NITS/DE*83009533. **1982.**

Wen. C. Y. Noncatalytic heterogeneous solid-fuel reaction models, *Ind. Eng. Chem.* **1968**, *60* (9), 34-54.

Westbrook, K, C.; Dryer, L. F. Simplified reaction mechanisms for the oxidation of hydrocarbon fuels in flames. *Combustion Science and Technology.* **1981,** *27*, 31-43.

World Coal Institute. *http://www.worldcoal.org/pages/content/index.asp?PageID=187*

Yang, Z.; Wang, Z.; Wu, Y.; Wang, J.; Lu, J.; Li, Z.; Ni, W. Dynamic model for an oxygen-staged slagging entrained flow gasifier. *Energy Fuels*, 2011, 25, 3646-3656.

Zheng, L.; Furinsky, E. comparison of Shell, Texaco, BGL and KRW gasifiers as part of IGGC plant computer simulations. *Energy Conversion and Management.* **2005,** *46*, 1767-1779.

Appendix: Recirculation model

This section briefly describes the heuristic recirculation model incorporated in the current study. In an industrial gasifier, two regions namely mixing and recirculation are known to exist at the immediate entrance of the gasifier. These two regions are crucial in maintaining stability of the ignition front as well as aiding in the initial drying and devolatilization processes. The recirculation model is thus used in the current model to mimic these two sections, shown in Figure A1 as regions 1 and 2 of lengths L_1 and L_2, respectively.

This model is based on the mixing and recirculation model seen in previous studies by Smith and Smoot[17] and Monaghan et al.[18]

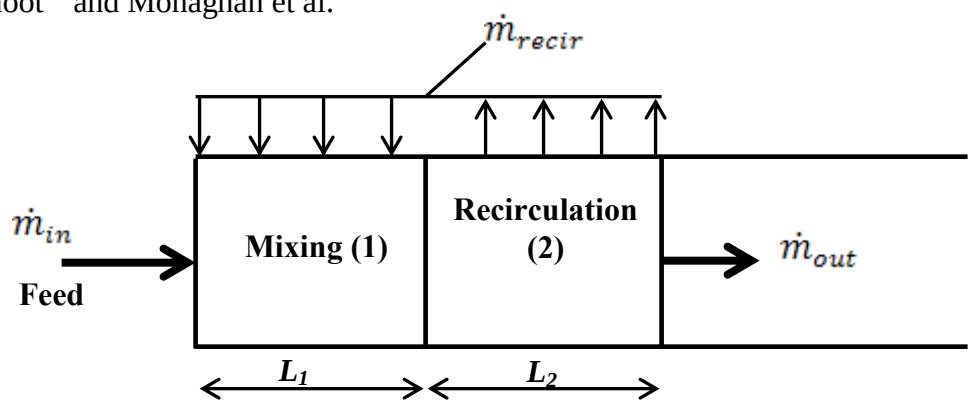

Figure A1: Illustration of the recirculation model

In the model, a fraction of the hotter gas phase stream from the recirculation section (2) of the gasifier is recirculated back to a colder region at the entrance of the reactor (region 1). The total mass recirculated (m_{recir}) is determined from the recirculation ratio (α), which is a parameter in the model, and the inlet gas feed flow rate (m_{in}):

$$\alpha = m_{recir} / m_{in} \tag{A.1}$$

The mass and energy balances in regions, 1 (mixing zone) and region 2 (recirculation zone) are modified to account for the recirculation as shown in Eqns. (A.2) and (A.3).

$$\frac{\partial(\rho_g \varepsilon)}{\partial t} + \frac{\partial(\rho_g \varepsilon U_g)}{\partial x} = (1-\varepsilon)\Gamma_{S-g} - m_{rg} + m_{mg} \tag{A.2}$$

$$\frac{\partial\lfloor \varepsilon\rho_g C_{p,g} T_g \rfloor}{\partial t} + \frac{\partial(U_g \varepsilon\rho_g C_{p,g} T_g)}{\partial x} = \frac{\pi D_i}{A_R}\left\{ e_g F_{w-g}\sigma\left[T_w^4 - T_g^4\right] + h_{w-g}\left[T_w - T_g\right]\right\}$$
$$-(1-\varepsilon)\frac{6}{d_p}\left\{ e_g F_{g-s}\sigma(T_g^4 - T_s^4) + h_{g-s}(T_g - T_s)\right\} + \sum_{j}^{\text{gas-phase reactions}} \varepsilon\left(-\Delta H_j\right) r_j - m_{rg} h_{rg} + m_{mg} h_{mg} \quad \text{(A.3)}$$

where m_{rg} and m_{mg} denote the mass of the gas recirculating from the recirculation zone (section 2) and that recirculating into the mixing zone (section1), respectively. The corresponding terms for the energy associated with the recirculating streams into or out of regions 1 and 2 are $m_{mg}h_{mg}$ and. $m_{rg}h_{rg}$, respectively, for which the specific enthalpy terms are calculated as

$$h_{mg} = \frac{1}{m}\sum_{k=1}^{m} h_k \quad \text{(A.4)}$$

$$h = \sum_{i=1}^{N} y_i h_i \quad \text{(A.5)}$$

$$h_i = h_0 + \int_{T_o}^{T} C_p dT \quad \text{(A.6)}$$

where *m* represents the total number of control volumes/cells in the recirculating region (section 2) and *i* represents the gas species. h_{rg} is the same as *h* of the control volume under consideration within section 2. m_{mg} and m_{rg} are calculated as

$$m_{mg} = \dot{m}_{recir} / (A_R L_1) \quad \text{(A.7)}$$

$$m_{rg} = \dot{m}_{recir} / (A_R L_2) \quad \text{(A.8)}$$

where A_R is the cross-sectional area.

The corresponding species balance equation in the above regions is written as

$$\frac{\partial}{\partial t}(\varepsilon\rho_g y_{gi}) + \frac{\partial}{\partial x}(\varepsilon\rho_g U_g y_{gi}) = R_{gi} - m_{rg} y_{gi} + m_{mg}\varpi_{gi} \quad (3)$$

where,

$$\varpi_{gi} = \frac{1}{n}\sum_{k=1}^{n} y_{gi,k}$$

y_{gi} is the mass fraction of the gas species in control volume k within the length L_1-L_2 and n is the total number of control volumes in length L_1- L_2. The lengths L_1 and L_2 are parameters in the model.

A recirculation ratio of 12-16% was found to be sufficient for initiating the ignition within 10% of the gasifier length for all the coals studied here and a recirculation ratio of 14.8% was used in most of the runs in this study.